Louisiana State University
LSU Digital Commons

2013

The development of capillary electrophoresis assays to study enzyme inhibition

Sherrisse Kelly Bryant
Louisiana State University and Agricultural and Mechanical College

Follow this and additional works at: https://digitalcommons.lsu.edu/gradschool_dissertations

 Part of the Chemistry Commons

THE DEVELOPMENT OF CAPILLARY ELECTROPHORESIS ASSAYS TO STUDY
ENZYME INHIBITION

A Dissertation

Submitted to the Graduate Faculty of the
Louisiana State University and
Agricultural and Mechanical College
in partial fulfillment of the
requirements for the degree of
Doctor of Philosophy

in

The Department of Chemistry

by
Sherrisse Kelly Bryant
B.S., Florida Agricultural and Mechanical University, 2007
August 2013

This dissertation is dedicated to my husband, Mark Bryant, and my parents, the late Alexander

D. Kelly III and Barbara Kelly.

ACKNOWLEDGEMENTS

Louis Stokes Alliance for Minority Participation and the Harriet G. Jenkins Predoctoral Fellowship program for providing opportunities for me to develop professionally.

Now, I must take the time to acknowledge the person who has had the most patience throughout this process, my husband, my love, Mark Bryant. Thank you for being my biggest supporter. Thank you for encouraging me as I pursued a doctoral degree and for being selfless. Thank you for motivating me and comforting me. There were others who were there for my graduate career and I must acknowledge them. I would like to acknowledge my mother for the phone calls, encouraging words, and advice, and my sisters (Lynne and Alexis). You all are always there for me. I would also like to thank my Godparents for being so helpful throughout this process. Additionally, I would like to thank one of my mentors, Dr. James Bouyer, for your encouragement and guidance in education and my personal life.

I have had to opportunity to experience graduate school with amazing colleagues and friends. Thank you all for the many conversations, late nights in the lab, dinners, spiritual conversations, your support, and all of the special moments we shared together. I also want to thank my other family members, friends, mentors, and church family for all of your support and encouragement.

Love always,

Sherrisse

TABLE OF CONTENTS

LIST OF TABLES

LIST OF FIGURES

ABSTRACT

New methods for studying enzymes and enzyme inhibition using capillary electrophoresis (CE) were developed and applied. Because CE is a separation technique, spectral interference is minimized by separation of substrates, products, inhibitors, and sample matrix components. Two types of CE enzyme assays were explored in this dissertation research. The first assay was based on optically gated vacancy capillary electrophoresis (OGVCE) with laser-induced fluorescence detection (LIF). This approach involves periodic photobleaching of fluorescent substrates and products. The initial goal of the study was to develop an assay for adenosine deaminase (ADA). A fluorescent ADA substrate was synthesized; however, the substrate was unusually photostable and could not be photobleached. In Chapter 2, a comparative study is presented that quantified the photostability of the fluorescent ADA substrate relative to other fluorophores that have been used for OGVCE in order to obtain a better understanding of the ideal properties of a dye for OGVCE assays. The development of an off-column CE assay for measuring acetyl coenzyme A carboxylase holoenzyme (holo-ACC) activity and inhibition is presented in Chapter 3. The two reactions catalyzed by the holo-ACC components, biotin carboxylase (BC) and carboxyltransferase (CT), were simultaneously monitored in the assay, which required successful separation of two substrates and two products using micellar electrokinetic chromatography (MEKC). Additionally, a previously reported off-column CE assay for only the CT component of ACC was optimized, and an off-column CE assay for only the BC component of ACC was developed. Finally, the CE-based enzyme assays developed in Chapter 3 were used for screening of botanical extracts against holo-ACC, BC and CT (Chapter 4). Compounds known to be present in the botanical extracts that inhibited holo-ACC were selected based on a detailed literature search and tested for inhibition of holo-ACC, BC and CT.

Synthetic compounds selected based on ligand homology studies were also tested for inhibition of holo-ACC. These CE assays were simple, off-column methods, where spectral interference and other limitations of previous methods were greatly reduced. The development of methods that can directly monitor reactants and products for multiple enzyme-catalyzed reactions will have impact beyond the enzymes presented in this dissertation.

CHAPTER 1. INTRODUCTION

1.1.   Enzyme Catalysis

Enzymes are proteins found in all living systems that function as catalysts for chemical reactions. Enzymes are essential for the function and regulation of cells, tissues, and organs [1]. At any point in time, there are thousands of chemical reactions occurring in living cells, and nearly all of them are catalyzed by enzymes. Therefore, enzymes are vital to the function of our bodies, and improper functioning of enzymes can lead to illness and disease. Like all proteins, enzymes are composed of one or more chains of amino acids. The structural organization of a protein is described using four levels known as the primary, secondary, tertiary, and quaternary structure. The linear sequence of amino acids, which is known as the primary structure, is genetically determined and unique to each protein. In the primary structure, the amino acids are linked by amide bonds [1, 2]. The secondary structure is a three-dimensional arrangement of the protein, which is driven by hydrogen bonding [1, 2]. The two most common types of secondary structure are α-helices and β-pleated sheets; however, other structures are also possible. Proteins usually adopt specific conformations in which hydrophobic amino acids are protected from the aqueous surroundings in a biological system [1]. The protein can assume a more compact three-dimensional structure, which is the tertiary structure. The tertiary structure is known as the active form of a protein (native structure), and enzymes consisting of a single polypeptide chain function in this conformation. Enzymes consisting of two or more polypeptide chains are referred to as multi-subunit enzymes and cannot function properly without the necessary subunits [1]. Each subunit is a polypeptide chain that has assumed a tertiary structure. The quaternary structure is based upon how the multiple polypeptide chains are arranged, where the arrangement

of polypeptide chains is based on noncovalent forces such as hydrogen bonds, ionic bonds, van der Waals interactions, and hydrophobic interactions [1, 2].

For every enzyme-catalyzed reaction, the enzyme must bind to a substrate, and in many cases there are two substrates and more than one reaction product. In enzyme-catalyzed reactions, the enzyme lowers the energy needed for a substrate to be converted to a product [1]. Enzymes are selective for their substrates, and substrates and enzymes have structures that complement each other. The active site of the enzyme typically is a crevice or cleft within the enzyme where the substrate binds and catalysis occurs. Typically, this binding occurs through weak attractions such as hydrogen bonds, ionic bonds, and van der Waals interactions [1-3].

Some enzymes require cofactors in order to function. Cofactors are nonprotein components such as metals and organic molecules, which are bound to the enzyme and are essential to its function [1, 3]. Cofactors that are required for the catalytic function of enzymes are also known as coenzymes. Many coenzymes are covalently bound to the enzyme and are referred to as prosthetic groups. The term holoenzyme is used to describe the catalytically active complex of protein and coenzyme(s) or prosthetic group(s), and the term apoenzyme is used to describe the catalytically inactive enzyme, which does not have the coenzyme(s) or prosthetic groups bound to it. A few common coenzymes are nicotinamide adenine dinucleotide (NAD^+), coenzyme A (CoA), and biotin [3].

1.1.1. Michaelis-Menten Kinetics

Chemical kinetics is the overall study of chemical reaction rates [3]. Chemical kinetics, specifically for enzyme-catalyzed reactions is known as enzyme kinetics [3]. Enzyme kinetics is used to study the roles of enzymes in metabolic reactions and determine how catalysis is accomplished. Enzyme kinetics provides valuable information such as the maximum reaction

velocity reached during catalysis, binding affinities of substrates to enzymes, and how the enzyme responds to different substrate concentrations [3]. Additionally, information obtained from enzyme kinetics experiments can be used to determine the mechanism by which catalysis occurs [3]. Enzyme kinetics is commonly described by the Michaelis-Menten model, which was proposed by Lenore Michaelis and Maud L. Menten in 1913 [4]. Equation 1.1 shows the typical progression of an enzyme-catalyzed reaction where each step is generally regarded as reversible. Once the enzyme (E) binds the substrate (S), an enzyme-substrate (ES) complex is formed, which is converted to an enzyme-product (EP) complex. Then, the reaction proceeds to yield free enzyme and product (P) once the enzyme-product complex dissociates.

$$E + S \overset{k_1}{\underset{k_{-1}}{\leftrightarrow}} ES \overset{k_2}{\underset{k_{-2}}{\leftrightarrow}} EP \overset{k_3}{\underset{k_{-3}}{\leftrightarrow}} E + P \qquad (1.1)$$
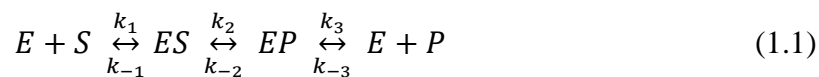
Simplifications of Equation 1.1 described by the Michaelis-Menten model rely on several assumptions. The binding of the enzyme and substrate to form the enzyme-substrate complex and the dissociation of the complex back to enzyme and substrate are assumed to be in equilibrium. This kinetic mechanism was analyzed and extended by Briggs and Haldane in 1925, who proposed the steady-state assumption, which is widely used for the determination of enzyme kinetics [5]. The steady-state assumption states that the concentration of the enzyme-substrate complex ([ES]) is constant because the enzyme-substrate complex forms as rapidly as it disappears [1, 3]. Therefore, [ES] is assumed to be constant throughout the time interval used to perform kinetic studies [1, 3]. Another assumption that is made for the simplification of Michaelis-Menten kinetics is that the reverse reaction (formation of the enzyme-substrate complex from enzyme plus product) is negligible [1, 3]. This is because the initial velocity of the reaction is observed (immediately after the enzyme and substrate are mixed). At these early time points, there is likely no conversion of the enzyme plus product to form the enzyme-substrate

3

complex because [P] is very low. Because [ES] is constant and the formation of product is irreversible, the velocity, or rate, of the enzymatic reaction is also constant. The rate is measured either as disappearance of substrate or formation of product. Using the aforementioned assumptions, the enzyme-catalyzed reaction scheme is simplified to Equation 1.2.

$$E + S \underset{k_{-1}}{\overset{k_1}{\leftrightarrow}} ES \overset{k_p}{\rightarrow} E + P \tag{1.2}$$

The first step is reversible because the enzyme-substrate complex can dissociate back to enzyme plus substrate, and the association and dissociation constants for this step are k_1 and k_{-1}, respectively. The dissociation constant for the second step is k_p. The ratio of the constants, (k_{-1} + k_p/k_1), is defined as the Michaelis constant, K_m, which is the substrate concentration at which the reaction rate is half of the maximum reaction rate [1]. The maximum rate of the reaction is defined as V_{max}. The V_{max} is reached once the enzyme is saturated with substrate [1]. In other words, all of the enzyme is in the form of the enzyme-substrate complex. These two constants along with the initial concentration of the substrate determine the initial rate of the reaction (v), according to the Michaelis-Menten equation (Equation 1.3).

$$v = \frac{V_{max}\,[S]}{K_m + [S]} \tag{1.3}$$

The Michaelis-Menten equation can be fit to a plot of v versus [S] called a substrate saturation curve, also known as a Michaelis-Menten plot (Figure 1.1). Using this plot, V_{max} and K_m can be determined as shown in Figure 1.1. Linear plots derived from the Michaelis-Menten equation can be used to further analyze enzymatic reactions. The Lineweaver-Burk double reciprocal plot is widely used (Figure 1.2). This plot is generated after taking the reciprocal of both sides of the Michaelis-Menten equation, which yields Equation 1.4.

$$\frac{1}{v} = \left(\frac{K_m}{V_{max}}\right)\left(\frac{1}{[S]}\right) + \frac{1}{V_{max}} \tag{1.4}$$

4

This equation is linear with a slope of K_m/V_{max} and a y-intercept of $1/V_{max}$ (Figure 1.2). In practice, nonlinear regression is used to determine K_m and V_{max} more precisely using computer programs designed to fit the rate versus concentration data to Equation 1.3 [6].
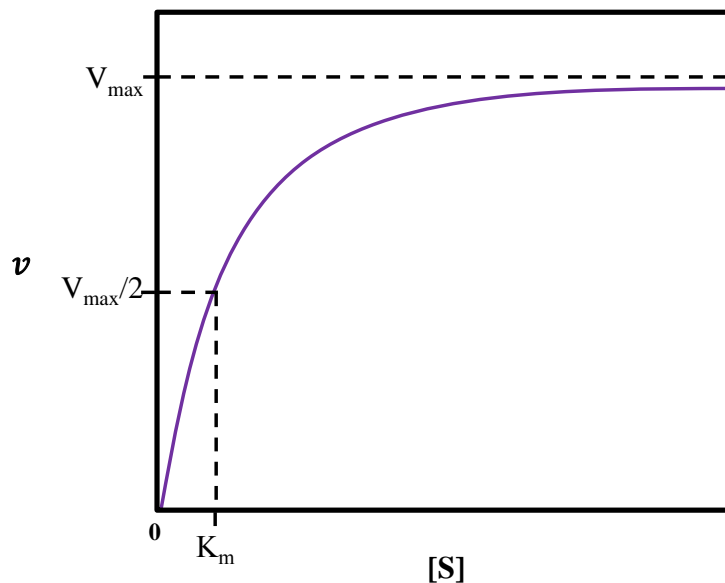
Figure 1.1. Michaelis-Menten plot. A plot of the reaction rate (v) versus substrate concentration, [S], where V_{max} is the maximum rate of the reaction and K_m is the Michaelis constant, which is the substrate concentration at which the reaction rate is half of V_{max}.
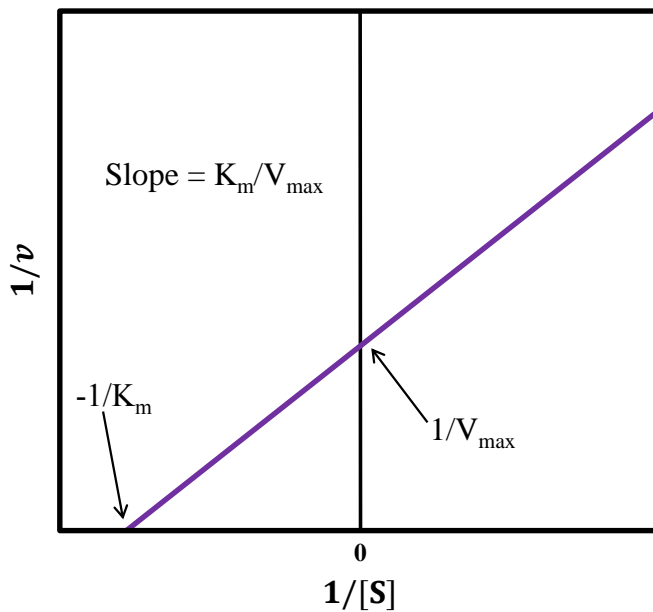
Figure 1.2. Lineweaver-Burk plot. A plot of the inverse of the rate versus the inverse of substrate concentration. K_m and V_{max} are defined in the text and in Figure 1.1.

1.2. Enzyme Inhibition

Because enzymes play a central role in important biochemical processes and metabolic pathways, it is important to understand the inhibition of enzymes. Enzyme inhibitors are targets for the development of a wide range of treatments for diseases such as cancer and diabetes [7, 8]. Studying enzyme inhibition is also important for understanding the mechanisms of enzymes. Additionally, enzyme inhibitors are used in agriculture as herbicides [9, 10]. Biological systems naturally regulate catalysis using enzyme inhibition. In 2000, Drews *et al.* reported that about 30% of drugs used clinically are therapeutically effective due to enzyme inhibition [11]. In 2002, Hopkins *et al.* reported that half of newly developed drugs inhibited target enzymes [12].

Enzyme inhibitors stop enzymes from catalyzing reactions or decrease the reaction rate [1, 7]. Inhibition of an enzyme-catalyzed reaction is analyzed using enzyme kinetics in order to determine binding affinities of an enzyme to an inhibitor, rates of inhibited reactions, inhibition constants, and types of inhibition. This information is used during the drug discovery process when potential inhibitors are screened for inhibition of target enzymes [7, 8]. Therefore, understanding enzyme kinetics and identifying enzyme inhibitors are both essential to the process of drug discovery.

Types of Inhibition

Enzyme inhibitors are classified as reversible and irreversible inhibitors [1-3]. Irreversible inhibitors form permanent, covalent bonds with the enzyme, and reduce or eliminate its activity. Reversible inhibitors bind noncovalently to the enzyme, and the enzyme-inhibitor complex dissociates very rapidly. The three subtypes of reversible enzyme inhibitors are competitive, noncompetitive and uncompetitive inhibitors.

Competitive inhibitors compete with the substrate for the active site of the enzyme and bind reversibly [1-3]. At high concentrations of substrate, the inhibitor is less likely to bind to the enzyme [1-3]. In competitive inhibition, the inhibitor affects K_m while V_{max} remains unaffected by the inhibitor as indicated in Equation 1.5 [1].

$$v = \frac{V_{max}[S]}{[S] + K_m \left(1 + \frac{[I]}{K_{is}}\right)} \qquad (1.5)$$

In this modified version of Equation 1.3, K_m is multiplied by $(1 + ([I]/K_{is})$, so the overall reaction rate, v, will be lower relative to an uninhibited reaction (Equation 1.3). At high concentrations of substrate, v is unaffected by [I]. The inhibition kinetic constant, K_{is}, can be determined by nonlinear fitting of Equation 1.5 to a plot of v versus [I]. Competitive inhibition can be identified using a Lineweaver-Burk plot (Figure 1.3). As shown in Figure 1.3, competitive inhibition results in lines that have the same y-intercept but different x-intercepts for plots of experiments using different inhibitor concentrations.
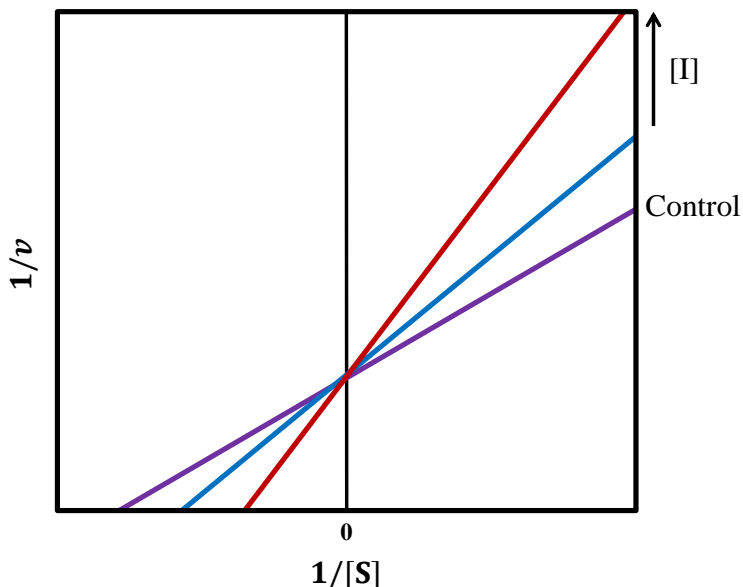
Figure 1.3. Lineweaver-Burk plot for competitive inhibition. A plot of the inverse of reaction rate versus the inverse of substrate concentration for a reaction without inhibitor (control) and two reactions with different inhibitor concentrations [I].

Uncompetitive inhibitors bind to the ES complex only [1-3]. Uncompetitive inhibitors affect K_m and V_{max} [1]. In the case of uncompetitive inhibition, the rate equation is Equation 1.6.

$$v = \frac{V_{max}[S]}{K_m + [S]\left(1 + \frac{[I]}{K_{ii}}\right)}$$

(1.6)

The inhibition constant, K_{ii}, is determined by nonlinear fitting of Equation 1.6. The Lineweaver-Burk plot for uncompetitive inhibition shows that both the x-intercept and y-intercept change with increasing [I], while the slope remains the same (Figure 1.4). As shown in Figure 1.4, uncompetitive inhibition results in a Lineweaver-Burk plot with parallel lines.
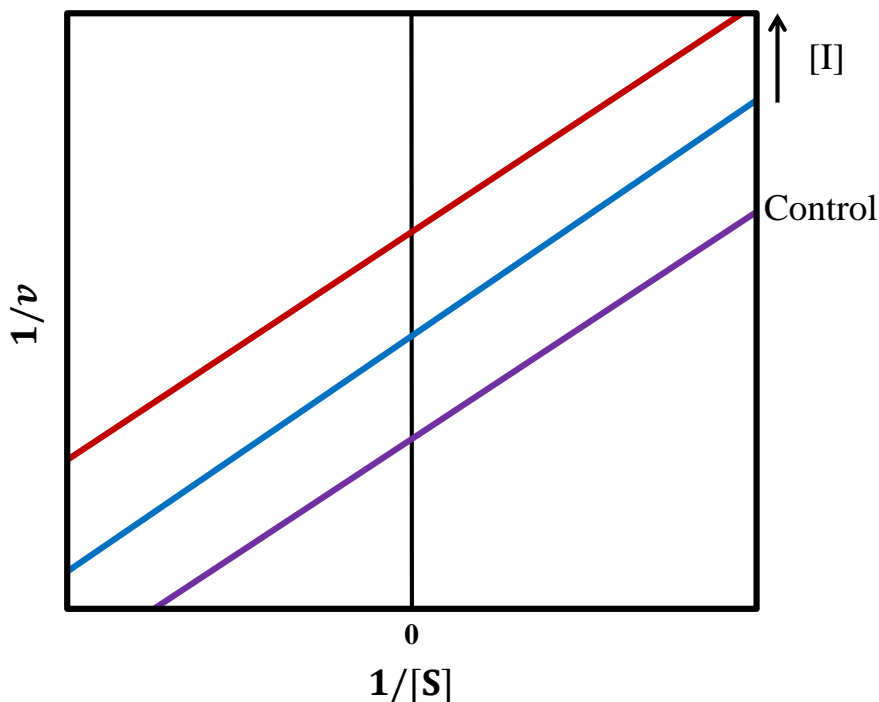
Figure 1.4. Lineweaver-Burk plot for uncompetitive inhibition. A plot of the inverse of reaction rate versus the inverse of substrate concentration for a reaction without inhibitor (control) and two reactions with increasing inhibitor concentrations [I].

Noncompetitive inhibitors can bind to the enzyme or the ES complex [1-3]. Unlike competitive inhibition, noncompetitive inhibition cannot be overcome by high substrate concentration [1-3]. There are two types of noncompetitive inhibition, pure and mixed. Pure

noncompetitive inhibition, where the binding of the inhibitor to the enzyme does not affect the binding of the substrate to the enzyme, is relatively uncommon. The rate equation for pure noncompetitive inhibition is Equation 1.7.

$$v = \frac{V_{max}[S]}{([S] + K_m)\left(1 + \frac{[I]}{K_{is}}\right)}$$

(1.7)

Pure noncompetitive inhibition decreases V_{max}, but does not affect the K_m [1]. The Lineweaver-Burk plot for pure noncompetitive inhibition shows that the y-intercept and slope increase with increasing [I], while the x-intercept remains unaffected.
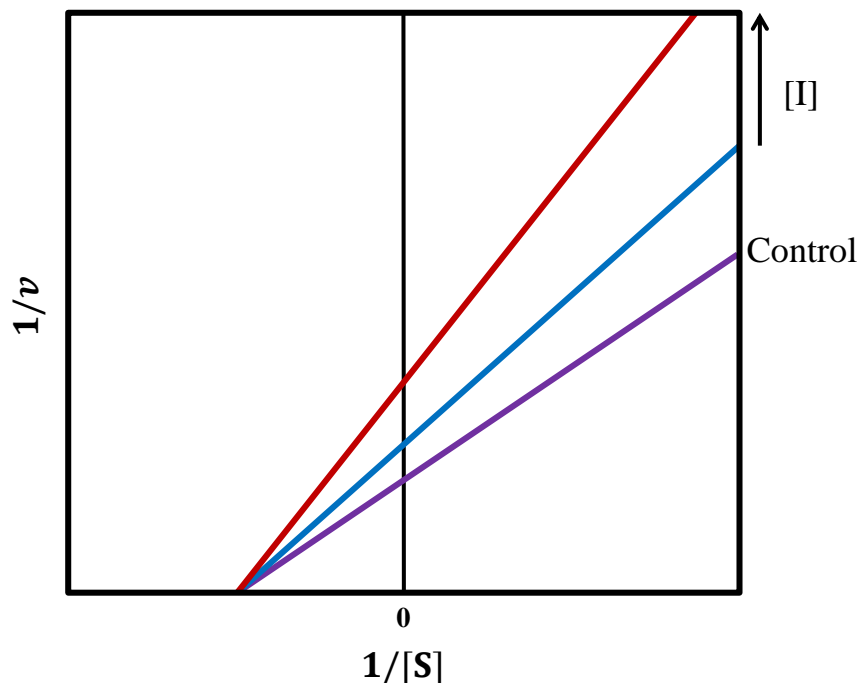
Figure 1.5. Lineweaver-Burk plot for pure noncompetitive inhibition. A plot of the inverse of reaction rate versus the inverse of substrate concentration for a reaction without inhibitor (control) and two reactions with increasing inhibitor concentrations [I].

In mixed noncompetitive inhibition, the binding of the inhibitor by the enzyme affects the binding of the substrate by the enzyme [1]. This can occur because the binding sites of the inhibitor and substrate are in close proximity or the binding of the inhibitor by the enzyme

9

induces a conformational change that impacts binding of the substrate. Equation 1.8 is the rate equation for mixed noncompetitive inhibition [1].

$$v = \frac{V_{max}[S]}{[S]\left(1 + \frac{[I]}{K_{ii}}\right) + K_m\left(1 + \frac{[I]}{K_{is}}\right)} \tag{1.8}$$

As shown in Equation 1.8, there are two inhibition constants, K_{ii} and K_{is}. When $K_{is} > K_{ii}$, the lines of the Lineweaver-Burk plot will cross below the x-axis (not shown); however, when $K_{ii} < K_{is}$, the lines will cross above the x-axis as shown in Figure 1.6. In mixed noncompetitive inhibition, both K_m and V_{max} are different when comparing the inhibited reactions to the uninhibited reaction [1].
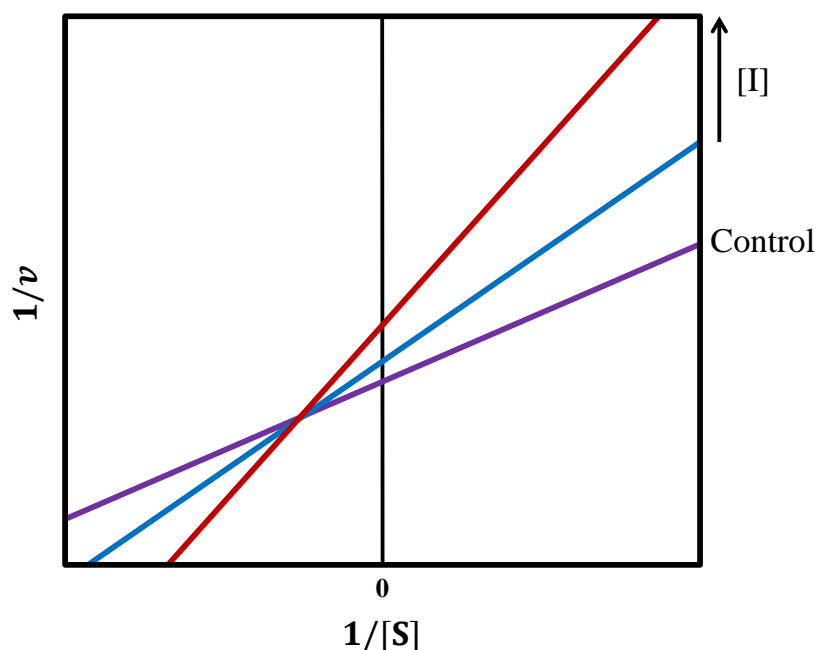
Figure 1.6. Lineweaver-Burk plot for mixed noncompetitive inhibition. A plot of the inverse of reaction rate versus the inverse of substrate concentration for a reaction without inhibitor (control) and two reactions with increasing inhibitor concentrations [I]. As shown in the plot, the slope of the line increases with increasing inhibitor concentration.

Substrate and product inhibition are also possible [2, 3]. Product inhibition typically occurs because the product is a substrate for the reverse reaction [2]. Therefore, the product can

bind to the enzyme and act similarly to a competitive inhibitor. Substrate inhibition occurs when the substrate or cofactor also has affinity for a non-active site on the enzyme. At high concentrations of the substrate or cofactor, binding to the enzyme can occur, resulting in substrate inhibition [3].

1.2.2. Botanicals as Enzyme Inhibitors

There are many different approaches that are used to identify enzyme inhibitors. Many of these approaches involve trial and error, such as high-throughput screening techniques, which involve screening libraries of synthetic molecules that may or may not inhibit the target enzyme [11]. Another approach involves screening botanical extracts for inhibition of targeted enzymes. For centuries, the medicinal properties of various botanicals have been investigated. A review of the literature shows that over the years, plants have had a major role as therapeutics for various diseases in the form of dietary supplements and drugs [13, 14], and botanical extracts have played a role in drug discovery [14-20]. In fact, a comprehensive study conducted by Newman *et al.* in 2006, indicated that 52% of 974 small molecule-based drugs developed from 1981-2006 were either natural products, derived from natural products, or synthetics that mimicked a natural product or had a natural product pharmacophore [20]. For example, metformin, which is commonly used to treat diabetes, is a biguanide derived from isoamylene guanidine which is found in in French lilac (*Galega officinalis*) [21]. Galanthamine (reminyl, galanta mind), which is used to treat Alzheimer's disease, can be isolated from plants such as the snow drop flower, daffodil, and spider lily [22]. It is effective at slowing the process of neurological degeneration because it inhibits the enzyme acetylcholinesterase [22-25]. A drug used to treat human immunodeficiency syndrome (HIV), calanolide A, can be isolated from a Malaysian rainforest

tree (*Calophyllum* lanigerum) [26-28] and is effective against type-1 HIV by inhibiting non-nucleoside reverse transcriptase [28-30].

1.3.   Enzyme Assays

Enzyme assays are performed to determine enzyme activity or the ability of an enzyme to catalyze the reaction of substrates to form products. This is done by monitoring the accumulation of product or reduction of substrate. Enzyme assays are frequently performed in chemical and biological sciences (including biomedicine), especially as part of the drug discovery process [1-3, 7]. Most traditional enzyme assays are carried out in cuvettes or microtiter wells, and the progress of the reaction is analyzed by using UV-Vis absorbance detection to measure the change in substrate or product absorbance over time [31]. Fluorescence detection is also commonly used for microplate reader based assays. Assays based on UV absorbance or fluorescence with UV excitation are prone to spectral interference by inhibitors and biological sample matrices, which is a significant limitation [31]. Some enzymes do not have a substrate or product that can be measured directly by absorbance or fluorescence detection, and in many of these cases, substrates or products are labeled with radioactive isotopes. Assays based on radiolabelling have significant disadvantages because they can be expensive and complex in practice due to health, waste and regulatory issues [31]. Another approach used when substrates and products can't be detected directly is the use of enzyme-coupled assays. In enzyme-coupled assays, the reactions of interest are coupled to other enzyme catalyzed reactions. The auxiliary enzymes used are referred to as coupling enzymes. Typically, a product for the reaction of interest will serve as a substrate for another enzyme-catalyzed reaction that can be monitored. Often, these assays involve the reduction of $NAD(P)^+$ to yield $NAD(P)H$ or the oxidation of $NAD(P)H$ to produce $NAD(P)^+$. Both processes can be monitored using absorbance or

fluorescence detection, which makes the use of these coupling reactions effective. Assays based on enzyme-coupled reactions are indirect and susceptible to false positives for inhibition studies because a potential inhibitor could be inhibiting the coupling enzymes, which is a major drawback [31].

Capillary Electrophoresis-Based Enzyme Assays

Capillary electrophoresis (CE) is a well-established separation technique that has been around for over 30 years. In 1981, Jorgenson and Luckas reported separations of amino acids and peptides using open glass capillaries and fluorescence detection [32]. Since then, this technique has been used for a wide array of applications including DNA sequencing, due to its advantages over other separation techniques, including high separation efficiency, simplicity, small sample volumes (nL) and rapid analysis times [33]. Additionally, CE can be coupled with UV-Vis absorbance, laser-induced fluorescence (LIF), mass spectrometry (MS), and electrochemical detection methods [34, 35]. This technique (Figure 1.7) employs a capillary which typically has an inner diameter ranging from 50 to 100 µm with a 360 µm outer diameter. Both ends of the capillary are immersed in buffer vials that contain electrodes, which are connected to a high voltage power supply. When a voltage is applied across the capillary, the analytes separate based on their electrophoretic mobility, which is related to the charge-to-size ratio of analytes.

It has been demonstrated that CE can be used effectively for performing quantitative enzyme assays and studying enzyme inhibition [36-39]. Using CE to investigate enzyme-catalyzed reactions has an advantage over traditional enzyme assays, which are often limited by spectral interference. Because CE is an electrophoretic separation technique, spectral interference is reduced by separation of substrates, products, inhibitors and sample matrix components. In addition, eliminating spectral interference allows direct monitoring of substrate depletion and

product formation in contrast to enzyme-coupled assays, which can result in false positives. Furthermore, when monitoring substrate depletion and/or product formation directly, radiolabels are not needed, which eliminates cost, health, waste and regulatory issues.
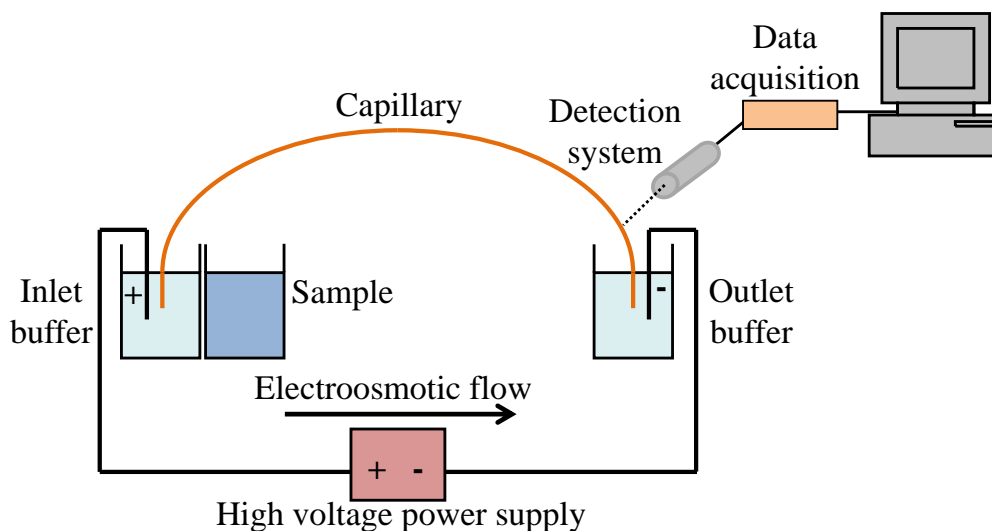
Figure 1.7. Schematic of a basic capillary electrophoresis system.

Enzyme assays based on CE can be homogeneous assays or heterogeneous assays. In homogenous assays, all assay components are in the solution phase. Homogeneous assays are further subcategorized: off-column (offline), on-column (online), and post-column. Heterogeneous assays refer to assays in which one of the assay components is immobilized, forming a microreactor [40]. Typically, the enzyme is immobilized inside the capillary on the capillary wall or on support surfaces such as silica beads or magnetic beads. The substrate is introduced into the capillary in the running buffer, and once the substrate and enzyme mix, product is formed. The product migrates through the capillary and is detected downstream. Heterogeneous assays have been extensively reviewed by Krenkova and Foret [40]. The research presented in this dissertation is focused on homogenous assays, and the two major types of homogenous assays, on-column and off-column, will be described.

1.3.2. On-Column CE Assays

In on-column CE assays, the enzyme-catalyzed reaction is initiated inside the capillary. This is generally carried out by injecting a plug of enzyme and a plug of substrate into the capillary and allowing them to mix, initiating the reaction. The first on-column CE enzyme assay was demonstrated by Bao and Regnier in 1992 [41]. A plug of enzyme was injected into a capillary filled with the substrate and a coenzyme required for the reaction. Product formation occurred as the enzyme migrated through the capillary and was detected by a downstream absorbance detector. The product formation was represented by a plateau in the resulting electropherogram. This type of CE-based assay was later termed electrophoretically mediated microanalysis (EMMA), and this format was defined as continuous engagement EMMA [42]. In continuous engagement EMMA, the substrate is often fluorogenic, which is a substrate that is nonfluorescent but produces a fluorescent product that can be detected by laser-induced fluorescence. Another format, in which the enzyme and substrate are injected in separate plugs and allowed to mix electrophoretically, was defined as transient engagement EMMA. In transient engagement EMMA, the plug with the slowest electrophoretic mobility is injected first. When the separation voltage is applied, the faster moving plug will pass the slower moving plug, initiating the enzymatic reaction, which results in a product peak being detected downstream [42].

Whisnant *et al.* used capillary electrophoresis with laser-induced fluorescence detection (CE-LIF) to study enzyme inhibition using a combination of both transient and continuous engagement EMMA [43]. The capillary was first filled with the fluorogenic substrate, AttoPhos, and running buffer. Then the enzyme, alkaline phosphatase, and the inhibitor, theophylline, were injected into the capillary as separate plugs. A constant potential was applied, and the enzyme

and inhibitor migrated through the substrate-filled capillary. As the reaction proceeded, fluorescent product was formed and detected as a plateau by a downstream LIF detector. The inhibitor plug was indicated by a negative peak in the plateau because the product formation decreased as the inhibitor zone mixed with the enzyme-substrate complex. The inhibition of alkaline phosphatase by different types of inhibitors was also studied using the same method [44]. More information about on-column CE assays can be found in reviews [37, 38]; this dissertation work focusses on off-column CE assays.

1.3.3. Off-column CE assays

In off-column CE assays the substrates, products, and inhibitors are mixed outside of the capillary, but one component is left out of the initial mixture, either the enzyme or the substrate. To initiate the reaction, the enzyme or substrate is added to the reaction mixture. Then a plug of the reaction mixture is sampled periodically by the CE instrument. Substrate depletion or product formation is monitored in the resulting electropherograms. A representative electropherogram for an off-column CE assay is shown in Figure 1.8. In the case where an inhibitor is present in solution, the substrate depletion and product formation will occur at decreased rates in comparison to a control assay. These types of assays have been performed in capillaries and microchips [37, 38]. Off-column assays are used for kinetic studies when the enzyme-catalyzed reaction is slow enough to be monitored periodically over a time frame that can range from several minutes to several hours or days.

The first off-column homogeneous CE enzyme assay for the determination of enzyme activity was demonstrated by Krueger *et al.* in 1991 for the analysis of endoproteinase Arg C [45]. In this assay, the adrenocorticotrophic hormone (ATCH (1-39)) peptide was incubated with endoproteinase Arg C in a reaction vial, and the mixture was periodically injected into the

16

capillary in order to monitor enzyme-catalyzed hydrolysis of 3 peptide bonds. In 1992, Landers *et al.* reported the determination of bacterial chloramphenicol acetyl transferase (CAT) activity using CE [46]. In this assay, the enzyme was incubated with acetyl coenzyme A and chloramphenicol, and after the incubation period, the mixture was injected into the capillary.
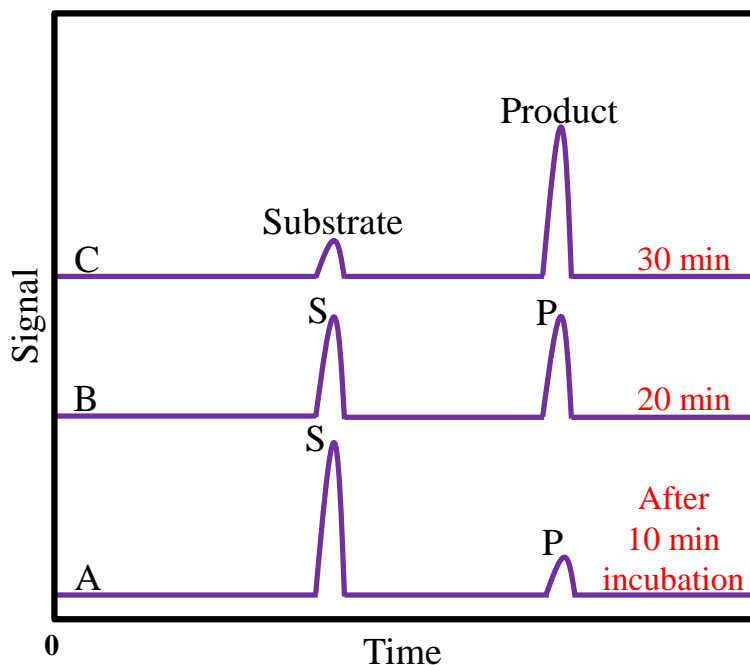
Figure 1.8. Sketch of electropherograms for the progress of a simple off-column CE enzyme assay where the depletion of substrate and formation of product are observed in 3 consecutive injections of the reaction mixture. Electropherogram A represents the first injection, B represents the second injection, and C represents the third injection.

The formation of products, coenzyme A and diacetyl chloramphenicol, and depletion of the substrates were observed. Pascual *et al.* reported CE-based studies of glutathione peroxidase activity where the separation and quantitation of reduced and oxidized glutathione were observed by CE [47]. In this study, sodium dodecyl sulfate was used to aid in the separation.

In off-column CE enzyme inhibition assays, the inhibitor is included in the reaction mixture. After the enzyme-catalyzed reaction is initiated, the mixture is injected into the CE instrument. Product formation in the inhibited reaction is compared to the product formation in a

control assay (no inhibitor present) using the resulting electropherograms. The first off-column CE enzyme inhibition assay was reported by Hoffmann *et al.* in 1995 [48]. The inhibition of dipeptidyl peptidase IV (DP-IV) by anti-DP IV antibodies was investigated using CE. Since that report, CE has been used to study the inhibition many of other enzymes. For example, in 1998, Kanie *et al.* studied the inhibition of galactosyltransferase using CE [49]. The GalTase-catalyzed transfer of uridine 5'-phosphonate galactose (UDP-gal), the substrate, to 4-methylyumbelliferyl 2-acetamido-2-deoxy-β-D-glucopyranoside (MU-GlcNAc), the product, was monitored by CE with absorbance detection. For the inhibition studies, UDP, a known GalTase inhibitor, was added to the reaction mixture and the inhibited reaction was monitored by CE [49]. In 2001, Change *et al.* developed a CE method with absorbance detection for studying the inhibition of angiotensin converting enzyme (ACE) by cultivated hot water *Cordyceps sinensis* extracts [50].

In order to decrease the analysis time for off-column assays, short end injection techniques have been developed [51-54]. In short end injection techniques, the sample vial is placed at the outlet end of the capillary, which is closer to the detection window than the inlet end. After injecting the sample from the outlet end, the separation is carried out using reverse polarity, which results in bulk electroosmotic flow toward the inlet end of the capillary.

1.3.4. Optical Gating Injections for CE

Optically gated vacancy capillary electrophoresis (OGVCE) is a technique where a solution containing a fluorescent compound or fluorescently labeled compound is continuously electrophoresed through the capillary and periodically photobleached at specific time intervals. This technique offers a potential advantage for development of CE enzyme assays because almost any fluorescent substrate with a high turnover rate that produces and is capable of being photobleached can be used with OGVCE. In OGVCE, a fluorescent substrate is incubated with

an enzyme offline, and the progress of the reaction is monitored as the mixture is continuously electrophoresed through a capillary and the reaction is monitored. Fluorogenic substrates are not required. Both the substrate and the product can be fluorescent. The need for a fluorogenic substrate limits the range of enzymes that can be studied using previously developed CE assays.

The instrument for OGVCE experiments is shown in Figure 1.9. The capillary is filled with the fluorescent compound during the entire experiment. The photobleaching beam from the laser is blocked by a computer-controlled shutter. When the shutter is opened, the bleaching
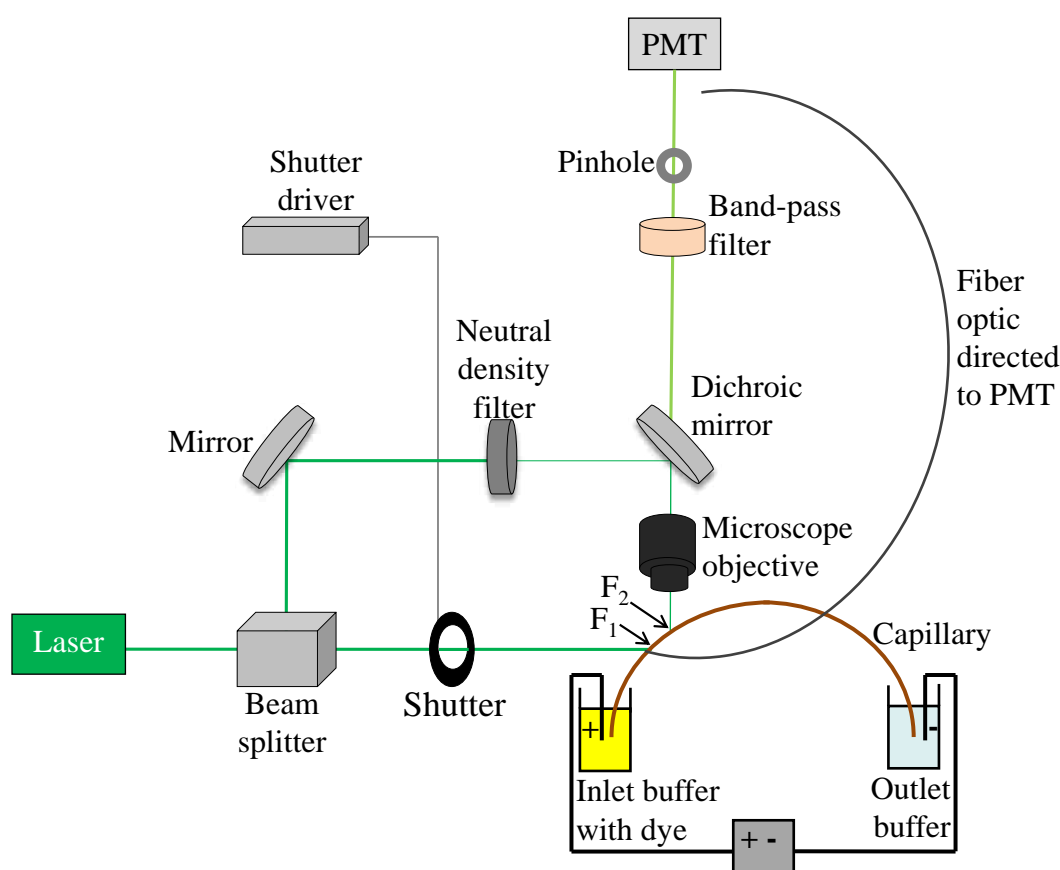
Figure 1.9. Schematic of the instrumentation for optically gated vacancy capillary electrophoresis (OGVCE).

beam is focused on the capillary. As the fluorescent dye migrates through the capillary, the opening of the shutter allows the high-powered beam to photobleach the dye at position F_1 in the

capillary window. The fluorescence emission is collected by a microscope objective at position F_2 in the capillary window, and the photobleached zone is observed as a negative peak (vacancy) in the resulting electropherogram (Figure 1.10). Additionally, an optical fiber is used to collect light each time the shutter is opened and direct it to the PMT for detection. This light creates a positive peak in electropherograms and represents the time at which the vacancies were created (Figure 1.10). When two dyes are present in solution, two separate negative peaks are observed in the electropherogram.
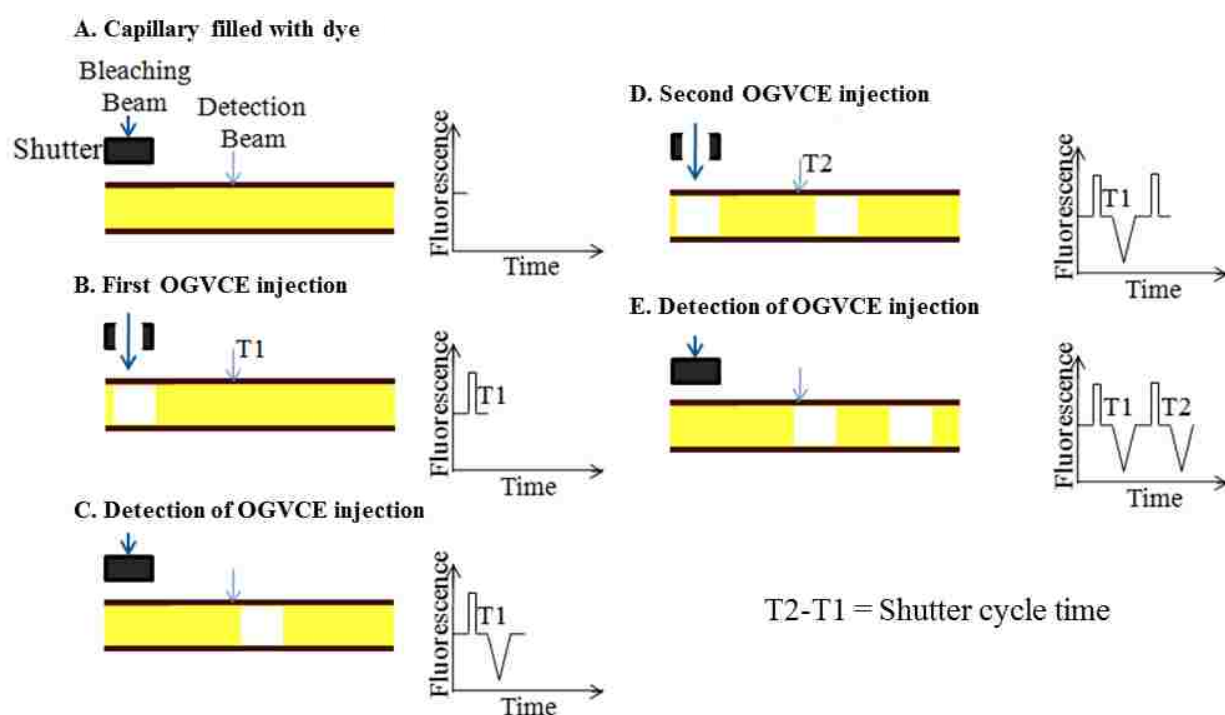
Figure 1.10. Schematic of the OGVCE method. A fluorescent dye is continuously electrophoresed through capillary, and the shutter is closed initially (A). When the shutter is opened, a photobleached zone is generated at F1, and the scattered light collected by an optical fiber is detected as a positive peak in the electropherogram (B). Then, the photobleached dye migrates to F2, where it is detected as a negative peak in the electropherogram (C). Steps B and C are repeated throughout the duration of the experiment (D and E).

In an off-column OGVCE enzyme assay, the enzyme is incubated with a fluorescent substrate in a reaction vial before electrophoresis is initiated. Then, the reaction mixture is

continuously sampled by electrophoresis as photobleaching occurs. As the enzyme catalyzes the reaction, two negative (vacancy) peaks, corresponding to the substrate and product, are observed in the resulting electropherogram (Figure 1.11). The fluorescent substrate and product peaks migrate at different rates due to their electrophoretic mobilities. As the reaction continues, the substrate peak decreases over time and the product peak increases. Figure 1.11 displays a schematic of an electropherogram for the progress of an OGVCE enzyme assay. Employing OGVCE injections offers advantages over traditional CE sample injections, because the reaction can be monitored every few seconds, depending on the difficulty of the separation [55, 56].
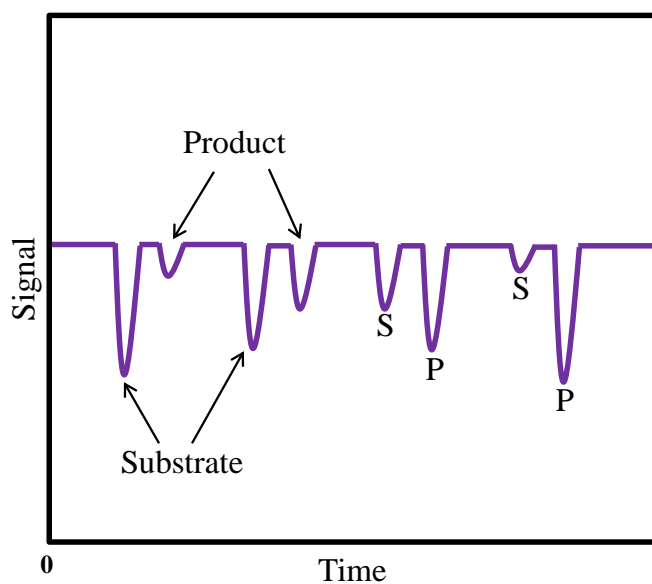
Figure 1.11. Sketch of an electropherogram for an OGVCE enzyme assay. After photobleaching of the reaction mixture occurs, the fluorescent substrate and product are detected as separate negative peaks in the electropherogram. The depletion of substrate and formation of product are observed as the reaction proceeds.

1.3.5. MEKC Modifications for Off-Column CE Assays

Micellar electrokinetic chromatography (MEKC), which was first reported by Terabe *et al.* in 1984 [57], has been widely used for the enhancement of CE separations [58, 59]. In MEKC, an ionic surfactant is added above its critical micelle concentration (CMC) to the

running buffer for a CE separation. The CMC is a concentration above which the surfactant molecules form micelles, which are aggregates of surfactants dispersed in a liquid colloid. Generally, micelles have a hydrophobic tail and hydrophilic head. Although the micelles are not stationary, they are similar to the stationary phase in chromatography and are referred to as a pseudostationary phase in MEKC. The surrounding solution is analogous to the mobile phase. Adding micelles to a CE running buffer is simple and can result in highly efficient separations and short analysis times [58, 59]. The most popular surfactant used for MEKC is sodium dodecyl sulfate (SDS). The CMC for SDS in pure water is approximately 8 mM [60].

Neutral molecules were not considered to be separable by CE until MEKC was developed [57]. In CE, neutral molecules travel with the electroosmotic flow (EOF). In MEKC, analytes partition between the pseudostationary phase and the separation buffer. Each analyte partitions between the micelles and separation buffer differently, which is why neutral analytes can be separated with MEKC [58, 59]. A schematic representation of MEKC is shown in Figure 1.12. Under electrophoresis conditions, anionic micelles are attracted to the anode; however, the EOF overcomes the electrophoretic migration of the micelles, resulting in migration of the micelles toward the cathode. Therefore, micelles migrate at a slower rate than the EOF [58, 59]. The use of MEKC for CE has been extensively reviewed by Terabe [58, 59].

Neutral analytes and analytes with similar charge-to-size ratios are often components of enzyme-catalyzed reactions. Therefore, MEKC has been used in the development of enzyme assays [61]. Most MEKC enzyme assays are off-column enzyme assays [61]. The enzyme is added into a reaction vial containing the reaction components in a buffer that does not contain the ionic surfactant. After incubation, the mixture is injected into the capillary, which is filled

with the buffer containing the surfactant. This off-column method is used because SDS and other common surfactants are known to denature proteins..
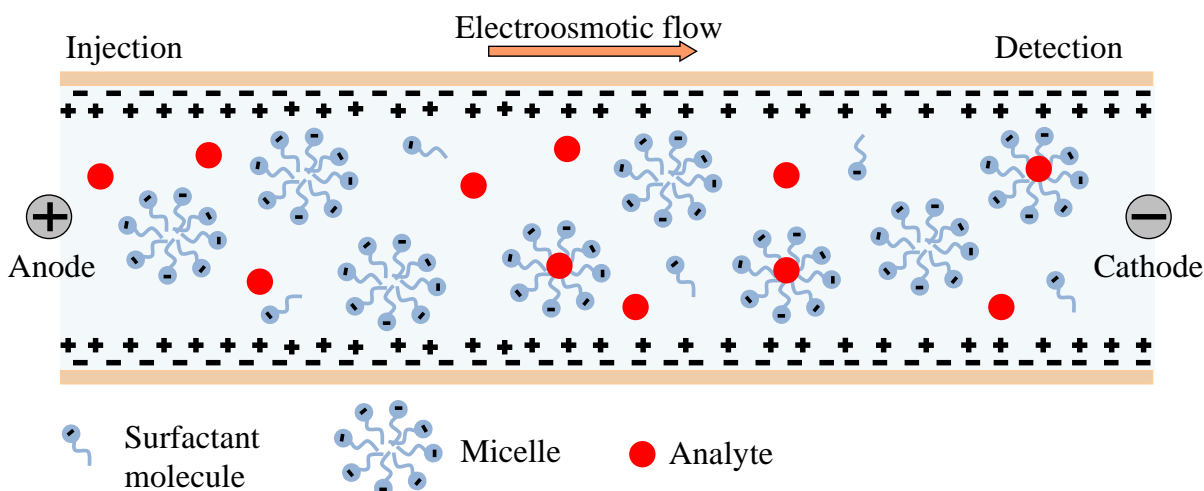
Figure 1.12. Schematic representation of the mechanism of MEKC separations. An ionic surfactant is added above its CMC to the running buffer for a CE separation, resulting in micelle formation. The analytes partition between the pseudostationary phase and the separation buffer. Although the micelles are attracted to the anode under electrophoresis conditions, the EOF overcomes that attraction and the micelles migrate toward the cathode at a slower rate than the EOF.

Many of the thousands of enzyme-catalyzed reactions occurring in a cell at any given time involve nucleotides. In fact, nucleotides are found as intermediates in nearly all aspects of metabolism [1]. For example, the nucleotide, adenosine 5′-triphosphate (ATP), serves as an energy carrier in numerous phosphate transfer enzyme-catalyzed reactions [1]. Because of the many advantages of MEKC for CE separations, MEKC is very attractive for the analysis of nucleotides and nucleosides, which can be difficult to separate using CE. Nucleosides are neutral, making them difficult to analyze using traditional CE. The separation of nucleotides by CE is difficult because some of them have poor peak shapes and similar charge-to-size ratios [62-66].

Many researchers have worked to improve the separation of nucleosides and nucleotides using MEKC. In 1989, Donlik *et al.* investigated several factors that affect the separation of oligonucleotides [62]. In this study, it was determined that using SDS as an additive in the background buffer enhanced the separation of polycytidines and eliminated the need for a coated capillary. In 1996, Uhrova *et al.* investigated separations of mono, di, and triphosphates of adenosine, guanosine, uridine and cytidine, and demonstrated enhancement of the separations using SDS [66]. Kawaruma *et al.* demonstrated enhancement of a CE separation of adenine, adenosine, and nucleotide isomers of adenosine using SDS in 1998 [64]. Also in 1998, Geldart reviewed the challenges faced when separating nucleotides using CE and methods that have been used to overcome those challenges, including MEKC [67].

Enzyme assays using MEKC with SDS have been developed for enzymes that catalyze reactions involving nucleosides and nucleotides, such as adenosine deaminase [68] and adenosine kinase [69]. In 2003, Carlucci *et al.* developed a CE methods for diagnosis and monitoring of adenosine deaminase (ADA) deficiency [68]. This enzyme, found in almost all human tissues, catalyzes the conversion of toxic adenosine (Ado) and 2'-deoxyadenosine (dAdo) to nontoxic inosine and 2'-deoxyinosine. Deficiency of ADA leads to severe combined immunodeficiency syndrome (SCID). As part of the method development, the authors successfully demonstrated the separation of 11 purine compounds, including Ado, dAdo, adenosine triphosphate (ATP), adenosine monophosphate (AMP), and dAMP, using SDS in the separation buffer. In 2006, Iqbal *et al.* published work on the development of off-column and on-column CE methods for screening and characterizing adenosine kinase inhibitors and substrates [69]. Adenosine kinase (AK) catalyzes the transfer of a phosphate group from ATP to adenosine, which results in the product, AMP. The authors successfully demonstrated an off-column assay

for AK using MEKC based on adding SDS into the separation buffer. In this assay, the AK-catalyzed phosphorylation of adenosine was successfully monitored, and adenosine derivatives were investigated as alternative substrates for AK.

1.4. Goals of this Research

The overall goal of the research presented in this dissertation was to develop new methods for studying enzymes and enzyme inhibition using CE. Traditional enzyme assays have significant limitations such as spectral interferences and indirect monitoring through the use of coupling enzymes, which limit the range of enzymes that can be studied. When using CE for enzyme assays, spectral interference and other limitations are minimized by separation of substrates, products, inhibitors and sample matrix components. An important objective of this research was to apply these newly developed CE assays to test botanical extracts and synthetic compounds for inhibition of specific enzymes that could not be studied using other methods.

Chapter 2. A comparison of the photostability of fluorophores commonly used for OGVCE was carried out as part of the overall goal of developing OGVCE-LIF enzyme assays. The OGVCE-LIF technique is based on photobleaching a fluorescent compound as it is continuously electrophoresed through a capillary. The initial goal of this project was to develop an OGVCE assay for adenosine deaminase (ADA); however, the fluorescent ADA substrate synthesized for the project (TNP-adenosine) was unusually photostable. As a result, the substrate could not be photobleached, and the OGVCE assay for ADA could not be developed. However, OGVCE-LIF was used to examine the photostability of fluorophores used for OGVCE, quantify the photostability of TNP-adenosine relative to those fluorophores, and gain a better understanding of the ideal properties of a dye for OGVCE assays.

Chapter 3. The main goal of this project was to develop an off-column CE assay for measuring holo-ACC activity and inhibition. Using CE to study ACC has advantages over previously developed ACC assays, which have limitations such as spectral interference, indirect monitoring through the use of coupling enzymes, and the use of radioactivity. Two important objectives for this project were to separate the two substrates and two products for the holo-ACC reaction and simultaneously monitor both reactions catalyzed by the holo-ACC components, BC and CT. Applying this CE assay to test known inhibitors of BC and CT for inhibition of holo-ACC inhibition was also an objective. Additional objectives for this project were to develop an off-column assay for the BC component of ACC and optimize a previously reported CE assay for the CT component.

Chapter 4. The goal of this project was to apply the CE-based enzyme assays developed in Chapter 3 to screen botanical extracts for inhibition of holo-ACC, BC and CT in order to identify natural products that inhibit ACC. A detailed literature search was used to identify specific compounds found in the botanical extracts that did inhibit holo-ACC. Compounds selected based on the literature search were also tested for inhibition of holo-ACC, BC and CT. A compound found in cranberry extracts that showed inhibition of holo-ACC, BC and CT was used as a model for ligand homology studies. Synthetic compounds identified from the ligand homology studies were also tested for holo-ACC inhibition. Furthermore, detailed steady-state kinetics studies were performed to determine patterns of inhibition for the compound that was used as a model for the ligand homology studies.

CHAPTER 2. COMPARISON OF FLUOROPHORES FOR OPTICALLY GATED VACANCY CAPILLARY ELECTROPHORESIS AND THE UNUSUAL PHOTOSTABILITY OF 2',3'-*O*-(2,4,6 TRINITROPHENYL) ADENOSINE

2.1. Introduction

Capillary electrophoresis (CE) can be used for performing on-column enzyme assays and for quantitative analysis of enzyme inhibition [39, 70]. Advantages provided by CE for enzyme assays include simplicity, rapid analysis times and consumption of small amounts of enzyme per assay [39]. Electrophoretically mediated microanalysis (EMMA) [71, 72] is a CE-based technique for carrying out on-column reactions and is often used to perform enzyme inhibition studies in capillaries and microchips [39, 70, 73]. Previously, Whisnant *et al.* developed a CE-based enzyme assay for alkaline phosphatase that combined continuous engagement EMMA and transient engagement EMMA and utilized laser-induced fluorescence (LIF) detection [43, 44]. These enzyme inhibition studies provided useful information about the enzyme of interest; however, the need for a fluorogenic substrate limits the range of enzymes that can be studied using this technique. A fluorogenic substrate is a nonfluorescent substrate that yields a fluorescent reaction product.

Capillary electrophoretic techniques using optically gated injections produce narrow sample plugs for high-speed separations in capillaries and microchips [74-78] and have been used for off-column enzyme assays in microchips [79, 80]. In these studies, the analytes of interest were fluorescently labeled and continuously introduced into the microcolumn by electrophoresis while being photobleached by a laser beam. The bleaching laser beam was blocked briefly (gated) to inject a short zone of fluorescent sample. The fluorescent zones were detected downstream by LIF, producing peaks in the resulting electropherograms. Optically gated vacancy capillary electrophoresis (OGVCE) uses a similar approach and instrumentation

27

[56, 81]. The fluorescent sample is continuously introduced into the microcolumn by electrophoresis, but the bleaching beam is blocked by a shutter. The shutter is opened briefly, which photobleaches the fluorescent species to produce a vacancy zone (negative peak). The resulting electropherogram contains vacancy peaks for each fluorescent analyte.

Optically gated vacancy capillary electrophoresis has been used for electroosmotic flow monitoring [55, 81, 82] and to perform separations in microchip devices [56]. Another potential application for OGVCE is to perform on-column enzyme assays using fluorescent rather than fluorogenic substrates. This would extend the range of enzymes that can be studied because effective fluorescent substrates are much easier to design and synthesize compared to fluorogenic substrates. For OGVCE-based enzyme assays, a fluorescent substrate requires several important characteristics. First, the fluorescent substrate requires a high reaction rate in the enzyme-catalyzed reaction of interest. Of course, the substrate should be highly fluorescent, and it should be possible to excite the fluorophore at wavelengths accessible with common and inexpensive laser sources. The fluorescent substrate and fluorescent reaction product also must be separable by CE, preferably using simple separation conditions. Finally, it must be possible to photobleach the fluorescent substrate and its reaction product at modest laser intensities. This last requirement is, in a sense, unorthodox. Photostability of a fluorophore is highly desirable for most applications.

In this chapter the photostability of several fluorophores used for OGVCE is examined. The photostability of a potential fluorescent substrate for the enzyme, adenosine deaminase (ADA), is studied also and compared to these fluorophores. The impacts of molar absorptivity and electrophoretic migration rates on photobleaching for OGVCE are considered. These studies

28

are important for determining which dyes perform best for OGVCE and for developing fluorescent substrates for OGVCE-based enzyme assays.

2.2. Materials and Methods

2.2.1. Chemicals

Adenosine, 2,4,6-trinitrobenzenesulfonic acid (TNBS) and fluorescein (sodium salt) were purchased from Sigma-Aldrich (St. Louis, MO). Sodium hydroxide and sodium phosphate and were purchased from Fisher Scientific (Fair Lawn, NJ). Calf intestinal adenosine deaminase was purchased from Roche Diagnostics (Indianapolis, IN). Coumarin 334 and rhodamine B were purchased from Acros Organics (Pittsburg, PA). Rhodamine 110 was purchased from Molecular Probes (Eugene, OR). All solutions were prepared using ultrapure water (> 18 MΩ-cm; ModuLab water system, United States Corp.; Palm Desert, CA).

2.2.2. Synthesis, storage and characterization of TNP-adenosine

Published procedures were used to synthesize TNP-adenosine [83, 84]. Briefly, adenosine was reacted with TNBS overnight at a 10:1 molar ratio of adenosine to TNBS in ultrapure water (adjusted to pH 10.5 with NaOH). After approximately 12 h, the reaction mixture was acidified to pH 4.0, and TNP-adenosine precipitated. The product was washed with an ice-cold acetone-benzene mixture and filtered. Then the product was dissolved in water, and NaOH was used to adjust the pH to neutral. The stock solution was stored at -20 ºC. An Econo-Pac 10 DG pre-packed polyacrylamide gel column from Bio-Rad Laboratories (Hercules, CA) was used to purify the TNP-adenosine. The column was equilibrated with 1.0 mM sodium phosphate buffer at pH 7.50, and a 3 mL sample in the same buffer was loaded onto the column. The same phosphate buffer was used to elute the components, and 0.5 mL fractions were collected. The TNP-adenosine was characterized using thin-layer chromatography, UV-VIS spectrophotometry

(Cary 50 Bio UV/Vis Spectrophotometer) and CE with UV-Vis absorbance detection at 210 nm as described in Section 2.3. Excitation-emission matrix spectra were collected for TNP-adenosine on a Horiba Yvon Fluorolog 3 spectrofluorometer (Edison, NJ).

2.2.3. Capillary Electrophoresis

For all CE experiments, fused-silica capillary (50 µm i.d./360 µm o.d.) purchased from Polymicro Technologies (Phoenix, AZ) was used. A MicroSolv window maker (Eatontown, NJ) was used to remove the polyimide coating to make a window for photobleaching and detection. Capillaries were rinsed with 1.0 M NaOH, ultrapure water and buffer for 10 min using a syringe pump at the beginning of each day. A power supply (Spellman CZE 1000R) was used to apply the potential for CE. Sodium phosphate buffer (20.0 mM, pH 7.55) was used for all experiments. For CE with UV absorbance detection (Acutect 500 detector) as described previously [85]. All buffers were filtered through a 0.2 µm nylon membrane (Whatman; Hillsboro, OR) prior to use for CE.

2.2.4. Optically Gated Vacancy Capillary Electrophoresis with LIF Detection

The capillary used for OGVCE studies was 76.1 cm (total length) and 43.3 cm to the window (effective length), and the applied potential was 369 V/cm (28.0 kV). The instrumentation for the OGVCE experiments was similar to that reported previously [55, 86]. A 457.9, 488.0, or 514.5 nm line from a Coherent (Santa Clara, CA) 90C Series argon ion laser passed through a cubic beamsplitter, and the beam was split for detection and photobleaching. The bleaching beam passed through a computer-controlled shutter and was focused on the capillary by a plano-convex lens. The power of the detection beam was reduced by a neutral density filter to 4.0 mW, and the light was directed to the capillary by a dichroic mirror. The light was focused onto the capillary by a 20× microscope objective, which also collected the

fluorescence emission. The distance between the detection beam and bleaching beam positions on the capillary was 470 μm, which was calculated as described previously [81]. The fluorescence passed through the dichroic mirror and was spectrally filtered by a band-pass filter before passing through an 800 μm pinhole for spatial filtering and being detected by a photomultiplier tube (PMT, HC120-01, Hamamatsu, Bridgewater, NJ) at 850 V. Light from the bleaching beam was collected by an optical fiber each time the shutter was opened and was also detected by the PMT. This light resulted in a positive peak in the electropherograms and marked the time at which the vacancy zones were created. A 250 Hz low-pass filter was used for filtering the PMT output, and a data acquisition board (BNC-2080, National Instruments, Austin, TX) was used for data collection at 200 Hz. Data collection and the shutter were controlled using a LabVIEW 5.0 program written in-house.

2.2.5.   OGVCE-LIF Flow Study

Three different flow rates, as well as several shutter opening times (25 ms to 2.5 s) were used for OGVCE experiments with rhodamine 110. The excitation wavelength was 488.0 nm, and the photobleaching beam and detection beam powers were 140.1 mW and 4.0 mW, respectively. The distance between the photobleaching beam and the detection beam at the capillary was increased to 1.0 cm from 470 μm for this study. The flow rate was changed by decreasing the applied potential in 10.0 kV increments (369 V/cm, 237 V/cm and 105 V/cm). Data were collected for 2 min for each combination of flow rate and shutter opening time.

2.2.6.   Enzyme Assay

This assay was performed using the OGVCE instrument described in Section 2.4; however, the photobleaching beam was blocked, and only LIF detection was performed using excitation at 488 nm. The detection beam power was 4.0 mW, and emission was collected using

a long-pass filter with a 550 nm cut-off. Adenosine deaminase (1 unit) was added to 150 μM TNP-adenosine in 20.0 mM sodium phosphate, pH 7.55 (200 μL total reaction volume) to initiate the enzyme-catalyzed reaction, and the mixture was immediately injected into the capillary for 0.5 s. Injections and separations were performed electrokinetically at 439 V/cm (25.0 kV). The injections were repeated every 3.0 min over a total of 40 min. For this study, the capillary used was 57.0 cm (total length) and 36.0 cm to the detection window (effective length).

2.3.   Results and Discussion

2.3.1. TNP-Adenosine

Figure 2.1 shows the structure of TNP-adenosine, which was synthesized with the goal of developing an enzyme assay for adenosine deaminase based on OGVCE. Fluorogenic substrates are not available for adenosine deaminase, but TNP-adenosine, which is highly fluorescent, has been reported to be a substrate for adenosine deaminase, forming the fluorescent product TNP-
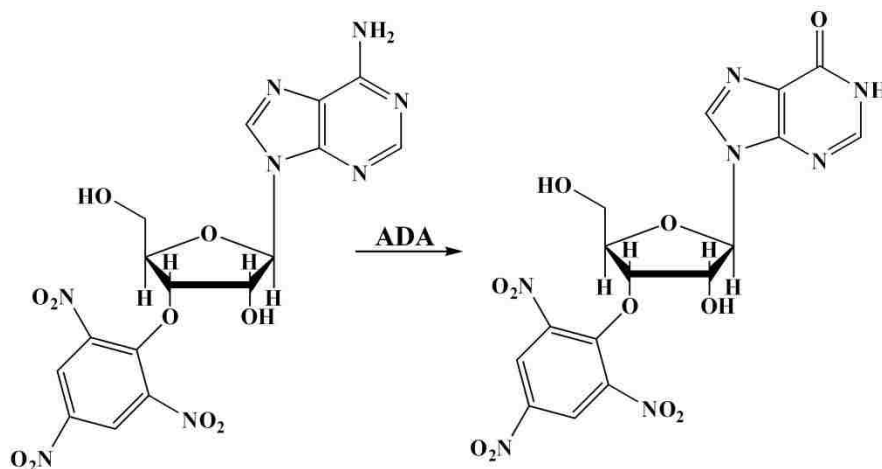
Figure 2.1. Adenosine deaminase catalyzes the reaction of TNP-adenosine to form TNP-inosine.

inosine (Figure 2.1) [87]. Absorbance spectra and excitation-emission matrix spectra were obtained for the synthesized TNP-adenosine. The visible absorbance maxima at 408 nm and 465 nm, were in accordance with literature reports [84, 87, 88]. The two excitation maxima at 408

nm and 466 nm and the emission maximum at 550 nm were also in consistent with reported values [87]. Finally, CE-LIF was used to confirm that ADA catalyzed the deamination of TNP-adenosine to form TNP-inosine (Figure 2.2). Adenosine deaminase was added to the reaction mixture, and injections were made from the reaction mixture at 3 min intervals. Immediately after the addition of ADA, a large TNP adenosine peak was detected at 2.65 min, and a small TNP-inosine peak was observed at 2.72 min. By 30 min nearly all of the TNP-adenosine had reacted to form TNP-inosine.
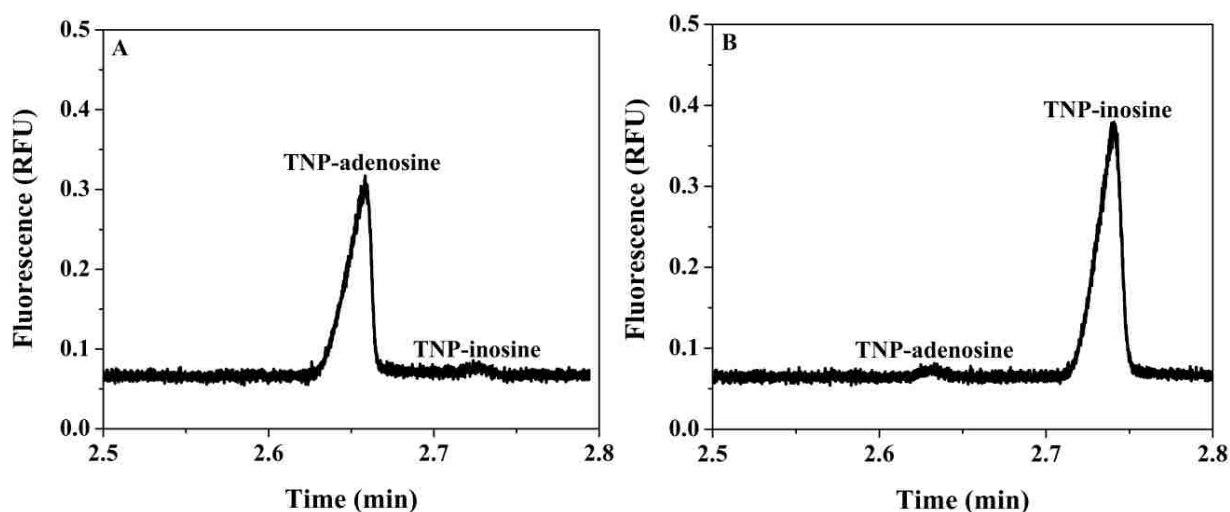
Figure 2.2. Electropherograms for the adenosine deaminase assay. (A) Immediately after the addition of adenosine deaminase (1 unit) to 150 μM TNP-adenosine, a large TNP adenosine peak and a small TNP-inosine peak were observed. (B) At 30 min after addition of adenosine deaminase, a large TNP-inosine peak was observed (product formation), and the TNP-adenosine peak has decreased. Electrokinetic injections (0.5 s) and separations were performed at 25.0 kV(439 V/cm). The sample buffer and separation buffer were both 20.0 mM sodium phosphate, pH 7.55. The electrophoretic current was 21.8 μA.

These experiments were repeated next with OGVCE instead of CE-LIF with an aim of using the fluorescent substrate for development of an on-column ADA assay. Surprisingly, no photobleaching was observed as shown in Figure 2.3. The power of the photobleaching beam (138.0 mW) at 457.9 nm was substantially higher than that used other published OGVCE studies at or near this wavelength (34.8-56.0 mW) [81, 82, 86, 89, 90] and is about 50% lower than the

maximum power used for bleaching the laser dye, rhodamine B, at 514.5 nm in a previous study (245 mW) [55]. This result suggests that TNP-adenosine is unusually resistant to photobleaching. Varying the concentration of the TNP-adenosine from 15 to 300 μM did not improve the ability to photobleach it. Changing the pH of the phosphate buffer to 6.5 and 6.0 as well as attempts to photobleach TNP-adenosine in a 50:50 mixture of ethanol and 20.0 mM sodium phosphate at pH 7.50 had no effect. This unexpected result for TNP-adenosine inspired a study to directly compare the photostability of several fluorophores commonly used for OGVCE and to examine related experimental issues that impact OGVCE and the extent of photobleaching.
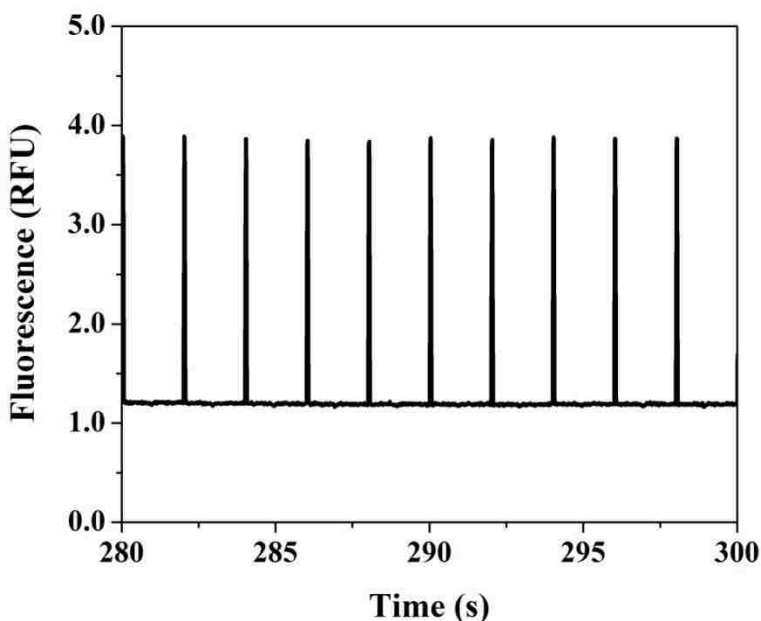
Figure 2.3. Attempted photobleaching of 150.0 μM TNP-adenosine. The shutter was opened for 50 ms every 2.00 s as TNP-adenosine was continuously introduced into the capillary by electrophoresis (369 V/cm). The power of the photobleaching was 138.0 mW, and the detection beam was 4.0 mW (λ = 457.9 nm). The sample and separation buffer were 20.0 mM sodium phosphate at pH 7.55.

2.3.2. Photostability of OGVCE dyes and TNP adenosine

A study was carried out to quantitatively compare the photobleaching of several dyes commonly used for OGVCE: coumarin 334, fluorescein, rhodamine 110, and rhodamine B.

Structures for these dyes are shown in Figure 2.4. The photobleaching of TNP-adenosine also was compared to that for these four dyes. The neutral dyes, coumarin 334, rhodamine B and rhodamine 110 have been used for continuous monitoring of electroosmotic flow dynamics in capillaries [55, 81, 86, 89, 90] and in microfabricated devices [82]. Fluorescein has been used for OGVCE separations in microfabricated devices [56].

Coumarin 334   **Fluorescein**

Rhodamine 110   **Rhodamine B**
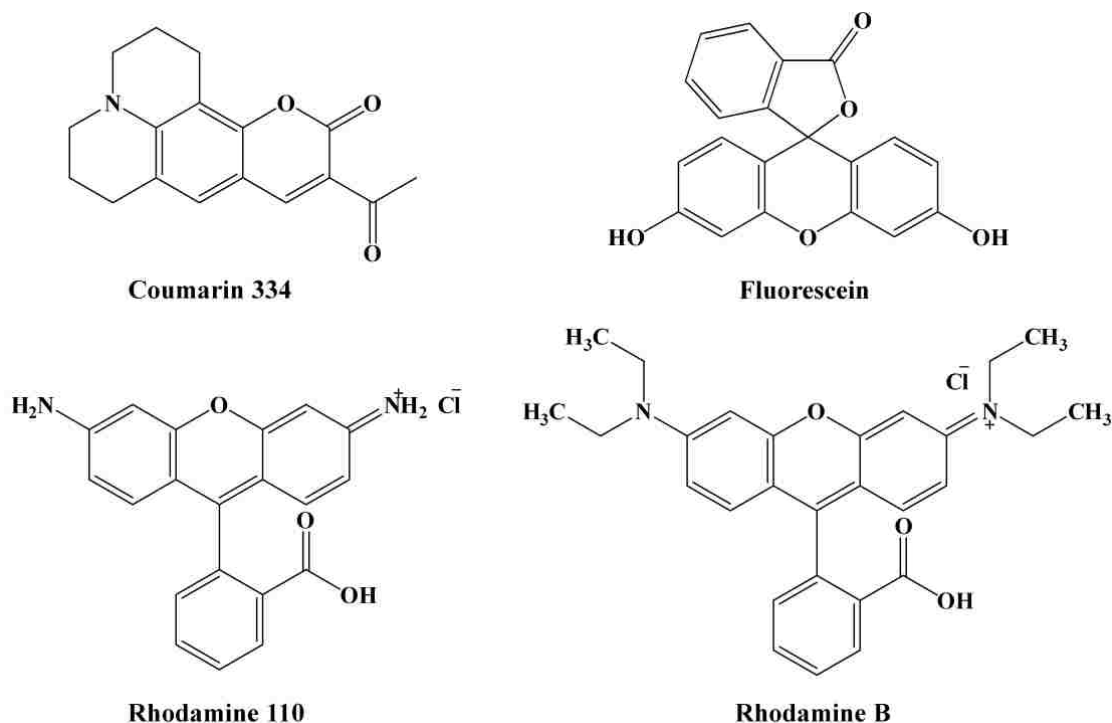
Figure 2.4. Structures of the dyes that were used for the comparative photobleaching study.

Absorbance spectra were measured in order to account for differences in molar absorptivity at the wavelength used for photobleaching of each dye. The concentrations of the dyes were adjusted so that the absorbance of the solution containing each dye was the same at their respective photobleaching/excitation wavelengths. The wavelengths, molar absorptivities and concentrations are listed in Table 1. Each dye was continuously introduced into the capillary by electrophoresis, and the dyes were photobleached every 1.00 s by opening the shutter blocking the bleaching beam for 50 ms. The results of this study are summarized in Table 2.1.

35

Table 2.1. Photobleaching percentages of dyes.

Dye	λ	ε	[C] (μM)	Bleaching Power (mW)	Bleaching (%)
TNP-adenosine	457.9	12,700	6.15	138.0	–
				–	–
Coumarin 334	457.9	49,500	1.58	140.2	83
				35.8	44
Fluorescein	488.0	52,100	1.55	140.2	96
				34.0	83
Rhodamine 110	488.0	14,600	5.40	140.2	37
				121.6	33
Rhodamine B	514.5	19,300	4.00	140.5	6
				91.5	4

The extent of photobleaching is reported as the photobleaching percentage, which is calculated according to Equation 2.1, where S_V, is the vacancy signal, which is the minimum

$$\left[\frac{S_B - S_V}{S_F - S_B}\right] \times 100\% \tag{2.1}$$

fluorescence of the negative peak resulting from photobleaching, S_F is the fluorescence signal when the dye is not photobleached (shutter closed), and S_B is the baseline signal in the absence of the fluorophore. These terms are shown graphically in Figure 2.5.

Photobleaching of each dye was determined at a bleaching beam power near 140 mW, which was the maximum that could be used with this system at all of the wavelengths of interest. Representative electropherograms (coumarin 334 and rhodamine B) are shown in Figure 2.6. Fluorescein was the most susceptible to photobleaching (96%), followed by coumarin 334 (83%), rhodamine 110 (37%) and rhodamine B (6%). As discussed in Section 3.1 and shown in Figure 2.3, TNP-adenosine did not photobleach significantly at any bleaching power tested.
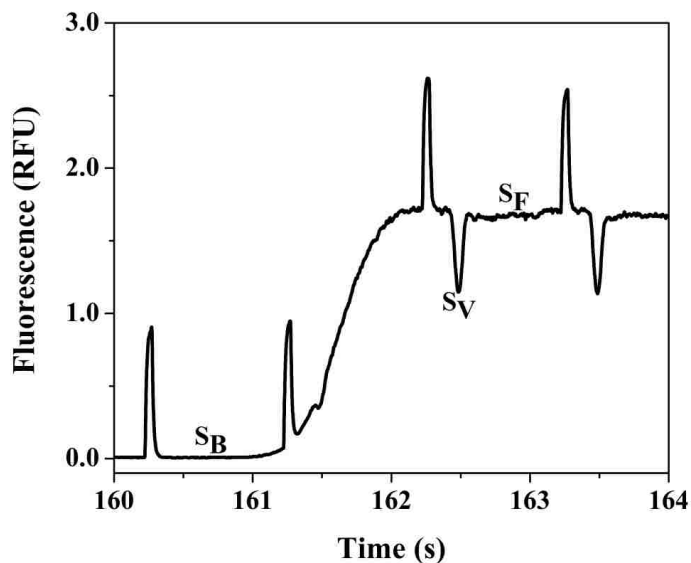
Figure 2.5. Electropherogram with photobleaching percentage variables labeled. The equation $[(S_F - S_V)/(S_F - S_B)] \times 100\%$, is used to determine the photobleaching percentage. The average fluorescence signal in the presence of the fluorophore is S_F, and the vacancy signal, S_V, is the minimum fluorescence of the negative peak resulting from photobleaching. The average baseline signal in the absence of fluorophore is S_B. This electropherogram is from rhodamine 110 (5.40 µM) photobleached with a 121.6 mW photobleaching beam power where the photobleaching percentage was 33%. The shutter was opened for 50 ms every 1.00 s. The excitation wavelength was 488.0 nm. The detection beam was 4.0 mW. Electrophoresis was performed at 28.0 kV (369 V/cm). The separation buffer was 20.0 mM sodium phosphate at pH 7.55.
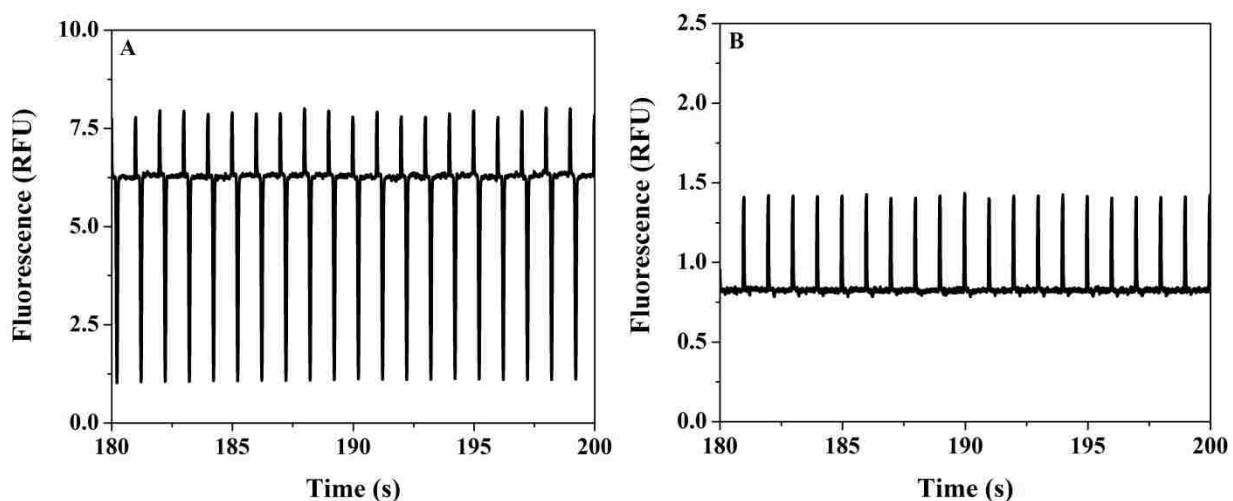
Figure 2.6. Photobleaching of (A) 1.58 µM coumarin 334 and (B) 4.00 µM rhodamine B with a 140 mW photobleaching beam power. The shutter was opened for 50 ms every 1.00 s. The excitation wavelengths were (A) 457.9 nm and (B) 514.5 nm. All other conditions are the same as in Figure 2.3. The distance between the detection beam and bleaching beam positions on the capillary was 470 µm.

37

As indicated in Table 1, the photobleaching power also was attenuated from 140 mW according to the molar absorptivity for each dye relative to that for TNP-adenosine. Under these conditions, the total absorbances of the solutions were different, but each dye molecule absorbed the same number of photons as TNP-adenosine at 138.0 mW. Figure 2.7 shows representative electropherograms for rhodamine 110 and fluorescein. The order of relative photobleaching did not change with TNP-adenosine (no photobleaching) and rhodamine B (4%) being the most resistant to photobleaching. Fluorescein was still 83% photobleached at only 34.0 mW, while coumarin 334 photobleaching dropped by almost a factor of two (83% to 44%) when the bleaching beam power was decreased to 35.8 mW. For rhodamine 110, the decrease in photobleaching (37% to 33%) was approximately proportional to the decrease in bleaching beam power (140.2 to 121.6 mW).
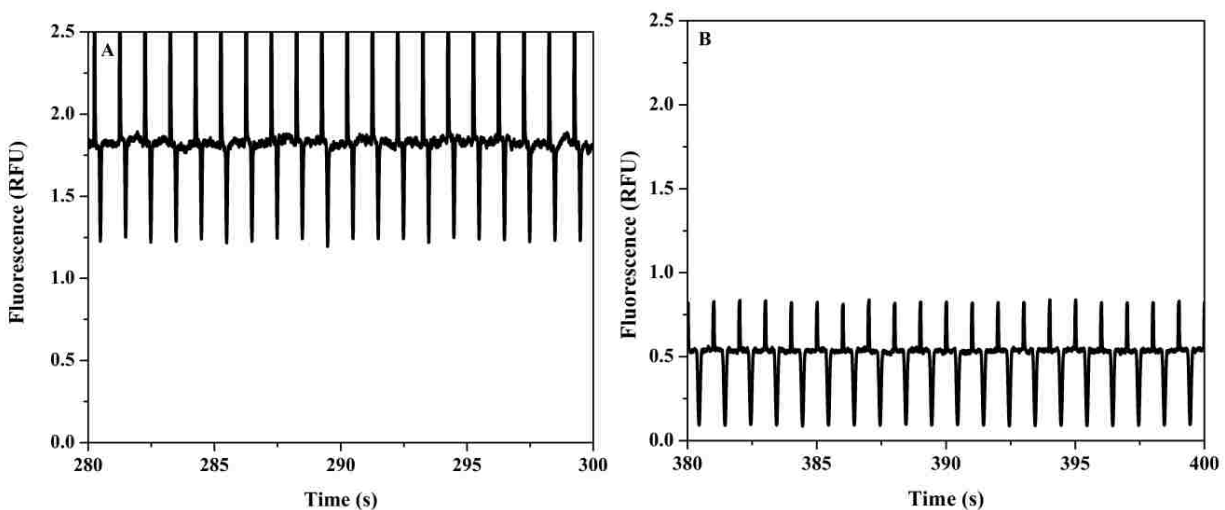
Figure 2.7. Electropherograms for photobleaching at reduced photobleaching power. (A) Rhodamine 110 (5.40 μM) was photobleached at 121.6 mW. (B) Fluorescein (1.55 μM) was photobleached at 34.0 mW. The shutter was opened for 50 ms every 1.00 s. The excitation wavelength was 488.0 nm. All other conditions were the same as in Figure 2.3.

Previously, the photobleaching properties of rhodamine B and fluorescein were investigated as part of studies of the photobleaching of organic laser dyes at micromolar

concentrations in methanol and in static solutions [91, 92]. In both studies, the photobleaching properties of the dyes were compared and contrasted to provide information about their use as laser dyes. For that application high photostability is beneficial. In one study, it was determined that the quantum efficiency of rhodamine B was 15 times smaller than that for fluorescein under pulsed photobleaching conditions [91]. In the other study, fluorescein was found to photobleach more readily than rhodamine B under continuous illumination at 514.5 nm, while fluorescein and rhodamine B had the same photobleaching properties under continuous illumination at 359.0 nm [92]. In studies conducted by Saylor, the photostability of fluorescein was investigated for fluid mechanics applications [93]. It was found that fluorescein was photobleached after only 1 ms of laser irradiation, which was not desirable for fluid mechanics experiments [93]. Hinkeldey *et al.* investigated the photostability of fluorescein for use in single-molecule applications requiring high photostability and concluded that fluorescein dyes were less photostable than borondipyrromethene (BODIPY) dyes [94]. The photobleaching properties of rhodamine B and fluorescein have also been investigated using independently using conventional optical gating [75] and OGVCE [55]. Tao *et al.* compared the photostability of fluorescein and orthophthalaldehyde/β-mercaptoethanol (OPA-βME) using conventional optical gating, and they found that fluorescein is substantially more stable than OPA-βME [75]. In a study conducted by Pittman *et al.*, it was found that rhodamine B only photobleached 30% when using a 230 mW photobleaching beam power (λ = 514.5 nm) and a shutter opening time of 75 ms while rhodamine B was electrophoresed at a field strength of 138 V/cm [55]. A detailed discussion directly comparing the photobleaching properties of common OGVCE dyes at typical conditions for this method has not been reported.

2.3.3. Migration Rate Study

The migration rate of a fluorophore should affect the photobleaching of a dye by OGVCE. Consider a dye molecule passing through the bleaching beam in a capillary. The migration rate of the molecule will affect the total number of photons the molecule is exposed to as it passes through the bleaching beam. Unless the molecules are all photobleached rapidly before they have passed through the bleaching beam, their migration rate will impact the total number of photons they are exposed to and, thus, the extent of photobleaching. Sugarman and Prud'homme examined the impact of photobleaching of fluorescein on the response of a laser-induced fluorescence detector for pressure-driven flow in capillaries [95]. In the study presented here, negatively charged fluorescein migrates more slowly through the bleaching beam compared to the neutral dyes (rhodamine B, rhodamine 110, and coumarin 334. The photobleaching of fluorescein and rhodamine 110 at different migration rates was investigated here in order to determine the extent to which migration speed impacted the photobleaching results for these dyes.

Panel A of Figure 2.8 shows the photobleaching of 5.40 µM rhodamine 110 at decreasing flow rates (EOF) when the shutter was opened every 15.00 s for 50 ms. The flow rate was changed by decreasing the applied voltage by 10.0 kV increments (369 V/cm, 237 V/cm, and 105 V/cm) every 2 min over a 6 min time frame. As seen in panel A of Figure 2.8, the photobleaching percentage actually decreased as the flow rate decreased. This unanticipated result occurred due to band broadening caused by molecular diffusion as the narrow vacancy zones travelled 1.0 cm to the detection beam spot [55, 82]. The experiment was repeated (Figure 2.8, panel B), but the shutter opening time was increased 20 fold (1.00 s instead of 50 ms), producing broader vacancy zones. The depth of these broader zones was not reduced

significantly by zone broadening, and the bleaching percentage increased with decreasing flow rate as expected. Similar experiments were performed with fluorescein (data not shown). Because fluorescein bleaches much more readily than the other dyes studied (Table 2.1), the changes in photobleaching percentage at different flow rates were minimal for these experimental conditions. Tao *et al.* studied the effect of migration rate for optically gated injections of amino acids derivatized by OPA-βME [75]. In those studies, the photobleaching beam was gated in order to form a zone of unbleached analytes to be separated and detected as peaks in the resulting electropherogram. They also concluded that longitudinal diffusion led to increased band broadening for slower migrating analytes as they traveled from the injection spot to the detection spot inside the capillary. Similar observations were made by Moore and Jorgenson for optically gated injections of compounds labeled with fluorescein isothiocyanate (FITC) [96].
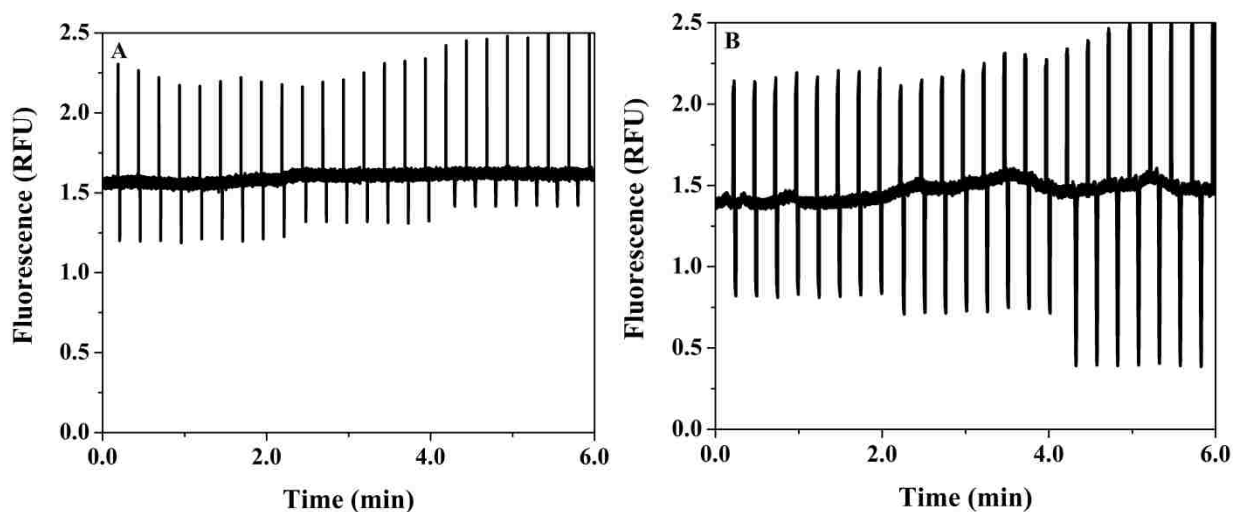
Figure 2.8. Photobleaching of 5.40 μM rhodamine 110 at decreasing flow rates when the shutter was opened every 15 s for (A) 50 ms and (B) 1.00 s. The flow was changed by decreasing the applied voltage to the capillary by 10.0 kV (369 V/cm, 237 V/cm, and 105 V/cm) every 2 min over a 6 min time period. The excitation wavelength was 488.0 nm. All other conditions are the same as in Figure 2.3.

2.4. Conclusions

The relative photostability of four fluorophores commonly used for OGVCE was studied quantitatively and compared to the photostability of TNP-adenosine. These studies will be beneficial for determining which dyes will perform best OGVCE studies and for developing fluorescent substrates for OGVCE-based enzyme assays. Fluorescein was found to be most susceptible to photobleaching, followed by coumarin 334 and rhodamine 110. Rhodamine B was the most photostable common OGVCE dye tested. The fluorescent substrate for adenosine deaminase, TNP-adenosine, didn't photobleach significantly under any conditions tested, making it unsuitable for development of an OGVCE enzyme assay. It was shown that rhodamine 110 photobleaching increased when the flow rate decreased in the absence of significant band broadening. High fluorescence for LIF detection and ease of photobleaching are the two most important properties of a dye for OGVCE, but other characteristics are also important. For example, a net neutral charge is essential for use of a dye for EOF measurements, and minimal adsorption to the capillary or microchip wall is important. For an OGVCE enzyme assay, the fluorescent substrate and product should be easily separable. Finally the wavelength needed for photobleaching and excitation ideally will match an inexpensive laser source.

CHAPTER 3. A CAPILLARY ELECTROPHORETIC ASSAY FOR ACETYL COA CARBOXYLASE[1]

The research presented in this chapter is based on a recent publication and was reproduced with permission from: Bryant, S. K., Waldrop, G. L., Gilman, S. D. A Capillary Electrophoretic Assay for Acetyl CoA Carboxylase, *Analytical Biochemistry*, 2013, 437 (1), 32-38.

3.1.   Introduction

Acetyl coenzyme A carboxylase (ACC) catalyzes the first committed and rate-limiting step in fatty acid biosynthesis in all bacteria, plants, and animals. The biotin-dependent carboxylation of acetyl coenzyme A (CoA) to form malonyl-CoA is carried out in two half-reactions (Figure 3.1) [97]. In the first half-reaction, biotin carboxylase (BC) catalyzes the conversion of adenosine triphosphate (ATP) to adenosine diphosphate (ADP), and the carboxylation of biotin, which *in vivo* is covalently attached to biotin carboxyl carrier protein (BCCP). In the second half-reaction, carboxyltransferase (CT) catalyzes the transfer of the carboxyl group on biotin to acetyl-CoA to form malonyl-CoA. In bacteria, BC, CT, and BCCP are separate proteins, and BC and CT retain their activity using free biotin in place of BCCP [97]. In eukaryotes, these three components of ACC are combined in one polypeptide [97]. Acetyl coenzyme A carboxylase is a target for the development of antibiotics [98, 99], herbicides [100], and therapeutic agents for metabolic syndrome (including obesity and type 2 diabetes) [101-105] and cancer [106, 107]. Thus, effective assays to measure the inhibition of ACC are desirable.

---

[1] *This chapter previously appeared as Bryant, S. K., Waldrop, G. L., Gilman, S. D. A Capillary Electrophoretic Assay for Acetyl CoA Carboxylase, Analytical Biochemistry, 2013, 437 (1), 32-38. It is reprinted with permission from Elsevier.*

Several assays have been developed to monitor the activity of isolated bacterial BC and CT, as well as holo-ACC from either bacterial or eukaryotic sources. Hereafter, holo-ACC will refer to the case when all three bacterial proteins, BC, CT, and BCCP are present in solution. Early studies of *E. coli* ACC utilized a radiolabeled bicarbonate fixation assay for determining the activity of holo-ACC and isolated BC [108]. Moreover, BC was also assayed with an enzyme-coupled assay, where ADP formation was monitored spectrophotometrically at 340 nm via NADH oxidation [108]. The enzymatic activity of isolated bacterial CT was commonly assayed in the reverse (nonphysiological) direction using either a radioactivity assay that measured the biotin-dependent decarboxylation of radiolabeled malonyl-CoA, or where acetyl-CoA production was coupled to the citrate synthase-malate dehydrogenase reaction and NAD^+ reduction was monitored spectrophotometrically at 340 nm [108]. More recently, Kroeger *et al.* developed an NADPH based spectrophotometric assay for holo-ACC, where malonyl-CoA reductase was used to catalyze the NADPH-dependent reduction of the product, malonyl-CoA [109]. In addition, Alves *et al.* reported an assay for holo-ACC based on HPLC with tandem mass spectrometry (LC-MS/MS), where the enzyme and substrates were incubated for 3 hr at room temperature and malonyl-CoA formation was monitored [110].
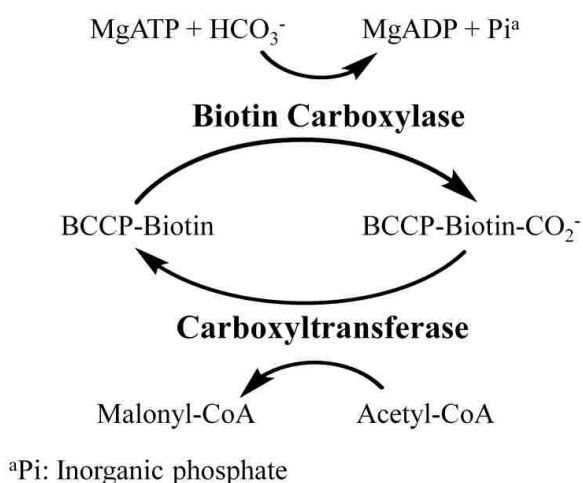
Figure 3.1. Acetyl-CoA carboxylase reaction scheme

Several of these assays for ACC have been adapted and optimized for high-throughput screening. Harwood *et al.* [103] developed a plate reader-based high-throughput screening assay for mammalian ACC based on the radiolabeled bicarbonate fixation assay of Guchhait *et al.* [108]. Subsequently, Santoro *et al.* developed a plate reader-based high-throughput screening assay for bacterial CT in the nonphysiological direction where citrate synthase was coupled to the production of acetyl-CoA and the product CoA was detected with DTNB (Ellman's Reagent) [111]. Soriano *et al.* developed a plate reader-based high-throughput assay for ACC that involved the use of ^{32}P-labeled ATP [112]. Seethala *et al.* developed a high-throughput assay for mammalian ACC where radiolabeled acetyl-CoA was used in an ACC/fatty acid synthase coupled assay and radiolabeled palmitic acid was detected [113]. Lui *et al.* reported two high-throughput assays for mammalian ACC where amplex red was used with two coupled enzyme-catalyzed reactions to detect phosphate by fluorescence or fluorescence polarization was used to monitor fluorescently labeled ADP binding to an anti-ADP antibody [114]. Chung *et al.* reported a high-throughput fluorescence assay where mammalian ACC activity was coupled to fatty acid synthase activity [115]. Recently Alves *et al.* developed a plate reader luminescence-based assay for assaying holo-ACC that monitored the depletion of ATP [110].

The previously developed assays each have significant limitations for screening of ACC inhibitors. The assays based on radiolabelling can be expensive and complex in practice due to health, waste and regulatory issues. The method based on LC-MS/MS provides comparable selectivity without the health and regulatory issues associated with radiolabelling, but it relies on complex methodology and expensive instrumentation. Assays based on enzyme-coupled reactions are inherently indirect and more susceptible to false positives for inhibition studies.

Additionally, spectrophotometric assays based on UV absorbance or fluorescence with UV excitation are prone to spectral interference by inhibitors and biological sample matrices.

Recently, we developed a simple capillary electrophoresis-based assay for the CT component of ACC using UV absorbance detection [116]. This method was developed to overcome spectral interference for particular inhibitors and botanical extracts that could not be assayed using the enzyme-coupled spectrophotometric method employed for the rest of the study [117]. Capillary electrophoresis (CE) has been used for a wide array of applications, and CE has several advantages including high separation efficiency, simplicity, small sample volume (nL) and rapid analysis times [33]. It has been demonstrated that CE can be used effectively for performing quantitative enzyme assays and studying enzyme inhibition [38, 39]. Because CE is an electrophoretic separation technique, spectral interference is reduced by separation of substrates, products, inhibitors and sample matrix components.

Herein, we report an off-column capillary electrophoretic assay to measure holo-ACC activity and inhibition that allows for simultaneous monitoring of the BC and CT catalyzed reactions. To our knowledge, this is the first report of simultaneous, direct monitoring of ATP and acetyl-CoA depletion, and ADP and malonyl-CoA production for determination of holo-ACC activity. Also, the CE assay for CT [116] has been optimized, and a CE assay for the BC component of ACC has been developed.

3.2.   Materials and Methods

3.2.1.   Reagents and assay solutions

Acetyl coenzyme A, malonyl-CoA, ATP, ADP, biocytin, dimethyl sulfoxide, potassium phosphate monobasic, potassium bicarbonate, benzoic acid, magnesium chloride and sodium dodecyl sulfate were purchased from Sigma-Aldrich (St. Louis, MO). (2E,4E,6E)-N-((S)-3-(((S)-

3-methyl-1-((3R,4S)-4-methyl-2,5-dioxopyrrolidin-3-yl)-1-oxobutan-2-yl)amino)-3-oxo-1-

phenylpropyl)octa-2,4,6-trienamide (andrimid) was a gift from Pfizer. 2-amino-N,N-

dibenzyloxazole-5-carboxamide was synthesized according to the protocol published by

Mochalkin *et al.* [99]. Tris(hydroxymethyl)aminomethane (tris) was purchased from Acros

Organics (Morris Plains, NJ). N-2-hydroxyethylpiperazine-N′-2-ethanesulfonic acid (HEPES)

was purchased from EMD Millipore (Billerica, MA), and sodium phosphate and sodium

hydroxide were purchased from Fisher Scientific (Fair Lawn, NJ). Biotin carboxylase and

carboxyltransferase from *Escherichia coli* were purified as described previously [117]. Biotin

carboxyl carrier protein was a gift from Pfizer. All solutions were prepared using ultrapure water

(> 18 MΩcm, ModuLab water system, United States Filter Corp., Palm Desert, CA). All buffers

were filtered through a 0.2 μm nylon membrane (Whatman; Hillsboro, OR) prior to use for CE.

3.2.2. Capillary electrophoretic enzyme assays

All assays were performed using a P/ACE MDQ system with UV absorbance detection

(photodiode array detector) from Beckman Coulter, Inc. (Brea, CA). The data were collected and

analyzed using 32 Karat 5.0 software from Beckman Coulter, Inc. Fused-silica capillary (50-μm

i.d./360-μm o.d.) was purchased from Polymicro Technologies (Phoenix, AZ) and cut to a total

length of 59.8 cm. The polyimide coating was removed using a MicroSolv CE window maker

(Eatontown, NJ) to make a 3-mm detection window at 49.8 cm (effective length). The capillary

was rinsed with 1.0 M NaOH, ultrapure water and 20.0 mM sodium phosphate buffer at pH 7.55

for 10.0 min at 20 psi for conditioning at the beginning of each day. All reaction vials were held

at 25 ºC and the capillary was held at 25 ºC. All injections were performed hydrodynamically at

0.5 psi for 10.0 s. All separations were performed using 30.0 kV (508 V/cm). All

electropherograms were plotted with absorbance at 256 nm.

All enzyme assay reaction samples were prepared in 5.00 mM potassium phosphate buffer at pH 7.55 (reaction buffer). The capillary was rinsed with the separation buffer for 30.0 s at 20 psi prior to each injection. All enzyme reactions were performed off-column in a 1.5 mL glass Beckman CE vial in a 1.0 mL total volume.

3.2.3. Carboxyltransferase CE assay

The assay mixture contained 250.0 μM malonyl-CoA and 4.00 mM biocytin in the reaction buffer. To initiate the reaction, CT was added to the reaction mixture to a final concentration of 10.0 μg/mL. The assay mixture was injected for CE analysis after 1.0 min and again after 9.5 min. The CT assay was carried out using 5.0 mM potassium phosphate buffer at pH 7.55, which was also used for the separation buffer.

3.2.4. Biotin carboxylase CE assay

The BC assay mixture contained 50.0 μM ATP, 2.5 mM $MgCl_2$, 50.0 mM biotin, 5.0 mM potassium bicarbonate and 200 μM benzoic acid (used as an internal standard) in the reaction buffer. To initiate the reaction, BC was added to the reaction mixture to a final concentration of 20.0 μg/mL, and the assay mixture was injected for CE analysis after 1.0 min and again after 12.0 min. The separation buffer contained 10.0 mM sodium phosphate and 20.0 mM sodium dodecyl sulfate at pH 7.55.

3.2.5. Holo-ACC CE assay

The holo-ACC assay mixture contained 25.0 μM ATP, 50.0 μM acetyl-CoA, 2.50 mM $MgCl_2$, 2.0 μM BCCP and 5.0 mM potassium bicarbonate in the reaction buffer. The reaction was initiated by adding BC and CT to a final concentration of 10.0 μg/mL in the assay mixture. The assay mixture was injected for CE analysis after 1.0 min and again after 9.5 min. 2-amino-N,N-dibenzyloxazole-5-carboxamide (212 μM) or andrimid (30.0 μM) was used for studying

inhibition of holo-ACC. Both inhibitors were dissolved in DMSO, and the assay mixtures contained 0.3% DMSO for those experiments. During preliminary studies, it was concluded that DMSO did not interfere with the enzymatic reaction or the separation of the substrates, products, and inhibitors. After adding BC (10.0 μg/mL) and CT (10.0 μg/mL) to the assay mixture containing inhibitor, the mixture was injected for CE analysis at 1.0 min and at 11.5 min. The separation buffer for all assays contained 10.0 mM sodium phosphate and 20.0 mM sodium dodecyl sulfate at pH 7.55.

3.3. Results and Discussion

3.3.1. Optimized CE assay for carboxyltransferase

We previously developed an off-column capillary electrophoretic assay for the CT component of ACC using UV absorbance detection [116]. The assay used in that study was functional but had not been optimized. The buffers for the sample (enzyme reaction mixture) and CE separation were substantially different in terms of composition and conductivity, which can lead to relatively poor CE peak shapes and separations [86, 118, 119]. The assay for CT was optimized primarily by matching the separation and enzyme reaction buffers. Both the enzyme reaction and separation buffers contained 5.0 mM potassium phosphate at pH 7.55. The reaction was monitored in the nonphysiological direction (malonyl-CoA reacts to form acetyl-CoA), and the reaction mixture contained the substrates, malonyl-CoA (250 μM) and biocytin (4.00 mM). Because the K_m of malonyl-CoA for CT is 100 μM [117], 250 μM malonyl-CoA was used. In bacteria, CT retains its activity using free biotin in place of the BCCP [97]. Biocytin, a more reactive analog of biotin where lysine is attached to the valeric acid carboxyl group (Figure 3.2), is commonly used when running the CT assay in the nonphysiological direction [117].
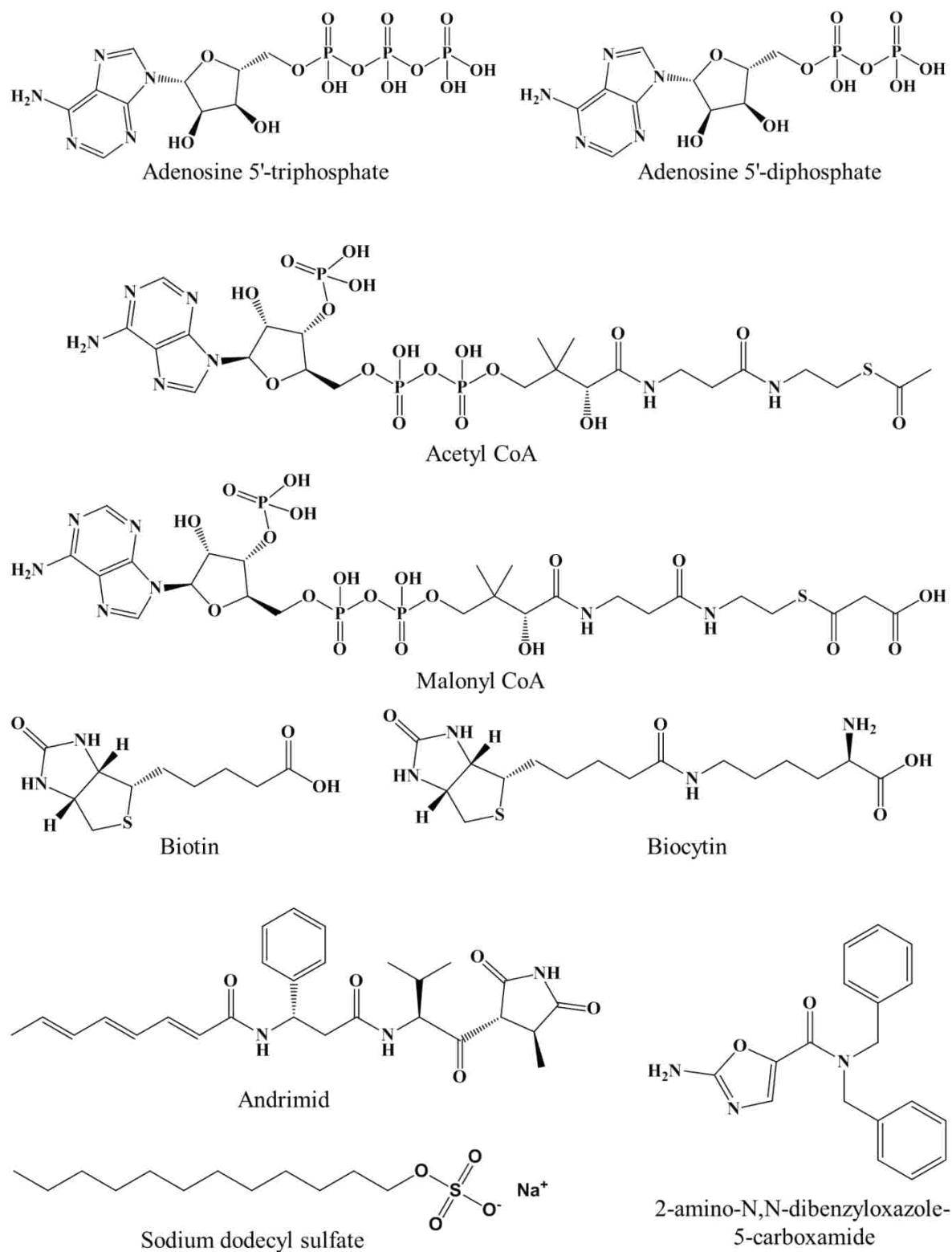
Figure 3.2. Structures of the compounds that were used to perform holo-ACC, CT, and BC assays.

Panel A of Figure 3.3 shows an electropherogram for 250 µM malonyl-CoA and 4.00 mM biocytin just prior to the addition of CT to initiate the reaction. A large malonyl-CoA peak is evident at 6.6 min. Panel B of Figure 3.3 shows an electropherogram 9.5 min after the addition of CT (final concentration, 10 µg/mL). A large acetyl-CoA peak with a migration time of 5.3 min is observed, and a very small malonyl-CoA peak is observed, indicating that the reaction was near completion. The peak shapes and separation of malonyl-CoA and acetyl-CoA were significantly improved relative to previous work as a result of optimizing the assay by better matching the sample buffer and separation buffer [116].
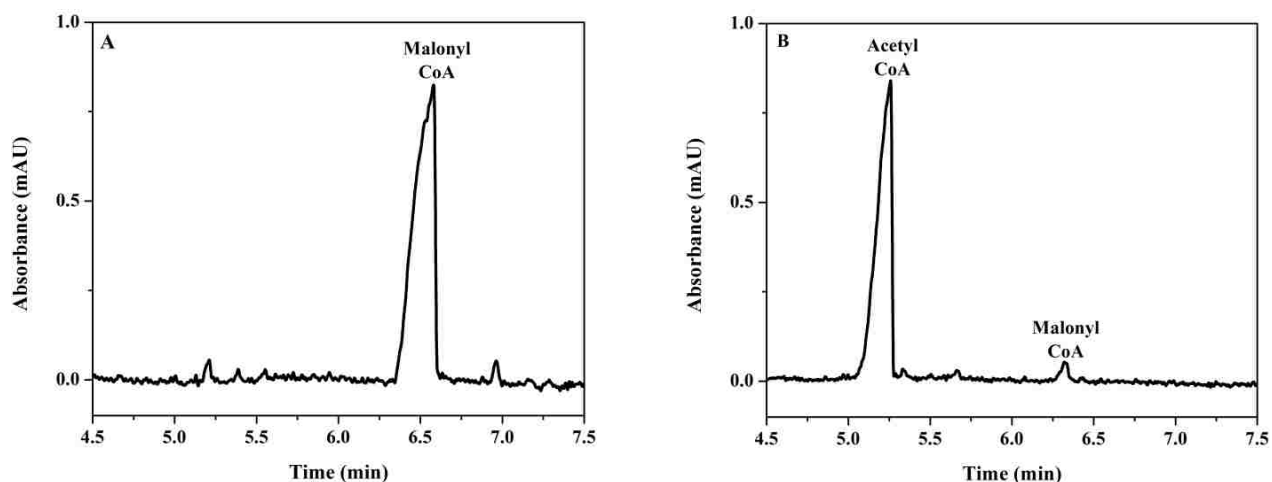
Figure 3.3. Electropherograms for the CT assay. (A) The assay reaction mixture contained 250 µM malonyl-CoA and 4.00 mM biocytin prior to addition of the enzyme. (B) At 9.5 min after addition of CT, a large acetyl-CoA peak was observed (product formation), and the malonyl-CoA peak had decreased. The sample buffer and separation buffer were both 5.0 mM potassium phosphate at pH 7.55. All injections were made at 0.5 psi for 10.0 s. The field strength for CE was 508 V/cm with a current of 11.1 µA.

3.3.2. Development of a CE assay for biotin carboxylase

An off-column CE assay for BC also was developed. Although ACC normally functions with both enzymes as holo-ACC, it is important to have assays for BC alone and CT alone. For example, these assays can be used to determine which part of ACC is being inhibited by a

molecule that inhibits holo-ACC. The assay reaction mixture contained ATP (50 μM) and biotin

(50 mM), as well as 2.5 mM $MgCl_2$, 5.0 mM potassium bicarbonate and 200 μM benzoic acid

(internal standard). The K_m for ATP in isolated BC is 80 μM [120], and an ATP concentration

(50 μM) was selected close to the K_m that resulted in a substrate peak with an adequate signal-to-

noise ratio for the assay. Biotin is needed in the reaction mixture because BC catalyzes the

carboxylation of biotin. Bicarbonate is the source of CO_2 for the carboxylation reaction, while

$MgCl_2$ is needed because BC activity requires two equivalents of the metal ion. One equivalent is

chelated to ATP such that the metal nucleotide chelate is the substrate for BC, while the other

metal ion binds in the active site and participates in catalysis [121]. Panel A of Figure 3.4 shows

an electropherogram for 50 μM ATP just prior to the addition of enzyme to initiate the reaction.
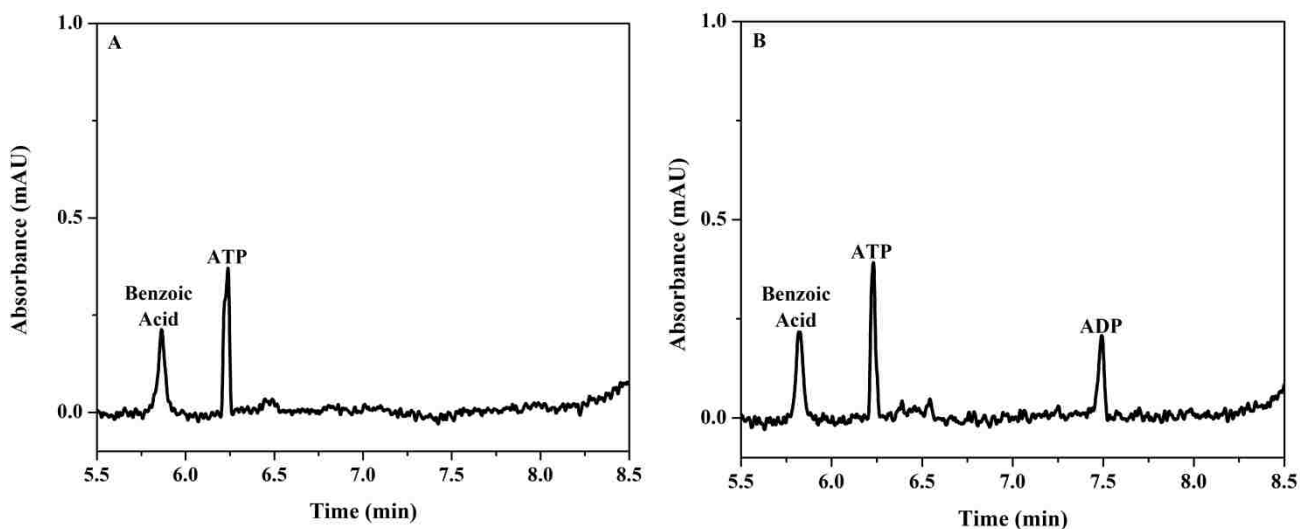
Figure 3.4. Electropherograms for the biotin carboxylase assay. (A) The reaction mixture contained 50 μM ATP, 2.5 mM $MgCl_2$, 50 mM biotin, 5.0 mM potassium bicarbonate and 200 μM benzoic acid prior to addition of the enzyme. (B) At 12.0 min after addition of BC, an ADP peak is observed (product formation). The sample buffer was 5.0 mM potassium phosphate at pH 7.55, and the separation buffer was 10.0 mM sodium phosphate at pH 7.55 with 20.0 mM SDS. All injections were made at 0.5 psi for 10.0 s. The field strength for CE was 508 V/cm with a current of 26.8 μA.

Panel B of Figure 3.4 shows an electropherogram at 12.0 min after the addition of BC (final BC concentration of 20 µg/mL). An ADP peak with a migration time of 7.5 min is observed, indicating that the reaction is proceeding. The development of the separation conditions used for this assay is described in Section 3.3.3.

3.3.3. Development of a CE assay for holo-ACC

The first step in the development of a CE assay for holo-ACC assay was to separate all of the substrates (ATP, acetyl-CoA) and products (ADP, malonyl-CoA) that have significant absorbance at 256 nm. A number of separation conditions were tested with a goal of identifying a buffer system that would allow resolution of the four molecules and also would be appropriate for the enzyme-catalyzed reactions. Because ACC functions well from pH 7.0 and 8.0, buffers were tested that could be used in that pH range. When using HEPES buffer alone (10.0 and 20.0 mM) at pH 7.55 or HEPES buffer with 2.0 mM KCl at pH 7.55, the 4 peaks were not fully resolved and the ATP peak width would range from 15 to 30 s. The separation was also attempted using 20.0 mM tris at pH 8.00, but similar results were obtained. Sodium dodecyl sulfate (SDS) was added to the separation buffer to improve the separation based on previous reports of separations of ATP and ADP for off-column enzyme assays and other applications [62, 63, 67-69]; however, the 4 peaks were not resolved using 20.0 mM HEPES with 15.0 mM SDS at pH 7.55. Attempts were made to add SDS to 20.0 mM HEPES buffer (pH 7.55) containing 2.0 mM KCl since the reaction buffer contained KCl, but the SDS precipitated out of solution upon KCl addition. Next, 10.0 mM sodium phosphate at pH 7.55 was used for the separation, but only 2 of the 4 peaks were resolved (Figure 3.5, panel A). Finally, resolution of all 4 peaks was achieved using 10.0 mM sodium phosphate with 20.0 mM SDS at pH 7.55, as shown in panel B of Figure 3.5.
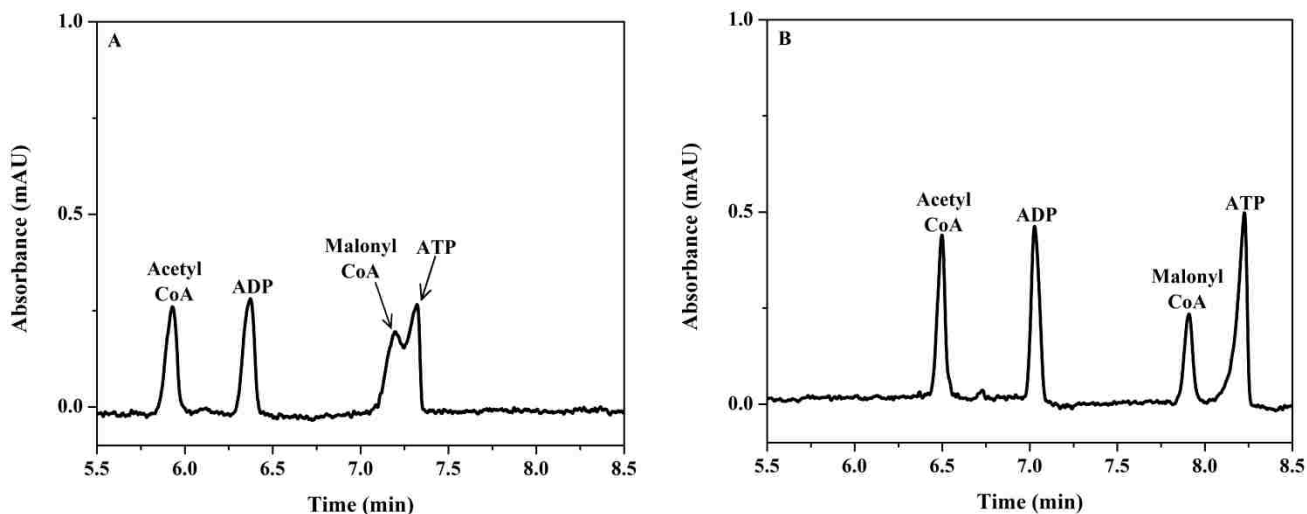
Figure 3.5. Electropherograms for separation of holo-ACC assay components. (A) Separation of a mixture of acetyl-CoA, malonyl-CoA, ATP and ADP (25 μM each). The sample and separation buffer was 10.0 mM sodium phosphate at pH 7.55. (B) The same sample separated using 10.0 mM sodium phosphate, pH 7.55 with 20.0 mM SDS as the separation buffer. All injections were made at 0.5 psi for 10.0 s. The field strength was 508 V/cm with a current of 19.0 μA for (A) and 25.2 μA for (B).

The substrate concentrations used for the holo-ACC assay were different than the concentrations used for assaying the individual components, BC and CT. The K_m for ATP in holo-ACC is 4 μM (T.C. Broussard and G.L. Waldrop, unpublished observations); however, a substantially higher ATP concentration of 25 μM was required to obtain an adequate signal-to-noise ratio. While the K_m for acetyl-CoA in holo-ACC is 0.5 mM, the concentration of acetyl-CoA used in the CE assay was only 50 μM because the ATP concentration was only 25 μM. The second half-reaction is limited by the amount of product produced in the first half-reaction (Figure 3.1), and higher concentrations of acetyl-CoA would not result in more malonyl-CoA production because ATP is the limiting reagent in this two-step reaction. Additionally, the reaction solution contained 2.5 mM $MgCl_2$, 2.0 μM BCCP, and 5.0 mM potassium bicarbonate, but it did not contain SDS, which would denature the proteins. Panel A of Figure 3.6 shows an electropherogram for 25 μM ATP and 50 μM acetyl-CoA just prior to the addition of enzyme to

initiate the reaction. Panel B of Figure 3.6 shows an electropherogram 9.5 min after the addition of BC and CT (final concentration of 10 μg/mL each). An ADP peak is observed with a migration time of 6.2 min, and a malonyl-CoA peak is observed with a migration time of 7.3 min, indicating that the reaction is proceeding. Furthermore, the necessary differences between the reaction solution and the separation buffer did not significantly degrade the separation as indicated in panel B of Figure 3.6.
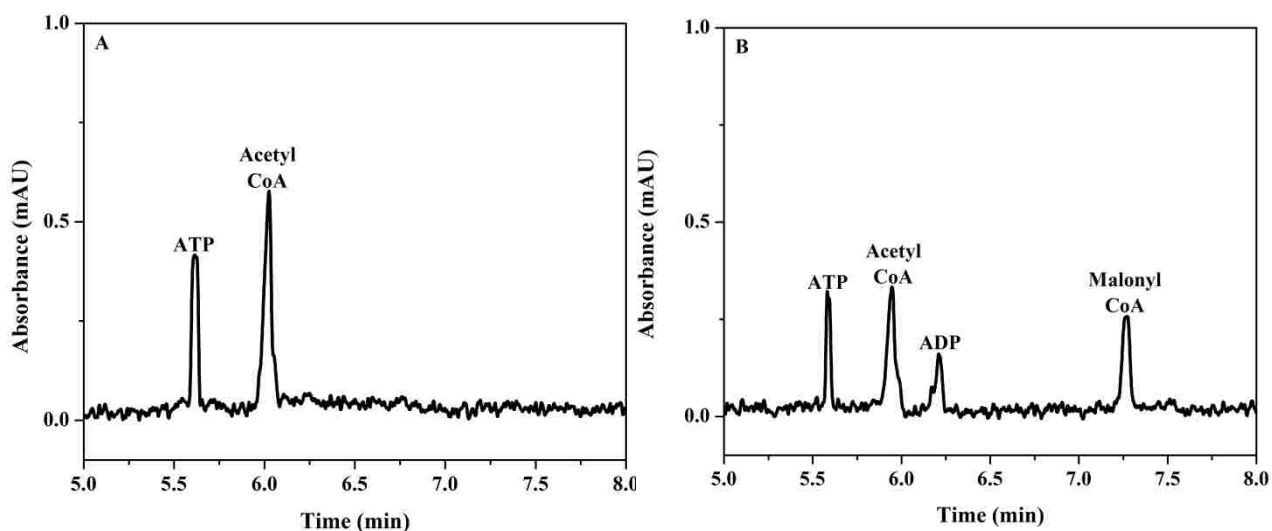
Figure 3.6. Electropherograms for the holo-ACC assay. (A) The reaction solution contained 25 μM ATP, 50 μM acetyl-CoA, 2.5 mM MgCl$_2$, 2.0 μM BCCP, and 5.0 mM potassium bicarbonate prior to the addition of 10.0 μg/mL of CT and 10.0 μg/mL of BC to initiate the reaction. (B) At 9.5 min after initiation of the reaction (addition of CT and BC), ADP and malonyl-CoA peaks were observed (product formation) and ATP and acetyl-CoA had decreased. The sample buffer was 5.0 mM potassium phosphate at pH 7.55 and the separation buffer was 10.0 mM sodium phosphate at pH 7.55 with 20.0 mM SDS. All injections were made at 0.5 psi for 10.0 s. The field strength for CE was 508 V/cm with a current of 24.6 μA.

Two well documented inhibitors of BC and CT were used to determine the effectiveness of the new CE assay for detecting inhibition of holo-ACC. The BC inhibitor used as a positive control was 2-amino-N,N-dibenzyloxazole-5-carboxamide (Figure 3.2), which was developed by Pfizer as an antibiotic [99]. This inhibitor concentration was tested first at 212 μM, which is well

above the IC$_{50}$ value of 0.125 μM reported by Mochalkin *et al.* [99]. The inhibitor has a strong

absorbance at 256 nm, so 3 peaks are observed instead of the usual 2 for ATP and acetyl-CoA

prior to the addition of the two enzymes (Figure 3.7, panel A). It is important to note the strong

absorbance of 2-amino-N,N-dibenzyloxazole-5-carboxamide. If the inhibitor, substrate, and

product absorb at the same wavelength, the inhibitor would significantly interfere with

traditional cuvette-based or plate reader-based assays due to spectral interference. Because CE is

a separation technique, the inhibitor can be physically separated from the substrates and

products, eliminating spectral interference. After adding CT and BC to the reaction mixture and

allowing the reaction to proceed for 11.5 min, no product formation was observed, indicating

strong inhibition (Figure 3.7, panel B).
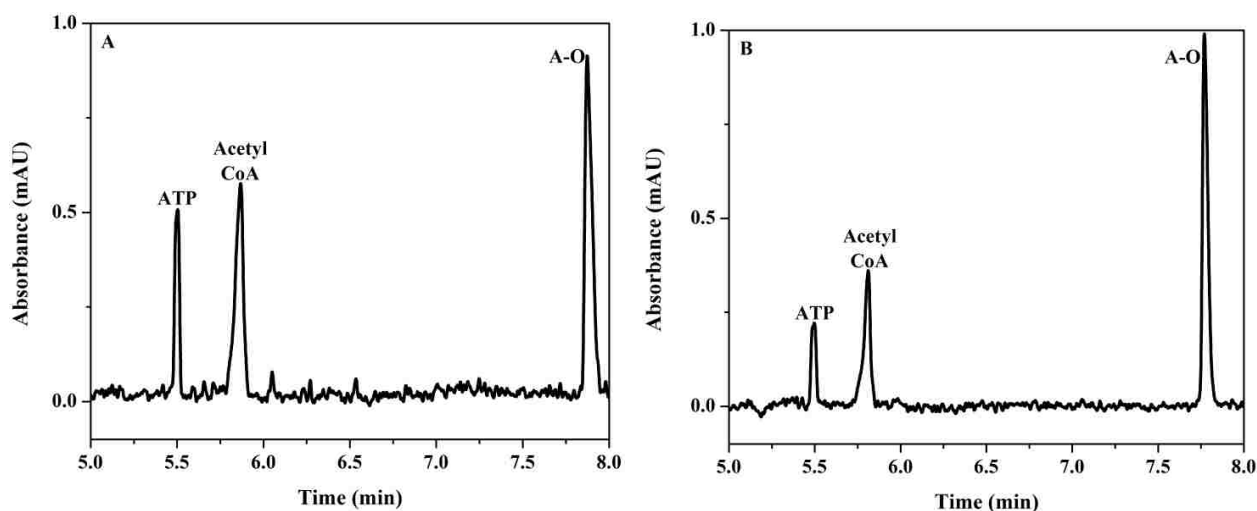
Figure 3.7. Electropherograms for the holo-ACC assay with 2-amino-N,N-dibenzyloxazole-5-carboxamide (A-O). (A) The reaction mixture contained 212 μM 2-amino-N,N-dibenzyloxazole-5-carboxamide, 25 μM ATP, 50 μM acetyl-CoA, 2.5 mM MgCl$_2$, 2.0 μM BCCP, and 5.0 mM potassium bicarbonate prior to the addition of addition of 10.0 μg/mL of CT and 10.0 μg/mL of BC to initiate the reaction. (B) At 11.5 min after initiation of the reaction there was no product formation observed. All other conditions are the same as in Figure 3.6.

This inhibitor was also tested near the IC$_{50}$ value at 0.20 μM using the same reaction time (11.5

min) and conditions. Product formation was observed at this concentration, but it was

56

significantly reduced compared to experiments without inhibitor. The ratio of peak areas for ADP/ATP decreased from 1.2 (no inhibitor) to 0.57 (0.20 μM 2-amino-N,N-dibenzyloxazole-5-carboxamide). Corresponding ratios for malonyl-CoA/acetyl-CoA were 0.79 (no inhibitor) and 0.55 (0.20 μM inhibitor). The IC_{50} was not determined here, but other studies have shown that this is possible using off-column CE assays [39].

Inhibition of holo-ACC using a known CT inhibitor, andrimid, also was studied [98]. Andrimid (Figure 3.2) is a natural product isolated from a marine isolate of *Pseudomonas fluorescens* that exhibits broad spectrum antibacterial activity [122]. A concentration of 30 μM was used, which is well above the IC_{50} value of 13 nM, reported by Freiberg *et al.* [98]. Electropherograms before addition of CT and BC and at 11.5 min after initiation of the reaction are shown in Figure 3.8. No product formation was observed. Unlike the BC inhibitor, andrimid does not absorb strongly at 256 nm. These results with inhibitors of both BC and CT are important because they show the assay can detect inhibition of bacterial holo-ACC, regardless of which half reaction the inhibitor is targeting.
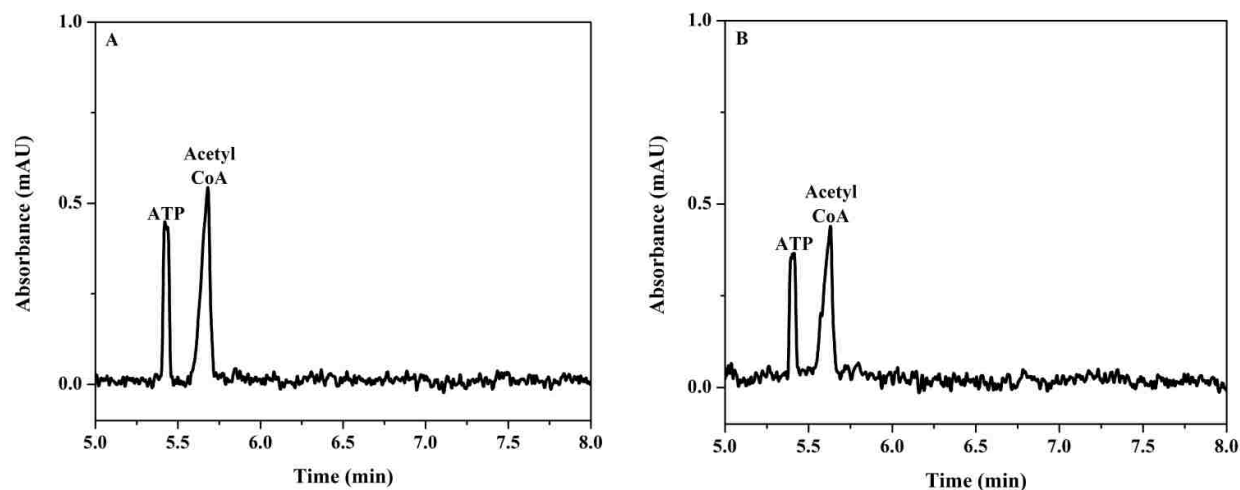
Figure 3.8. Electropherograms for the holo-ACC assay with andrimid. (A) The reaction mixture contained 30 μM andrimid, 25 μM ATP, 50 μM acetyl-CoA, 2.5 mM $MgCl_2$, 2.0 μM BCCP, and 5.0 mM potassium bicarbonate prior to the addition of 10.0 μg/mL of CT and 10.0 μg/mL and 10.0 μg/mL of BC to initiate the reaction. (B) At 11.5 min after initiation of the reaction, no production formation was observed. All other conditions are the same as in Figure 3.6.

3.4.   Conclusions

The first off-column capillary electrophoretic assay for holo-ACC that allows for simultaneous monitoring of the holo-ACC components, BC and CT, is described. For this assay, acetyl-CoA, malonyl-CoA, ATP, and ADP were separated by CE. The assay allows for simultaneous screening of inhibitors against BC and CT by directly monitoring the depletion of ATP and acetyl-CoA, and the concomitant production of ADP and malonyl-CoA. A CE assay for the BC component of ACC and an optimized CE assay for the CT component of ACC have been demonstrated. The CE assays for holo-ACC and the individual components BC and CT eliminate disadvantages that have been associated with previously developed ACC assays such as, spectral interference, the use of radioactive materials, consumption of large sample amounts, and indirect monitoring, which could lead to false positives. One drawback of this CE-based method is that the ATP and acetyl-CoA concentrations were limited to 50 μM and above because UV absorbance detection was used with a 50 μm internal diameter capillary. While several of the previously published assays for holo-ACC used ATP and acetyl-CoA concentrations above 50 μM, it is desirable to have the capability to use substrate concentrations below 50 μM. Because ACC is a target for the development of therapeutic agents for metabolic syndrome (including obesity and type 2 diabetes) and cancer as well as antibiotics and herbicides, this assay will be beneficial for efficient inhibitor screening and could lead to new discoveries of antibiotics, herbicides, and treatments for metabolic syndrome and cancer. Finally, the development of methods that can directly monitor reactants and products for multiple enzyme-catalyzed reactions will have impact beyond studying ACC.

CHAPTER 4. IDENTIFICATION OF BACTERIAL ACETYL COA CARBOXYLASE INHIBITORS DERIVED FROM BOTANICAL EXTRACTS

4.1.   Introduction

The development of antibiotic resistant bacteria is an emerging problem with potentially catastrophic consequences [123, 124]. The dramatic increase in resistant bacteria in recent years is primarily from overuse of antibiotics in both human therapy and agricultural settings [125]; however, even without overuse, bacterial resistance to an antibiotic will appear soon after its introduction in the clinic [126]. Thus, unlike other drugs, antibiotics are only effective for a limited time, which means there is a constant need for new antibiotics. Unfortunately, there has been a steady decline in the number of antibiotics approved by the FDA. Only two antibiotics were approved by the FDA from 2008-2010 [127, 128]. One reason for the lack of new antibiotics is that the current arsenal of antibiotics is directed at a limited number of targets ($<$ 30) [129], and there is an urgent need for new antibiotic targets. One potential new target for antibacterial therapy is acetyl-CoA carboxylase (ACC) [98, 99, 130].

ACC catalyzes the committed and rate-limiting step in fatty acid biosynthesis in all bacteria, plants, and animals. Since bacteria only use fatty acids for membrane biogenesis, inhibiting the activity of ACC will limit cell wall biosynthesis, ultimately resulting in cell death [130]. Catalysis by ACC involves the biotin-dependent carboxylation of acetyl-CoA to form malonyl-CoA and is carried out in two half-reactions (Figure 4.1) [97]. First, the biotin carboxylase (BC) component of ACC catalyzes the ATP-dependent carboxylation of biotin, which is covalently attached to biotin carboxyl carrier protein (BCCP) *in vivo*. Second, the carboxyltransferase (CT) component of ACC catalyzes the transfer of the carboxyl group from biotin to acetyl-CoA to form malonyl-CoA. In bacteria, BC, CT, and BCCP are separate proteins, and BC and CT retain their activity and can utilize free biotin in place of BCCP [97].

Both the BC and the CT components of bacterial ACC have been validated as targets for antibacterial development. CT was first identified as the target for the antibacterial natural products andrimid and moiramide B [98], while BC was identified as the target for several synthetic antibacterial agents: pyridopyrimidines [131], amino-oxazoles [99], and benzimidazole carboxamides [132]. Although these CT and BC inhibitors showed both *in vivo* and *in vitro* antibacterial activity against a variety of Gram-negative and Gram-positive pathogens, these compounds never advanced to clinical testing, leaving a promising new antibacterial target (ACC) without any new lead compounds.

$$MgATP + HCO_3^- \qquad MgADP + Pi^a$$

Biotin Carboxylase

$$BCCP\text{-}Biotin \qquad BCCP\text{-}Biotin\text{-}CO_2^-$$

Carboxyltransferase

$$Malonyl\text{-}CoA \qquad Acetyl\text{-}CoA$$

aPi: Inorganic phosphate
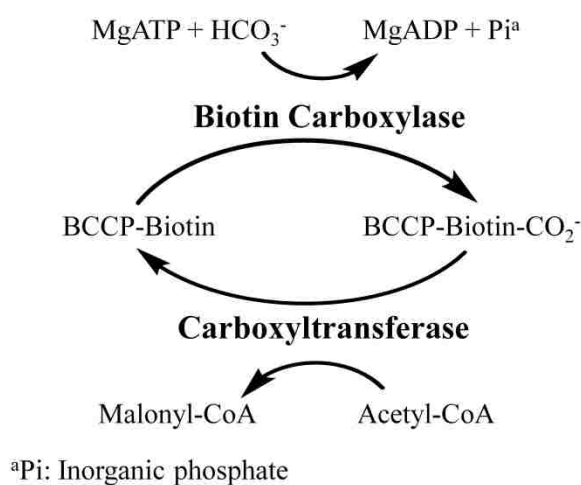
Figure 4.1. Acetyl-CoA carboxylase reaction scheme.

Greater than 75% of the antibiotics used to treat infectious disease originated as natural products,[133] but the pharmaceutical industry has largely abandoned testing for new leads based on natural products [15, 16]. One reason botanicals remain unexplored as a primary source of natural products is due to the inherent complexity of botanical extracts. The complex chemical mixtures of botanical samples are often incompatible with most of the high-throughput screening methods and assays used in the pharmaceutical industry [15, 16]. Thus, simple, efficient and

cost-effective assays that can accommodate complex mixtures of chemicals, such as botanical extracts, are required.

Capillary electrophoresis (CE) is a common separation technique that can be used for quantitative enzyme assays and studying enzyme inhibition [39, 134]. Enzyme assays based on CE are attractive for testing inhibition by complex samples like botanical extracts since spectral interference is greatly reduced by separation of substrates, products, inhibitors and sample matrix components. Additionally CE provides high separation efficiencies and peak capacities, simplicity, small sample volumes (nL) and rapid analysis times [33]. Previously, we developed a simple, off-column CE assay for the CT component of ACC using UV absorbance detection, which eliminated spectral interference for cinnamon extracts and related molecules that could not be assayed using the enzyme-coupled spectrophotometric method employed for the rest of the study [116, 117]. More recently, we optimized the CT assay, developed a CE assay for BC and reported the first assay for holo-ACC activity and inhibition that simultaneously monitored ATP, ADP, acetyl-CoA and malonyl-CoA [135].

Herein, we report the identification of natural products that inhibit ACC, which may serve as lead compounds for antibacterial development. These compounds were identified by screening botanical extracts against ACC using a recently developed CE assay [135]. Based on selected extracts that inhibited ACC in this assay, specific compounds likely to be responsible for this inhibition were identified using a combination of literature research and computational methods. Several of these compounds were tested for ACC inhibition using the CE assay.

4.2.   Materials and Methods

4.2.1. Reagents and assay solutions

Acetyl coenzyme A, malonyl coenzyme A, adenosine 5'-triphosphate, adenosine 5'-diphosphate, adenosine, biocytin, dimethyl sulfoxide, potassium phosphate monobasic, potassium bicarbonate, magnesium chloride, sodium dodecyl sulfate, nutmeg oil, myricetin, quercetin, malvidin chloride, 3,5,7-trihydroxyflavone (galangin), anrantine osage orange, eucalyptol, terpineol, caryophyllene oxide, linalool, β-caryophyllene, α-humulene, borneol, camphor, eugenol, estragole, carvacrol, and St. John's Wort were purchased from Sigma-Aldrich (St. Louis, MO). 3,6-dihydroxyflavone was purchased from Alfa Aesar (Ward Hill, MA). N-2-hydroxyethylpiperazine-N′-2-ethanesulfonic acid (HEPES) was purchased from EMD Millipore (Billerica, MA), and sodium phosphate and sodium hydroxide were purchased from Fisher Scientific (Fair Lawn, NJ). Biotin carboxylase and carboxyltransferase from *Escherichia coli* were purified as described previously [117, 120]. Biotin carboxyl carrier protein was a gift from Pfizer. All other botanical extracts were provided by The Center for Research on Botanicals and Metabolic Syndrome (Baton Rouge, LA). All solutions were prepared using ultrapure water (> 18 MΩ-cm, ModuLab water system, United States Filter Corp., Palm Desert, CA). All buffers were filtered through a 0.2 μm nylon membrane (Whatman; Hillsboro, OR) prior to use for CE.

4.2.2. Capillary electrophoretic assays.

All CE assays for holo-ACC, BC and CT were performed using a P/ACE MDQ system with UV absorbance detection (photodiode array detector) from Beckman Coulter, Inc. (Brea, CA) as described by Bryant, *et al.*[135]. All solutions for the enzyme-catalyzed reaction were prepared in 5.00 mM potassium phosphate buffer at pH 7.55 (reaction buffer). All enzyme reactions were performed off-column in a 1.5 mL glass Beckman CE vial with a total volume of

1.0 mL. The separation buffer for all assays contained 10.0 mM sodium phosphate and 20.0 mM sodium dodecyl sulfate at pH 7.55. The capillary was rinsed for 30 s prior to each injection, and the reaction mixtures were injected prior to addition of the enzyme at 1.0 min and 9.5 min after the addition of enzyme. All electropherograms were plotted with absorbance at 256 nm.

The holo-ACC assay solution contained 25.0 μM ATP, 50.0 μM acetyl-CoA, 2.50 mM $MgCl_2$, 2.0 μM BCCP, 5.0 mM potassium bicarbonate and 200 μM adenosine (internal standard) in the reaction buffer. The reaction was initiated by adding BC and CT to a final concentration of 10.0 μg/mL in the assay mixture. The BC assay mixture contained 50.0 μM ATP, 2.5 mM $MgCl_2$, 50.0 mM biotin, 5.0 potassium bicarbonate and 200 μM adenosine in the reaction buffer. To initiate the reaction, BC was added to the reaction mixture to a final concentration of 20.0 μg/mL. The CT assay mixture contained 250.0 μM malonyl-CoA, 4.00 mM biocytin and 200 μM adenosine in the reaction buffer. To initiate the reaction, CT was added to the reaction mixture to a final concentration of 10.0 μg/mL. When botanical extracts and specific compounds were tested for inhibition of holo-ACC, BC and CT, the extracts and compounds were added to the reaction mixture prior to the addition of enzyme. Botanical extracts were added to the reaction mixture at a final concentration of either 300 μg/mL or 30 μg/mL. All botanical extracts and potential inhibitors were dissolved in either water, DMSO, methanol or ethanol according to their solubilities (Tables 4.1, 4.2, 4.3, and 4.4). Only compounds dissolved in water or DMSO displayed inhibition of holo-ACC. Therefore, control assays were carried out containing 1% DMSO in the reaction mixture. It was concluded that 1% DMSO (the highest percentage of DMSO used in these studies) did not interfere with the enzymatic reaction or the separation of the substrates, products, and inhibitors. The ratios of the peak areas of products to substrates (ADP / ATP and malonyl-CoA / acetyl-CoA) were used to determine whether or not inhibition

occurred when a botanical extract or potential inhibitor were present in the solution. The ratios obtained during the inhibition studies were compared to the ratios for a control assay that was performed on the same day.

4.2.3. Steady State Kinetics

Biotin carboxylase activity and holo-ACC activity were both measured with a spectrophotometric assay in which the production of ADP was coupled to pyruvate kinase and lactate dehydrogenase, and the oxidation of NADH was monitored at 342 nm [120, 136]. Carboxyltransferase activity was measured in the reverse direction with a spectrophotometric assay in which the production of acetyl-CoA was coupled to the combined citrate synthase-malate dehydrogenase reaction requiring NAD^+ reduction [117]. All measurements were carried out in a volume of 0.5 mL in 1 cm path length quartz cuvettes. All reaction mixtures contained 10% DMSO to ensure that quercetin remained in solution during the course of the studies. Control assays containing 10% DMSO were also performed.

4.2.4. Ligand homology study

A computational ligand homology approach was used to identify potential inhibitors of ACC. Quercetin was used as a model for the ligand homology studies. A variety of software was used for the studies including *e*SimDock, DrugScore and AutoDock Vina software.

4.3.   Results

4.3.1. Screening of botanical extracts against holo-ACC.

A small library of botanical extracts provided by The Center for Research on Botanicals and Metabolic Syndrome was screened for inhibition of holo acetyl-coA carboxylase with a goal of identifying natural products that inhibit this enzyme. Many of these botanical extracts contained molecules that absorb strongly at UV and visible wavelengths. A photo of the

dissolved extracts is shown in Figure 4.2. The coupled enzyme assay normally used for holo-ACC [136] is based on measurement of NADH absorbance at 340 nm and could not be used for screening these extracts due to spectral interference. Instead, a recently developed CE assay for ACC[135] was used to screen the botanical extracts for holo-ACC inhibition.

Figure 4.2. Sample vials containing botanical extracts (300 μg/mL).

The CE assay is less susceptible to spectral interference since substrates and products are separated from many potential interfering species in the test samples [116, 135]. An example of this is presented in panel A of Figure 4.3, which shows an electropherogram of a reaction mixture containing a curcumin extract (Table 1) prior to the addition of CT and BC to initiate the enzyme assay. Peaks are observed in panel A of Figure 4.3 for 25 μM ATP, 50 μM acetyl-CoA, and the curcumin extract (7.9 min). Although panel A of Figure 4.3 shows absorbance at 256 nm,

the wavelength used for this CE assay, the curcumin extract absorbs strongly at 340 nm, and inhibition of holo-ACC could not be carried out using the more common coupled enzyme assay due to spectral interference [116, 135].
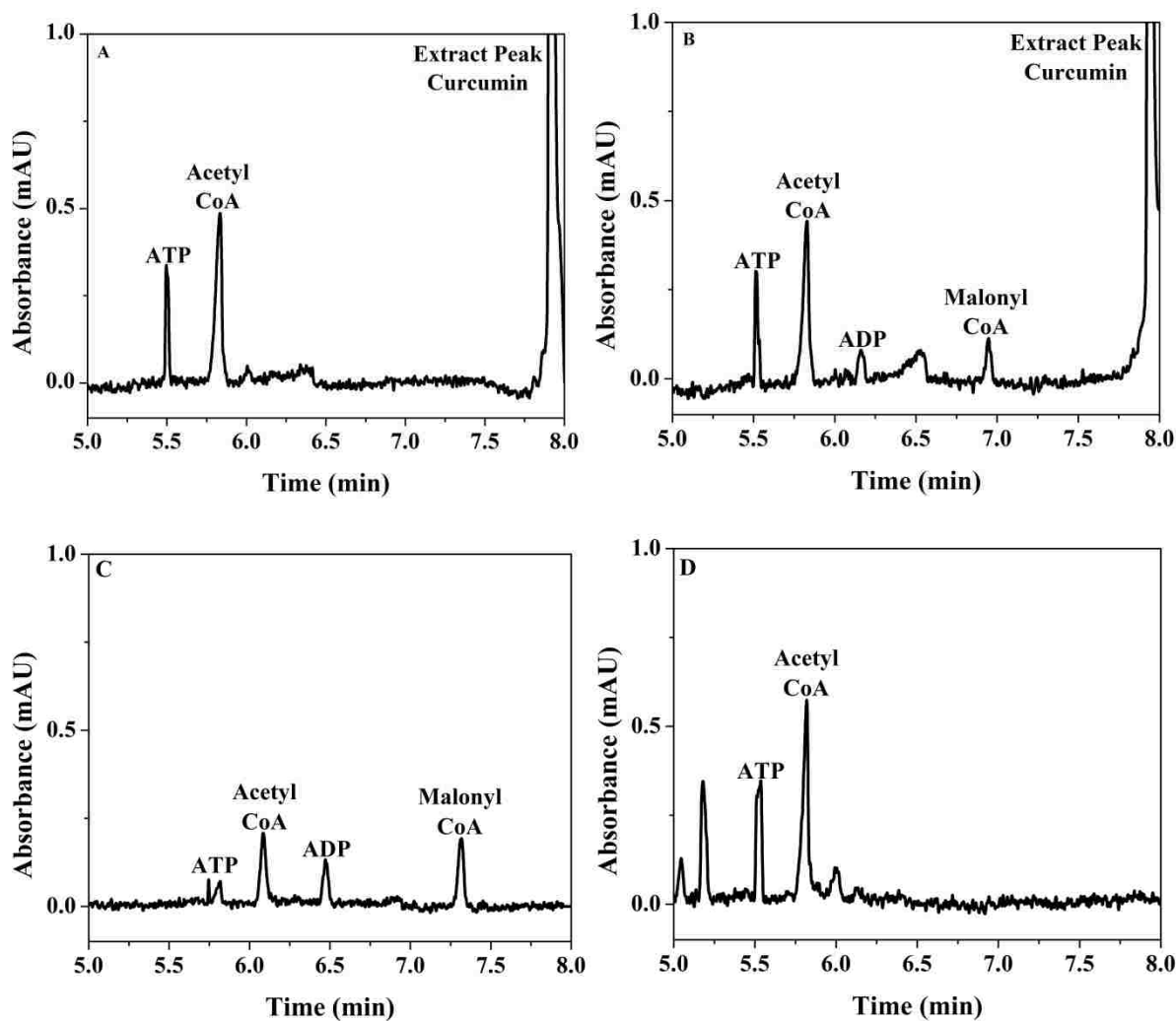
Figure 4.3. Electropherograms for the holo-ACC assay. (A) The reaction mixture contained 300 µg/mL of curcumin extract, 25 µM ATP, 50 µM acetyl-CoA, 2.5 mM MgCl$_2$, 2.0 µM BCCP, and 5.0 mM potassium bicarbonate prior to the addition of addition of 10.0 µg/mL of CT and 10.0 µg/mL of BC to initiate the reaction. (B) A 9.5 min after initiation of the reaction for the same sample shown in panel A, a decreased amount of ADP and malonyl-CoA formation was observed when compared to the control assay shown in panel C, indicating weak inhibition. (C) Control assay (no inhibitor) at 9.5 min after the addition of CT and BC to initiate the reaction. (D) Assay with 300 µg/mL cranberry CE at 9.5 min after the addition of CT and BC to initiate the reaction shows no product formation, indicating inhibition.

66

Panel B of Figure 4.3 shows an electropherogram 9.5 min after the addition of BC and CT to start the assay. A small ADP peak is observed at 6.2 min, and a malonyl-CoA peak is observed at 6.9 min, indicating that the reaction is proceeding. However, when the product formation at 9.5 min was compared to a control assay (no extract present) at the same reaction time (Figure 4.3, panel C), production of ADP and malonyl-CoA was significantly reduced in the presence of the curcumin extract. An example of strong inhibition is shown in panel D of Figure 4.3 for a cranberry extract (cranberry CE, Table 4.1). In this experiment, formation of the products ADP and malonyl-CoA was not observed even after a 9.5 min reaction time. It is important to note that there are three extract peaks from the cranberry extract very close to ATP and acetyl-CoA, again illustrating the importance of using the CE assay for these studies.

A total of 18 botanical extracts were blindly tested for their ability to inhibit holo-ACC using the CE-based screening assay. At a concentration of 300 µg/mL, ten of these extracts significantly inhibited holo-ACC (Table 4.1). Strong inhibition was defined as inhibition when the malonyl-CoA peak was below the limit of quantification at reaction time of 9.5 min. Extracts that significantly reduced the formation of ADP and malonyl-CoA at a reaction time of 9.5 min, but did not meet the definition of strong inhibitors were classified as weak inhibitors. The four extracts that were strong inhibitors at 300 µg/mL were diluted to 30 µg/mL and tested with the CE assay. All four of these extracts were classified as weak inhibitors at 30 µg/mL.

Holo-ACC is a multifunctional enzyme composed of two enzymatic components, which catalyze two coupled reactions, so all the extracts that inhibited holo-ACC were subsequently screened against CT and BC separately using the CE assays developed by Bryant *et al.*[135]. The results from these studies are presented in Table 4.1. All ten extracts that inhibited holo-ACC

also inhibited CT, but the only botanical extracts that inhibited both CT and BC were two cranberry extracts, cranberry CE and cranberry 90MX.

Table 4.1. Inhibition of holo-ACC, CT and BC by botanical extracts.[*]

Extract Name	Holo-ACC Inhibition	CT Inhibition	BC Inhibition	Solvent
Cranberry CE	Strong	Strong	Strong	Water
Cranberry 90MX	Weak	Weak	Strong	Water
Holy Basil	Strong	Strong	None	Water
Rubus Caesius	Strong	Strong	None	DMSO
Artemisia Scoparia	Strong	Weak	None	DMSO
Curcumin	Weak	Strong	None	DMSO
Inula Helenium	Weak	Strong	None	DMSO
PMI 5011 (Artemisia Dracunculus)	Weak	Weak	None	DMSO
Artemisia Rutifolia	Weak	Weak	None	DMSO
Artemisia Santolinifolia	Weak	Weak	None	DMSO
BM4 (Bitter Melon)	None	N/A	N/A	DMSO
Avocado	None	N/A	N/A	Water
BMSB (Bitter Melon)	None	N/A	N/A	Water
Inula Grandis	None	N/A	N/A	DMSO
Blueberry	None	N/A	N/A	Water
BMV (Bitter Melon)	None	N/A	N/A	DMSO
St. John's Wort	None	N/A	NA	Ethanol
Nutmeg Oil	None	N/A	N/A	DMSO

* The final extract concentration in the reaction mixture was 300 μg/mL.
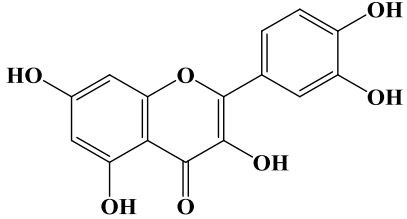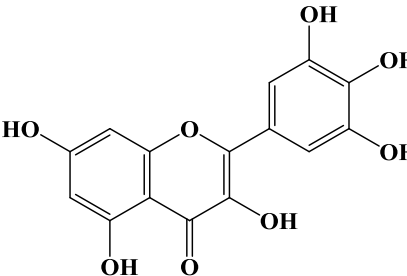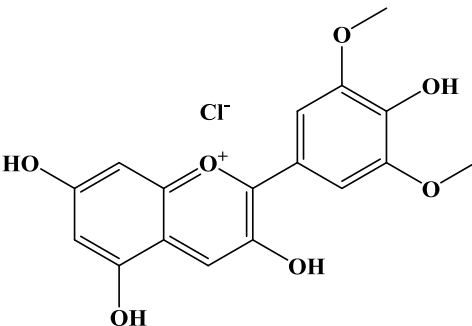
4.3.2. Screening of specific compounds against holo-ACC

The surprising result that 10 of the 18 botanical extracts screened inhibited holo-ACC necessitated making a choice as to which extract would be used for identification of specific natural products that inhibit ACC. Cranberry was selected for several reasons. First, the two cranberry extracts were the only extracts that inhibited both BC and CT in addition to holo-ACC. An equally important rationale for concentrating on the cranberry extracts is that the chemical makeup of cranberries is well documented in the literature [137-140], which simplifies identification of the molecule(s) in the extracts potentially responsible for the enzyme inhibition. The literature on the chemical composition of cranberries was studied carefully in order to identify commercially available compounds as potential ACC inhibitors for testing.

A total of 14 compounds were identified, acquired and screened against holo-ACC. Three of these were known to be present in cranberry extracts (Table 4.2), and the remaining compounds were known to be present in other extracts that inhibited holo-ACC (Table 4.3). The compounds in Table 4.2 were chosen based on their commercial availability as well as their structural similarity to known synthetic inhibitors of BC [99, 131]. Out of 14 compounds tested, quercetin and myricetin showed inhibition of holo-ACC activity (Table 4.2). At 250 μM, quercetin was a weak inhibitor while myricetin was a strong inhibitor using the same criteria for classification used for the botanical extracts. Myricetin was also tested at 25 μM and found to inhibit holo-ACC weakly. Interestingly, malvidin, which is similar in structure to quercetin and myricetin (Table 4.2) did not inhibit holo-ACC. Lastly, consistent with both cranberry extracts, quercetin and myricetin also inhibited the individual half-reactions catalyzed by BC and CT. Conventional steady-state kinetic analysis was used to study the inhibition of holo-ACC, BC and CT by quercetin and myricetin. This study was very difficult to conduct because of spectral

interference at 340 nm by quercetin and myricetin. The results obtained for these inhibition studies were initially difficult to interpret. Finally it was determined that quercetin and myricetin inhibited the coupling enzymes used in the assay. The conventional assay for holo-ACC could not be used to study these extracts and compounds.

Table 4.2. Inhibition of holo-ACC by compounds abundant in cranberry.

Compound	Structure	Concentration (µM)	Inhibition of Holo-ACC
Quercetin		250 25	Weak Weak
Myricetin		250 25	Strong Weak
Malvidin		250	None

*These compounds were dissolved in 100% DMSO and the reaction mixtures contained 0.25% DMSO.

70
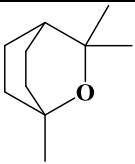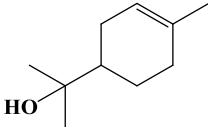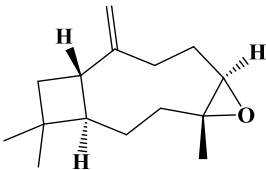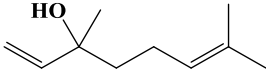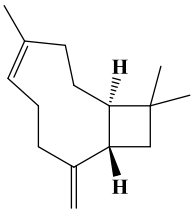
4.3.3. Ligand Homology Studies

The natural products, quercetin and myricetin, that were discovered to be holo-ACC inhibitors based on botanical screen, can serve as structural leads to identify other compounds, both synthetic and natural products, that inhibit holo-ACC. A straightforward computational approach was used to search for structurally related holo-ACC inhibitors. The computational approach taken in this study was a ligand homology analysis using eSimDock, DrugScore and AutoDock Vina software. These ligand homology studies identified 353 molecules as potential holo-ACC inhibitors. Of the 300 molecules identified, three were chosen for further testing based on their structural similarity to quercetin and myricetin and their commercial availability. The three compounds selected for analysis were: anrantine osage orange, 3,6-dihydroxyflavone, and galangin (Table 4.4). All three compounds selected contain a carbonyl group attached to fused six-membered rings. The compounds were analyzed for inhibition holo-ACC using the CE assay. Anrantine osage orange was found to be a strong inhibitor of holo-ACC at 250 μM, and it was a weak inhibitor at 25 μM. Galangin and 3,6-dihydroxflavone could not be tested at 250 μM due to low solubility, but they were tested at lower concentrations. 3,6-Dihydroxflavone weakly inhibited holo-ACC at 25 μM and 50 μM. Galangin was a weak holo-ACC inhibitor at 200 μM but showed no inhibition at 100 μM.

4.4. Conclusions
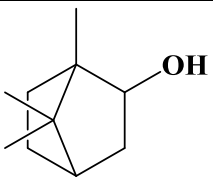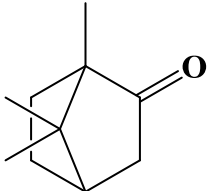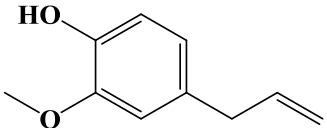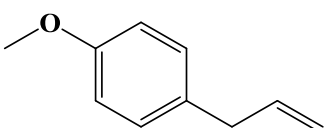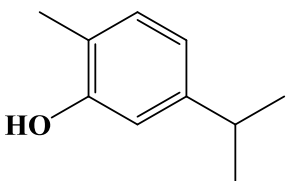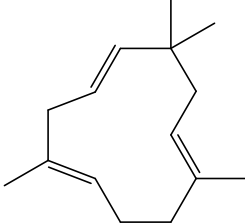
The importance of developing CE assays for ACC was validated in these studies. A total of 18 botanical extracts were screened for inhibition of holo-ACC. Using the CE assay to screen botanical extracts resulted in reduced spectral interference, which limits traditional enzyme assay techniques. Out of the 18 botanical extracts screened, ten inhibited holo-ACC. The ten extracts that inhibited holo-ACC all inhibited CT, and two of the ten (both from cranberry) inhibited BC.

Table 4.3. Compounds found in botanical extracts other than cranberry.[*]

Compound	Structure	Solvent
Eucalyptol		DMSO
Terpineol		DMSO
Caryophyllene Oxide		Methanol
Linalool		DMSO
β-Caryophyllene		DMSO
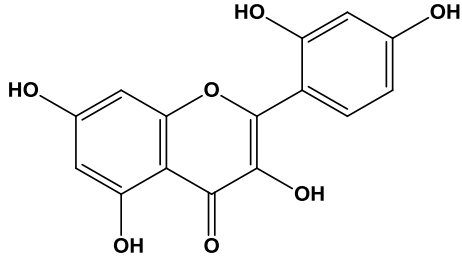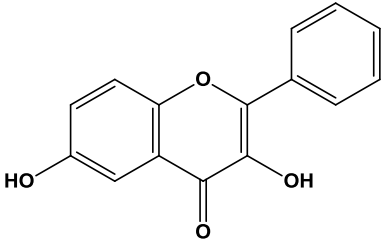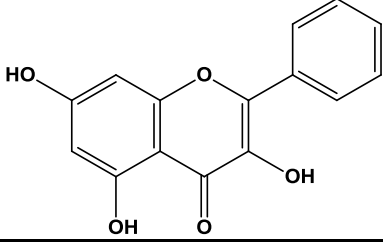
[*]The compounds were dissolved in their respective solvents (100%) and the final concentration of solvent in the assay mixtures was between 0.25% and 0.32%.

Table 4.3 continued. Compounds found in botanical extracts other than cranberry.[*]

Compound	Structure	Solvent
Borneol		Ethanol
Camphor		Ethanol
Eugenol		DMSO
Estragole		DMSO
Carvacrol		DMSO
α-Humulene		DMSO

[*]The compounds were dissolved in their respective solvents (100%) and the final concentration of solvent in the assay mixtures was between 0.25% and 0.32%.

Table 4.4. Inhibition of holo-ACC by compounds identified through ligand homology studies.

Compound	Structure	Concentration (μM)	Inhibition of Holo-ACC
Anrantine Osage Orange		250 25	Strong Weak
3,6-Dihydroxyflavone		50 25	Weak Weak
Galangin		200 100	Weak None

[*]The compounds were dissolved in their respective solvents (100%) and the final concentration of solvent in the assay mixtures was between 0.25% and 0.32%.

Furthermore, 14 specific compounds found in the botanical extracts that inhibited holo-ACC were identified based on a detailed literature search and tested for inhibition of holo-ACC, BC and CT. Interestingly, only quercetin and myricetin, both abundant in cranberry, showed inhibition of holo-ACC. Quercetin and myricetin inhibited both of the individual components, BC and CT, as well. Quercetin was used as a model for ligand homology studies and synthetic compounds that could potentially inhibit ACC were identified based on the studies. Three

compounds selected from the ligand homology studies were screened for holo-ACC inhibition and found to inhibit holo-ACC. The overall strategy of using CE to identify inhibitors by initially screening botanical extracts and ending with testing natural products or synthetic molecules that mimic natural products, can be employed for economic and efficient identification of inhibitors of other enzymes in the future.

CHAPTER 5. CONCLUSIONS AND FUTURE DIRECTIONS

5.1. <u>Conclusions</u>

The research presented in this dissertation resulted in the development and application of new methods for studying enzymes and enzyme inhibition using capillary electrophoresis (CE). In Chapter 2, a fluorescent adenosine deaminase (ADA) substrate, 2',3'-*O*-(2,4,6 trinitrophenyl) adenosine (TNP-adenosine), was found to be unusually photostable and could not be photobleached. The photostability of TNP-adenosine was compared quantitatively to that of common OGVCE fluorophores. Of the common OGVCE fluorophores investigated, fluorescein was found to be most susceptible to photobleaching, followed by coumarin 334 and rhodamine 110. Rhodamine B was the most photostable common OGVCE dye tested; however, the photostability of TNP-adenosine, which did not photobleach at all, exceeded that of rhodamine B. Another conclusion drawn from Chapter 2 was that the migration rate of a dye through a capillary can contribute significantly to its photobleaching percentage. These studies contribute to a better understanding of the ideal properties of a dye for OGVCE assays. This information will be useful for determining which dyes should be used for OGVCE studies and for developing fluorescent substrates for OGVCE-based enzyme assays.

In Chapter 3, simple, and efficient assays for studying acetyl coenzyme A carboxylase holoenzyme (holo-ACC) activity and inhibition were developed. The first off-column CE assay for simultaneously monitoring the two reactions catalyzed by the holo-ACC components, biotin carboxylase (BC) and carboxyltransferase (CT), was developed. The holo-ACC substrates (ATP and acetyl-CoA) and products (ADP and malonyl-CoA) were separated using micellar electrokinetic chromatography (MEKC). This assay allowed for concurrent screening of inhibitors against BC and CT by directly monitoring ATP and acetyl-CoA depletion, and the

concomitant production of ADP and malonyl-CoA. The CE assay was also applied to test known inhibitors of BC and CT inhibition of holo-ACC inhibition. The development of this assay is very important because many enzymes have multiple components and simultaneous monitoring of multiple enzyme-catalyzed reactions is desirable. Additionally, a previously reported off-column CE assay for only the CT component of ACC was optimized, and an off-column CE assay for only the BC component of ACC was developed. The CE assays for holo-ACC and the individual components, BC and CT, eliminate disadvantages that have been associated with previously developed ACC assays such as, spectral interference, the use of radioactivity, consumption of large amounts of enzyme, and indirect monitoring through the use of coupling enzymes, which could lead to false positives. These CE assays will be beneficial for efficient inhibitor screening because ACC is a target for the development of therapeutic agents for metabolic syndrome (including obesity and type 2 diabetes), cancer, antibiotics and herbicides. Efficient screening of compounds for inhibition of ACC could lead to new discoveries of antibiotics, herbicides, and treatments for metabolic syndrome and cancer.

In Chapter 4, 18 botanical extracts were screened for inhibition of holo-ACC, which further demonstrates the importance of developing CE assays for ACC. Botanical extracts are complex samples; however, because CE is an electrophoretic separation technique, spectral interference is reduced by separation of substrates, products, inhibitors and sample matrix components. Out of the 18 botanical extracts screened, ten inhibited holo-ACC. The ten extracts that inhibited holo-ACC all inhibited CT, and two of the ten (both from cranberry) inhibited BC. Specific compounds found in the botanical extracts that inhibited holo-ACC were identified based on a detailed literature search and tested for inhibition of holo-ACC, BC and CT. Out of 14 compounds tested, quercetin and myricetin, both abundant in cranberry, showed inhibition of

holo-ACC. Quercetin and myricetin inhibited both of the individual components, BC and CT, as well. Synthetic compounds identified through ligand homology studies using quercetin as a model were also screened for holo-ACC inhibition. Three compounds identified based on the ligand homology studies were found to inhibit holo-ACC. The overall strategy of using CE to identify inhibitors by initially screening botanical extracts and ending with testing natural products or synthetic molecules that mimic natural products, can be employed for economic and efficient identification of inhibitors of other enzymes in the future.

5.2. Future Directions

The OGVCE-LIF technique is very useful for enzyme assays because enzymes that do not have fluorogenic substrates can be investigated. Therefore, the development of OGVCE-LIF assays for adenosine deaminase and other enzymes that do not have fluorogenic substrates is still desirable. Now that a better understanding of the ideal properties of a substrate for OGVCE assays has been gained, other fluorescent adenosine derivatives [141-143] and fluorescent adenosine nucleoside derivatives [144, 145] can be explored as potential substrates for ADA and examined for compatibility with OGVCE in order to develop an OGVCE assay for ADA. Furthermore, other enzymes that do not have fluorogenic substrates can also be explored for the development of an OGVCE-LIF assay.

In Chapter 4, the assays developed in Chapter 3 were successfully used for the screening of botanical extract and potential inhibitors for inhibition of holo-ACC, and new ACC inhibitors were identified. Next, the antimicrobial activity of the newly discovered inhibitors will be investigated. The information obtained from those studies will be useful in determining whether or not these new ACC inhibitors can be used in the development of antibiotics to combat the emerging antibiotic resistance problem. Three synthetic compounds identified through ligand

homology studies were found to inhibit holo-ACC in Chapter 4; however, several other compounds identified through ligand homology could also be tested for ACC inhibition. In this dissertation, there was also strong focus on the cranberry botanical extracts, but eight other botanical extracts were found to inhibit holo-ACC. Those eight botanical extracts will be investigated in more detail. A literature search will be used to identify and select compounds found in the botanical extracts that inhibit holo-ACC, and those compounds will be tested for ACC inhibition as well. If any of the compounds show inhibition of ACC, ligand homology studies could be used to identify other potential ACC inhibitors. Synthetic compounds identified through ligand homology could also be screened for ACC inhibition. Finally, the antimicrobial activity of the compounds that inhibit holo-ACC will be investigated.

REFERENCES

[1] R.H. Garrett, C.M. Grisham, Biochemistry, 3rd Edition, 2004.

[2] R.A. Copeland, Enzymes: A Practical Introduction to Structure, Mechanism, and Data Analysis, Second Edition, 2000.

[3] V. Leskovac, Comprehensize Enzyme Kinetics, New York, 2003.

[4] L. Michaelis, M.L. Menten, The Kinetics of the Inversion Effect, Biochem. Z., 49 (1913) 333-369.

[5] G.E. Briggs, J.B.S. Haldane, A Note on the Kinetics of Enzyme Action, Biochem. J., 19 (1925) 338-339.

[6] W.W. Cleland, Statistical Analysis of Enzyme Kinetic Data, Adv. Enzymol. Relat. Areas Mol. Biol., 29 (1967) 1-&.

[7] R.A. Copeland, Evaluation of Enzyme Inhibitors in Drug Discovery: A Guide for Medicinal Chemists and Pharmacologists., John Wiley & Sons, Inc., Hoboken, 2005.

[8] R.A. Copeland, M.R. Harpel, P.J. Tummino, Targeting Enzyme Inhibitors in Drug Discovery, Expert Opin. Ther. Targets, 11 (2007) 967-978.

[9] C.A. Ryan, Protease Inhibitors in Plants - Genes for Improving Defenses against Insects and Pathogens, Annu. Rev. Phytopathol., 28 (1990) 425-449.

[10] F. Jamal, P.K. Pandey, D. Singh, M.Y. Khan, Serine Protease Inhibitors in Plants: Nature's Arsenal Crafted for Insect Predators, Phytochemistry review, (2012).

[11] J. Drews, Drug Discovery: A Historical Perspective, Science, 287 (2000) 1960-1964.

[12] A.L. Hopkins, C.R. Groom, The Druggable Genome, Nat. Rev. Drug Discov., 1 (2002) 727-730.

[13] I. Raskin, D.M. Ribnicky, S. Komarnytsky, N. Ilic, A. Poulev, N. Borisjuk, A. Brinker, D.A. Moreno, C. Ripoll, N. Yakoby, J.M. O'Neal, T. Cornwell, I. Pastor, B. Fridlender, Plants and Human Health in the Twenty-First Century, Trends Biotechnol., 20 (2002) 522-531.

[14] B. Schmidt, D.M. Ribnicky, A. Poulev, S. Logendra, W.T. Cefalu, I. Raskin, A Natural History of Botanical Therapeutics, Metabolism-Clinical and Experimental, 57 (2008) S3-S9.

[15] M.S. Butler, The Role of Natural Product Chemistry in Drug Discovery, J. Nat. Prod., 67 (2004) 2141-2153.

[16] F.E. Koehn, G.T. Carter, The Evolving Role of Natural Products in Drug Discovery, Nat. Rev. Drug Discov., 4 (2005) 206-220.

[17] B.B. Mishra, V.K. Tiwari, Natural Products: An Evolving Role in Future Drug Discovery, Eur. J. Med. Chem., 46 (2011) 4769-4807.

[18] M.J. Balunas, A.D. Kinghorn, Drug Discovery from Medicinal Plants, Life Sci., 78 (2005) 431-441.

[19] A.L. Harvey, Natural Products in Drug Discovery, Drug Discov. Today, 13 (2008) 894-901.

[20] D.J. Newman, G.M. Cragg, Natural Products as Sources of New Drugs over the Last 25 Years, J. Nat. Prod., 70 (2007) 461-477.

[21] K. Cusi, R.A. DeFronzo, Metformin: A Review of Its Metabolic Effects, Diabetes Rev., 6 (1998) 89-131.

[22] M. Heinrich, H.L. Teoh, Galanthamine from Snowdrop - the Development of a Modern Drug against Alzheimer's Disease from Local Caucasian Knowledge, J. Ethnopharmacol., 92 (2004) 147-162.

[23] T. Pirttila, G. Wilcock, L. Truyen, C.V. Damaraju, Long-Term Efficacy and Safety of Galantamine in Patients with Mild-to-Moderate Alzheimer's Disease: Multicenter Trial, Eur. J. Neurol., 11 (2004) 734-741.

[24] J.J. Sramek, E.J. Frackiewicz, N.R. Cutler, Review of the Acetylcholinesterase Inhibitor Galanthamine, Expert Opin. Investig. Drugs, 9 (2000) 2393-2402.

[25] B. Ibach, E. Haen, Acetylcholinesterase Inhibition in Alzheimer's Disease, Curr. Pharm. Design, 10 (2004) 231-251.

[26] Y. Kashman, K.R. Gustafson, R.W. Fuller, J.H. Cardellina, J.B. McMahon, M.J. Currens, R.W. Buckheit, S.H. Hughes, G.M. Cragg, M.R. Boyd, Hiv Inhibitory Natural-Products .7. The Calanolides, a Novel Hiv-Inhibitory Class of Coumarin Derivatives from the Tropical Rain-Forest Tree, Calophyllum-Lanigerum, J. Med. Chem., 35 (1992) 2735-2743.

[27] S.S. Yang, G.M. Cragg, D.J. Newman, J.P. Bader, Natural Product-Based Anti-Hiv Drug Discovery and Development Facilitated by the NCI Developmental Therapeutics Program, Journal of Natural Products, 64 (2001) 265-277.

[28] D.L. Yu, M. Suzuki, L. Xie, S.L. Morris-Natschke, K.H. Lee, Recent Progress in the Development of Coumarin Derivatives as Potent Anti-HIV Agents, Med. Res. Rev., 23 (2003) 322-345.

[29] R.W. Buckheit, E.L. White, V. Fliakas-Boltz, J. Russell, T.L. Stup, T.L. Kinjerski, M.C. Osterling, A. Weigand, J.P. Bader, Unique Anti-Human Immunodeficiency Virus Activities of

the Nonnucleoside Reverse Transcriptase Inhibitors Calanolide a, Costatolide, and Dihydrocostatolide, Antimicrob. Agents Chemother., 43 (1999) 1827-1834.

[30] M.J. Currens, R.J. Gulakowski, J.M. Mariner, R.A. Moran, R.W. Buckheit, K.R. Gustafson, J.B. McMahon, M.R. Boyd, Antiviral Activity and Mechanism of Action of Calanolide a against the Human Immunodeficiency Virus Type-1, J. Pharmacol. Exp. Ther., 279 (1996) 645-651.

[31] R.A. Copeland, Enzymes: A Practical Introduction to Structure, Mechanism, and Data Analysis, Second Edition, 2000.

[32] J.W. Jorgenson, K.D. Lukacs, Zone Electrophoresis in Open-Tubular Glass-Capillaries, Anal. Chem., 53 (1981) 1298-1302.

[33] Handbook of Capillary and Microchip Electrophoresis and Associated Microtechniques (3rd Edn.) Edited by J. P. Landers, 2008.

[34] K. Swinney, D.J. Bornhop, Detection in Capillary Electrophoresis, Electrophoresis, 21 (2000) 1239-1250.

[35] K.B. Tomer, L.J. Deterding, C.E. Parker, Capillary Electrophoresis Coupled with Mass Spectrometry, Adv. Chromatogr. (N. Y.), 35 (1995) 53-99.

[36] J.J. Bao, J.M. Fujima, N.D. Danielson, Determination of Minute Enzymatic Activities by Means of Capillary Electrophoretic Techniques, J. Chromatogr., B, 699 (1997) 481-497.

[37] Y. Fan, G.K.E. Scriba, Advances in-Capillary Electrophoretic Enzyme Assays, J. Pharm. Biomed. Anal., 53 (2010) 1076-1090.

[38] Z. Glatz, Determination of Enzymatic Activity by Capillary Electrophoresis, J. Chromatogr., B: Biomed. Sci. Appl., 841 (2006) 23-37.

[39] R. Chantiwas, X. Yan, S.D. Gilman, Microfluidics for Studying Enzyme Inhibition, Biol. Appl. Microfluid., (2008) 135-170.

[40] J. Krenkova, F. Foret, Immobilized Microfluidic Enzymatic Reactors, Electrophoresis, 25 (2004) 3550-3563.

[41] J. Bao, F.E. Regnier, Ultramicro Enzyme Assays in a Capillary Electrophoretic System, J. Chromatogr., 608 (1992) 217-224.

[42] F.E. Regnier, D.H. Patterson, B.J. Harmon, Electrophoretically-Mediated Microanalysis (EMMA), TrAC, Trends Anal. Chem., 14 (1995) 177-181.

[43] A.R. Whisnant, S.E. Johnston, S.D. Gilman, Capillary Electrophoretic Analysis of Alkaline Phosphatase Inhibition by Theophylline, Electrophoresis, 21 (2000) 1341-1348.

[44] A.R. Whisnant, S.D. Gilman, Studies of Reversible Inhibition, Irreversible Inhibition, and Activation of Alkaline Phosphatase by Capillary Electrophoresis, Anal. Biochem., 307 (2002) 226-234.

[45] R.J. Krueger, T.R. Hobbs, K.A. Mihal, J. Tehrani, M.G. Zeece, Analysis of Endoproteinase Arg-C Action on Adrenocorticotropic Hormone by Capillary Electrophoresis and Reversed-Phase High-Performance Liquid-Chromatography, J. Chromatogr., 543 (1991) 451-461.

[46] J.P. Landers, M.D. Schuchard, M. Subramaniam, T.P. Sismelich, T.C. Spelsberg, High-Performance Capillary Electrophoretic Analysis of Chloramphenicol Acetyl Transferase-Activity, J. Chromatogr., 603 (1992) 247-257.

[47] P. Pascual, E. Martinezlara, J.A. Barcena, J. Lopezbarea, F. Toribio, Direct Assay of Glutathione-Peroxidase Activity Using High-Performance Capillary Electrophoresis, J. Chromatogr., B: Biomed. Sci. Appl.,, 581 (1992) 49-56.

[48] T. Hoffmann, D. Reinhold, T. Kahne, J. Faust, K. Neubert, R. Frank, S. Ansorge, Inhibition of Dipeptidyl-Peptidase-IV (DP-IV) by Anti-DP-IV Antibodies and Nonsubstrate X-X-Pro-Oligopeptides Ascertained by Capillary Electrophoresis, J. Chromatogr., A, 716 (1995) 355-362.

[49] Y. Kanie, A. Kirsch, O. Kanie, C.H. Wong, Enzymatic Assay of Galactosyltransferase by Capillary Electrophoresis, Anal. Biochem., 263 (1998) 240-245.

[50] B.W. Chang, R.L.C. Chen, I.J. Huang, H.C. Chang, Assays for Angiotensin Converting Enzyme Inhibitory Activity, Anal. Biochem., 291 (2001) 84-88.

[51] X. Cahours, C. Viron, P. Morin, I. Renimel, P. Andre, M. Lafosse, Short-End Injection Procedure in Capillary Electrophoresis for Determination of Enzymatic Reaction Kinetics, Anal. Chim. Acta, 441 (2001) 15-21.

[52] Z. Glatz, P. Bouchal, O. Janiczek, M. Mandl, P. Ceskova, Determination of Rhodanese Enzyme Activity by Capillary Zone Electrophoresis, J. Chromatogr., A, 838 (1999) 139-148.

[53] X. Hai, X. Wang, M. El-Attug, E. Adams, J. Hoogmartens, A. Van Schepdael, In-Capillary Screening of Matrix Metalloproteinase Inhibitors by Electrophoretically Mediated Microanalysis with Fluorescence Detection, Anal. Chem., 83 (2011) 425-430.

[54] S. Van Dyck, S. Vissers, A. Van Schepdael, J. Hoogmartens, Kinetic Study of Angiotensin Converting Enzyme Activity by Capillary Electrophoresis after in-Line Reaction at the Capillary Inlet, J. Chromatogr., A, 986 (2003) 303-311.

[55] J.L. Pittman, S.D. Gilman, K.F. Schrum, On-Line Monitoring of Electroosmotic Flow for Capillary Electrophoretic Separations, Analyst (Cambridge, U. K.), 126 (2001) 1240-1247.

[56] J.L. Pittman, A.I. Terekhov, S.W. Suljak, S.D. Gilman, Optically Gated Vacancy Electrophoresis in Microfluidic Devices, Anal. Chim. Acta, 496 (2003) 195-204.

[57] S. Terabe, K. Otsuka, K. Ichikawa, A. Tsuchiya, T. Ando, Electrokinetic Separations with Micellar Solutions and Open-Tubular Capillaries, Anal. Chem., 56 (1984) 111-113.

[58] S. Terabe, Capillary Separation: Micellar Electrokinetic Chromatography, Annu. Rev. Anal. Chem., 2009, pp. 99-120.

[59] S. Terabe, Micellar Electrokinetic Chromatography, Handb. Capillary Microchip Electrophor. Assoc. Microtech. (3rd Ed.), (2008) 109-133.

[60] P. Mukerjee, K.J. Mysels, Critical Micelle Concentrations of Aqueous Surfactant Systems (NSRDS-NBS 36), 1971.

[61] T. Krizek, A. Kubickova, Microscale Separation Methods for Enzyme Kinetics Assays, Anal. Bioanal. Chem., 403 (2012) 2185-2195.

[62] V. Dolnik, J.P. Liu, J.F. Banks, M.V. Novotny, P. Bocek, Capillary Zone Electrophoresis of Oligonucleotides - Factors Affecting Separation, J. Chromatogr., 480 (1989) 321-330.

[63] P. Elisabeth, M. Yoshioka, T. Sasaki, M. Senda, Separation of Nucleotides Using Micellar Electrokinetic Capillary Chromatography, J. Chromatogr., A, 806 (1998) 199-207.

[64] K. Kawamura, Capillary Electrophoretic Separation of Mono- and Dinucleotides of Adenosine Using Cyclodextrin Solutions with $MgCl_2$ Additive, J. Chromatogr., A, 802 (1998) 167-177.

[65] T. Tsuda, K. Takagi, T. Watanabe, T. Satake, Separation of Nucleotides in Organs of Guinea-Pig by Capillary Zone Electrophoresis, J. High Resolut. Chromatogr., 11 (1988) 721-723.

[66] M. Uhrova, Z. Deyl, M. Suchanek, Separation of Common Nucleotides, Mono-, Di- and Triphosphates, by Capillary Electrophoresis, J. Chromatogr., B, 681 (1996) 99-105.

[67] S.E. Geldart, P.R. Brown, Analysis of Nucleotides by Capillary Electrophoresis, J. Chromatogr., A, 828 (1998) 317-336.

[68] F. Carlucci, A. Tabucchi, A. Aiuti, F. Rosi, F. Floccari, R. Pagani, E. Marinello, Capillary Electrophoresis in Diagnosis and Monitoring of Adenosine Deaminase Deficiency, Clin. Chem., 49 (2003) 1830-1838.

[69] J. Iqbal, J.C. Burbiel, C.E. Muller, Development of Off-Line and On-Line Capillary Electrophoresis Methods for the Screening and Characterization of Adenosine Kinase Inhibitors and Substrates, Electrophoresis, 27 (2006) 2505-2517.

[70] J. Zhang, J. Hoogmartens, A.V. Schepdael, Recent Developments and Applications of EMMA in Enzymatic and Derivatization Reactions, Electrophoresis, 31 (2010) 65-73.

[71] J. Bao, F.E. Regnier, Ultramicro Enzyme Assays in a Capillary Electrophoretic System, J. Chromatogr., 608 (1992) 217-224.

[72] F.E. Regnier, D.H. Patterson, B.J. Harmon, Electrophoretically-Mediated Microanalysis (EMMA), TrAC, Trends Anal. Chem., 14 (1995) 177-181.

[73] J. Saevels, K. Van den Steen, A. Van Schepdael, J. Hoogmartens, Study of the Competitive Inhibition of Adenosine Deaminase by Erythro-9-(2-Hydroxy-3-Nonyl)Adenine Using Capillary Zone Electrophoresis, J. Chromatogr., A, 745 (1996) 293-298.

[74] C.A. Monnig, J.W. Jorgenson, On-Column Sample Gating for High-Speed Capillary Zone Electrophoresis, Anal. Chem., 63 (1991) 802-807.

[75] L. Tao, J.E. Thompson, R.T. Kennedy, Optically Gated Capillary Electrophoresis of O-Phthalaldehyde/Beta-Mercaptoethanol Derivatives of Amino Acids for Chemical Monitoring, Anal. Chem., 70 (1998) 4015-4022.

[76] R.T. Kennedy, Bioanalytical Applications of Fast Capillary Electrophoresis, Anal. Chim. Acta, 400 (1999) 163-180.

[77] J.A. Lapos, A.G. Ewing, Injection of Fluorescently Labeled Analytes into Microfabricated Chips Using Optically Gated Electrophoresis, Anal. Chem., 72 (2000) 4598-4602.

[78] E.S. Roddy, H.W. Xu, A.G. Ewing, Sample Introduction Techniques for Microfabricated Separation Devices, Electrophoresis, 25 (2004) 229-242.

[79] H. Xu, A.G. Ewing, A Rapid Enzyme Assay for Beta -Galactosidase Using Optically Gated Sample Introduction on a Microfabricated Chip, Anal. Bioanal. Chem., 378 (2004) 1710-1715.

[80] H. Xu, A.G. Ewing, High-Throughput Enzyme Assay on a Multichannel Microchip Using Optically Gated Sample Introduction, Electrophoresis, 26 (2005) 4711-4717.

[81] K.F. Schrum, J.M. Lancaster, III, S.E. Johnston, S.D. Gilman, Monitoring Electroosmotic Flow by Periodic Photobleaching of a Dilute, Neutral Fluorophore, Anal. Chem., 72 (2000) 4317-4321.

[82] J.L. Pittman, C.S. Henry, S.D. Gilman, Experimental Studies of Electroosmotic Flow Dynamics in Microfabricated Devices During Current Monitoring Experiments, Anal. Chem., 75 (2003) 361-370.

[83] M. Azegami, K. Iwai, Specific Modification of Nucleic Acids and Their Constituents with Trinitrophenyl Group, J. Biochem., 55 (1964) 346-348.

[84] M. Azegami, K. Iwai, Trinitrophenylation of Nucleic Acids and Their Constituents, J. Biochem., 78 (1975) 409-420.

[85] Y.H. Rezenom, A.D. Wellman, L. Tilstra, C.D. Medley, S.D. Gilman, Separation and Detection of Individual Submicron Particles by Capillary Electrophoresis with Laser-Light-Scattering Detection, Analyst (Cambridge, U. K.), 132 (2007) 1215-1222.

[86] J.L. Pittman, H.J. Gessner, K.A. Frederick, E.M. Raby, J.B. Batts, S.D. Gilman, Experimental Studies of Electroosmotic Flow Dynamics During Sample Stacking for Capillary Electrophoresis, Anal. Chem., 75 (2003) 3531-3538.

[87] T. Hiratsuka, Biological-Activities and Spectroscopic Properties of Chromophoric and Fluorescent Analogs of Adenine Nucleoside and Nucleotides, 2',3'-O-(2,4,6-Trinitrocyclohexadienylidene) Adenosine Derivatives, Biochim. Biophys. Acta., 719 (1982) 509-517.

[88] T. Hiratsuka, K. Uchida, Preparation and Properties of 2'(or 3')-O-(2,4,3-Trinitrophenyl)Adenosine 5'-Triphosphate, an Analog of Adenosine Triphosphate, Biochim. Biophys. Acta, Gen. Subj., 320 (1973) 635-647.

[89] J.F. O'Grady, K.Y. Noonan, P. McDonnell, A.J. Mancuso, K.A. Frederick, Detecting Deviations from Pure Eof During CE Separations, Electrophoresis, 28 (2007) 2385-2390.

[90] K.E. Swords, P.B. Bartline, K.M. Roguski, S.A. Bashaw, K.A. Frederick, Assessment of Polyelectrolyte Coating Stability under Dynamic Buffer Conditions in CE, J. Sep. Sci., 34 (2011) 2427-2432.

[91] D. Beer, J. Weber, Photobleaching of Organic Laser Dyes, Opt. Commun., 5 (1972) 307-309.

[92] J. Weber, Continuously Uv-Bleaching of Organic Laser Dyes, Phys. Lett. A, 45A (1973) 35-36.

[93] J.R. Saylor, Photobleaching of Disodium Fluorescein in Water, Exp. Fluids, 18 (1995) 445-447.

[94] B. Hinkeldey, A. Schmitt, G. Jung, Comparative Photostability Studies of Bodipy and Fluorescein Dyes by Using Fluorescence Correlation Spectroscopy, Chemphyschem, 9 (2008) 2019-2027.

[95] J.H. Sugarman, R.K. Prudhomme, Effect of Photobleaching on the Output of an On-Column Laser Fluorescence Detector, Ind. Eng. Chem. Res., 26 (1987) 1449-1454.

[96] A.W. Moore, J.W. Jorgenson, Study of Zone Broadening in Optically Gated High-Speed Capillary Electrophoresis, Anal. Chem., 65 (1993) 3550-3560.

[97] J.E. Cronan, G.L. Waldrop, Multi-Subunit Acetyl-CoA Carboxylases, Prog. Lipid Res., 41 (2002) 407-435.

[98] C. Freiberg, N.A. Brunner, G. Schiffer, T. Lampe, J. Pohlmann, M. Brands, M. Raabe, D. Haebich, K. Ziegelbauer, Identification and Characterization of the First Class of Potent Bacterial Acetyl-CoA Carboxylase Inhibitors with Antibacterial Activity, J. Biol. Chem., 279 (2004) 26066-26073.

[99] I. Mochalkin, J.R. Miller, L. Narasimhan, V. Thanabal, P. Erdman, B. Cox Philip, J.V.N.V. Prasad, S. Lightle, D. Huband Michael, C.K. Stover, Discovery of Antibacterial Biotin Carboxylase Inhibitors by Virtual Screening and Fragment-Based Approaches, ACS Chem. Biol., 4 (2009) 473-483.

[100] M.D. Devine, A. Shukla, Altered Target Sites as a Mechanism of Herbicide Resistance, Crop Prot., 19 (2000) 881-889.

[101] L. Abu-Elheiga, M.M. Matzuk, K.A.H. Abo-Hashema, S.J. Wakil, Continuous Fatty Acid Oxidation and Reduced Fat Storage in Mice Lacking Acetyl-CoA Carboxylase 2, Science, 291 (2001) 2613-2616.

[102] L. Abu-Elheiga, W. Oh, P. Kordari, S.J. Wakil, Acetyl-CoA Carboxylase 2 Mutant Mice Are Protected against Obesity and Diabetes Induced by High-Fat/High-Carbohydrate Diets, Proc. Natl. Acad. Sci. U. S. A., 100 (2003) 10207-10212.

[103] H.J. Harwood, Jr., S.F. Petras, L.D. Shelly, L.M. Zaccaro, D.A. Perry, M.R. Makowski, D.M. Hargrove, K.A. Martin, W.R. Tracey, J.G. Chapman, W.P. Magee, D.K. Dalvie, V.F. Soliman, W.H. Martin, C.J. Mularski, S.A. Eisenbeis, Isozyme-Nonselective N-Substituted Bipiperidylcarboxamide Acetyl-CoA Carboxylase Inhibitors Reduce Tissue Malonyl-CoA Concentrations, Inhibit Fatty Acid Synthesis, and Increase Fatty Acid Oxidation in Cultured Cells and in Experimental Animals, J. Biol. Chem., 278 (2003) 37099-37111.

[104] K.L. Levert, G.L. Waldrop, J.M. Stephens, A Biotin Analog Inhibits Acetyl-CoA Carboxylase Activity and Adipogenesis, J. Biol. Chem., 277 (2002) 16347-16350.

[105] L. Abu-Elheiga, H.M. Wu, Z.W. Gu, R. Bressler, S.J. Wakil, Acetyl-CoA Carboxylase 2(-/-) Mutant Mice Are Protected against Fatty Liver under High-Fat, High-Carbohydrate Dietary and De Novo Lipogenic Conditions, J. Biol. Chem., 287 (2012) 12578-12588.

[106] A. Beckers, S. Organe, L. Tinunermans, K. Scheys, A. Peeters, K. Brusselmans, G. Verhoeven, J.V. Swinnen, Chemical Inhibition of Acetyl-CoA Carboxylase Induces Growth Arrest and Cytotoxicity Selectively in Cancer Cells, Cancer Res., 67 (2007) 8180-8187.

[107] C. Wang, C.X. Xu, M.W. Sun, D.X. Luo, D.F. Liao, D.L. Cao, Acetyl-CoA Carboxylase-Alpha Inhibitor Tofa Induces Human Cancer Cell Apoptosis, Biochem. Biophys. Res. Commun., 385 (2009) 302-306.

[108] R.B. Guchhait, S.E. Polakis, P. Dimroth, E. Stoll, J. Moss, M.D. Lane, Acetyl Coenzyme-A Carboxylase System of Escherichia-Coli - Purification and Properties of Biotin Carboxylase,

Carboxyltransferase, and Carboxyl Carrier Protein Components, J. Biol. Chem., 249 (1974) 6633-6645.

[109] J.K. Kroeger, J. Zarzycki, G. Fuchs, A Spectrophotometric Assay for Measuring Acetyl-Coenzyme A Carboxylase, Anal. Biochem., 411 (2011) 100-105.

[110] J. Alves, L. Westling, E.C. Peters, J.L. Harris, J.W. Trauger, Cloning, Expression, and Enzymatic Activity of Acinetobacter Baumannii and Klebsiella Pneumoniae Acetyl-Coenzyme a Carboxylases, Anal. Biochem., 417 (2011) 103-111.

[111] N. Santoro, T. Brtva, S. Vander Roest, K. Siegel, G.L. Waldrop, A High-Throughput Screening Assay for the Carboxyltransferase Subunit of Acetyl-CoA Carboxylase, Anal. Biochem., 354 (2006) 70-77.

[112] A. Soriano, A.D. Radice, A.H. Herbitter, E.F. Langsdorf, J.M. Stafford, S. Chan, S.H. Wang, Y.H. Liu, T.A. Black, Escherichia Coli Acetyl-Coenzyme A Carboxylase: Characterization and Development of a High-Throughput Assay, Anal. Biochem., 349 (2006) 268-276.

[113] R. Seethala, Z.P. Ma, R. Golla, D. Cheng, A Homogeneous Scintillation Proximity Assay for Acetyl Coenzyme - A Carboxylase Coupled to Fatty Acid Synthase, Anal. Biochem., 358 (2006) 257-265.

[114] Y.C. Liu, L. Zalameda, K.W. Kim, M.H. Wang, J.D. McCarter, Discovery of Acetyl-Coenzyme a Carboxylase 2 Inhibitors: Comparison of a Fluorescence Intensity-Based Phosphate Assay and a Fluorescence Polarization-Based ADP Assay for High-Throughput Screening, Assay Drug Dev. Technol., 5 (2007) 225-235.

[115] C.C. Chung, K. Ohwaki, J.E. Schneeweis, E. Stec, J.P. Varnerin, P.N. Goudreau, A. Chang, J. Cassaday, L.H. Yang, T. Yamakawa, O. Kornienko, P. Hodder, J. Inglese, M. Ferrer, B. Strulovici, J. Kusunoki, M.R. Tota, T. Takagi, A Fluorescence-Based Thiol Quantification Assay for Ultra-High-Throughput Screening for Inhibitors of Coenzyme A Production, Assay Drug Dev. Technol., 6 (2008) 361-374.

[116] G. Meades, Jr., R.L. Henken, G.L. Waldrop, M.M. Rahman, S.D. Gilman, G.P.P. Kamatou, A.M. Viljoen, S. Gibbons, Constituents of Cinnamon Inhibit Bacterial Acetyl CoA Carboxylase, Planta Med., 76 (2010) 1570-1575.

[117] C.Z. Blanchard, G.L. Waldrop, Overexpression and Kinetic Characterization of the Carboxyltransferase Component of Acetyl-CoA Carboxylase, J. Biol. Chem., 273 (1998) 19140-19145.

[118] M.C. Breadmore, M. Dawod, J.P. Quirino, Recent Advances in Enhancing the Sensitivity of Electrophoresis and Electrochromatography in Capillaries and Microchips (2008-2010), Electrophoresis, 32 (2011) 127-148.

[119] Z. Mala, P. Gebauer, P. Bocek, System Effects in Sample Self-Stacking CZE: Single Analyte Peak Splitting of Salt-Containing Samples, Electrophoresis, 30 (2009) 866-874.

[120] C.Z. Blanchard, Y.M. Lee, P.A. Frantom, G.L. Waldrop, Mutations at Four Active Site Residues of Biotin Carboxylase Abolish Substrate-Induced Synergism by Biotin, Biochemistry, 38 (1999) 3393-3400.

[121] I. Mochalkin, J.R. Miller, A. Evdokimov, S. Lightle, C. Yan, C.K. Stover, G.L. Waldrop, Structural Evidence for Substrate-Induced Synergism and Half-Sites Reactivity in Biotin Carboxylase, Protein Sci., 17 (2008) 1706-1718.

[122] J. Needham, M.T. Kelly, M. Ishige, R.J. Andersen, Andrimid and Moiramides A-C, Metabolites Produced in Culture by a Marine Isolate of the Bacterium Pseudomonas-Fluorescens - Structure Elucidation and Biosynthesis, J. Org. Chem., 59 (1994) 2058-2063.

[123] C. Nathan, Fresh Approaches to Anti-Infective Therapies, Science Translational Medicine, 4 (2012).

[124] J. Spizek, J. Novotna, T. Rezanka, A.L. Demain, Do We Need New Antibiotics? The Search for New Targets and New Compounds, J. Ind. Microbiol. Biotechnol., 37 (2010) 1241-1248.

[125] H. Nikaido, Multidrug Resistance in Bacteria, Annu. Rev. Biochem., 2009, pp. 119-146.

[126] A.L. Demain, J. Spizek, The Antibiotic Crisis, Adv. Mol. Cell. Microbiol., 22 (2012) 26-43.

[127] M.S. Butler, M.A. Cooper, Antibiotics in the Clinical Pipeline in 2011, J. Antibiot., 64 (2011) 413-425.

[128] M.A. Cooper, D. Shlaes, Fix the Antibiotics Pipeline, Nature, 472 (2011) 32-32.

[129] E.D. Brown, G.D. Wright, New Targets and Screening Approaches in Antimicrobial Drug Discovery, Chem. Rev., 105 (2005) 759-774.

[130] G.L. Waldrop, Acetyl-CoA Carboxylase as a Target for Antibacterial Development, Adv. Mol. Cell. Microbiol., 22 (2012) 208-219.

[131] J.R. Miller, S. Dunham, I. Mochalkin, C. Banotai, M. Bowman, S. Buist, B. Dunkle, D. Hanna, H.J. Harwood, M.D. Huband, A. Karnovsky, M. Kuhn, C. Limberakis, J.Y. Liu, S. Mehrens, W.T. Mueller, L. Narasimhan, A. Ogden, J. Ohren, J. Prasad, J.A. Shelly, L. Skerlos, M. Sulavik, V.H. Thomas, S. VanderRoest, L.A. Wang, Z.G. Wang, A. Whitton, T. Zhu, C.K. Stover, A Class of Selective Antibacterials Derived from a Protein Kinase Inhibitor Pharmacophore, Proc. Natl. Acad. Sci. U. S. A., 106 (2009) 1737-1742.

[132] C.C. Cheng, G.W. Shipps, Z.W. Yang, B.Y. Sun, N. Kawahata, K.A. Soucy, A. Soriano, P. Orth, L. Xiao, P. Mann, T. Black, Discovery and Optimization of Antibacterial AccC Inhibitors, Bioorg. Med. Chem. Lett., 19 (2009) 6507-6514.

[133] D.J. Newman, G.M. Cragg, K.M. Snader, Natural Products as Sources of New Drugs over the Period 1981-2002, J. Nat. Prod., 66 (2003) 1022-1037.

[134] H. Nehme, R. Nehme, P. Lafite, S. Routier, P. Morin, New Development in in-Capillary Electrophoresis Techniques for Kinetic and Inhibition Study of Enzymes, Anal. Chim. Acta, 722 (2012) 127-135.

[135] S.K. Bryant, G.L. Waldrop, S.D. Gilman, A Capillary Electrophoretic Assay for Acetyl CoA Carboxylase, Anal. Biochem., 437 (2013) 32-38.

[136] T. Broussard, A.E. Price, S.M. Laborde, G.L. Waldrop, Complex Formation and Regulation of Escherichia Coli Acetyl-CoA Carboxylase, Biochemistry, (2013) In press.

[137] H. Chen, Y.G. Zuo, Y.W. Deng, Separation and Determination of Flavonoids and Other Phenolic Compounds in Cranberry Juice by High-Performance Liquid Chromatography, J. Chromatogr., A, 913 (2001) 387-395.

[138] S. Hakkinen, M. Heinonen, S. Karenlampi, H. Mykkanen, J. Ruuskanen, R. Torronen, Screening of Selected Flavonoids and Phenolic Acids in 19 Berries, Food Res. Int., 32 (1999) 345-353.

[139] S.H. Hakkinen, S.O. Karenlampi, I.M. Heinonen, H.M. Mykkanen, A.R. Torronen, Content of the Flavonols Quercetin, Myricetin, and Kaempferol in 25 Edible Berries, J. Agric. Food Chem., 47 (1999) 2274-2279.

[140] J.M. Harnly, R.F. Doherty, G.R. Beecher, J.M. Holden, D.B. Haytowitz, S. Bhagwat, S. Gebhardt, Flavonoid Content of Us Fruits, Vegetables, and Nuts, J. Agric. Food Chem., 54 (2006) 9966-9977.

[141] G. O'Mahony, E. Ehrman, M. Grotli, Adenosine-Based Fluorosides Containing a Novel Heterocyclic Ring System, Collection Symposium Series, 7 (2005) 233-237.

[142] P. Virta, T. Holmstrom, T. Munter, T. Nyholm, L. Kronberg, R. Sjoholm, Fluorescent 7- and 8-Methyl Etheno Derivatives of Adenosine and 6-Amino-9-Ethylpurine: Syntheses and Fluorescence Properties, Nucleosides, Nucleotides & Nucleic Acids, 22 (2003) 85-98.

[143] K.F. Yip, K.C. Tsou, Synthesis of Fluorescent Adenosine Derivatives, Tetrahedron Lett., (1973) 3087-3090.

[144] M.E. Hawkins, W. Pfleiderer, O. Jungmann, F.M. Balis, Synthesis and Fluorescence Characterization of Pteridine Adenosine Nucleoside Analogs for DNA Incorporation, Anal. Biochem., 298 (2001) 231-240.

[145] A. Leskovar, J. Reinstein, Photophysical Properties of Popular Fluorescent Adenosine Nucleotide Analogs Used in Enzyme Mechanism Probing, Arch. Biochem. Biophys., 473 (2008) 16-24.

APPENDIX 1. TOWARD TOTAL AUTOMATION OF MICROFLUIDICS FOR EXTRATERRESTIAL IN SITUANALYSIS[2]

The studies described herein were conducted at the National Aeronautics and Space Agency Jet Propulsion Laboratory (NASA-JPL) and published in collaboration with other researchers. I worked at NASA-JPL as a Summer 2010 NASA Harriett G. Jenkins Fellowship Program Mini Research Award recipient. I submitted a proposal for the competitive award and was selected to receive funding for my summer work at NASA-JPL. My role was to automate lab-on-a-chip instrumentation for end-to-end analysis of amino acids. I successfully carried out automated on-chip fluorescence derivatization of amino acids and on-chip pumping and mixing of buffers and samples, resulting in an end-to-end analysis of amino acid samples that was completely controlled using a computer. I achieved the automation and performed initial optimization of the derivatization, mixing and separation steps, and further optimization of the method to complete the work for the manuscript was performed by the other authors.

Introduction

One of the primary goals of planetary exploration is to determine the potential for past, present, or future life on extraterrestrial bodies. Despite multiple orbiter and landed missions to extraterrestrial bodies such as Mars and Titan, we still know relatively little about their detailed chemical composition. Quantitative chemical compositional analysis provides vital chemical information on the processes that shape these environments, including details on abiotic or potentially biotic sources of organic chemistry. For example, abiotic processes lead to a racemic statistical distribution of organic molecules, while biotic processes enrich the few organic

---

molecules essential for life resulting in homochirality.[1-2] In order to learn as much as possible about these environments, which may contain only trace quantities of organic material, fully-automated instrumentation capable of sensitive analysis of a broad range of organic molecules is needed.

Capillary electrophoresis (CE) is a powerful liquid-based chemical analytical technique that has been widely used for the analysis of a large range of biomolecules,[3-8] including amino acids,[9-12] and thus is a well-suited technique for *in situ* extraterrestrial chemical analyses. CE provides highly efficient separations with minimal sample consumption and short analysis times. There have been significant developments in the field of CE in the last decade in miniaturization to create portable separation and detection units.[13-16] In the field of planetary exploration, miniaturized CE systems have been incorporated into instrument prototypes for detection of life on other planetary bodies, including Mars.[17-20] CE has proven to be easily miniaturized to lab-on-a-chip (LOC) systems offering great versatility, custom design, high throughput, and even lower volumes and times of analysis.[13] These microchip-CE devices (µCE) have low mass, volume, and power requirements, making them well-suited for the scientific payloads of planetary probes.

Although several materials can be used to fabricate microchips, glass is highly suitable for *in situ* planetary exploration due to its compatibility with planetary protection and contamination control procedures used to ultrasterilize spacecraft probes and instruments. Additionally, the surface chemistry of glass is well understood, which allows precise control of electro-osmotic flow, yielding highly efficient and reproducible electrophoretic separations. Finally, glass microchips have high mechanical strength, high chemical resistance, low conductivity, and are compatible with optical detection techniques.[21]

A μCE analysis requires fluidic manipulation, which involves the incorporation of valves or switches into the design. A variety of microfabricated valves and pumps have been reported for on-chip fluidic manipulation.[22-31] Multiple devices for *in situ* planetary analyses have been published based on these devices, including simple fluidic routing structures, based on pneumatically actuated monolithic membrane microvalves.[17, 19] These devices rely on a polymer elastomer, which can be PDMS or a fluorinated polymer such as Teflon or perfloropolyether.[29-30] Typically, PDMS is used in the laboratory because it allows easy and for rapid prototyping. While work to partially automate sample processing steps including fluorescent derivatization, serial dilutions, and mixing with a standard have been reported, to date these methods have inadequately integrated sample processing steps with sample analysis into a single device. Although the Mars Organic Analyzer (MOA) incorporated fluidic routing features into microfluidic systems, these methods required operator involvement and the use of PEEK tubing interfaces between two separate microdevices. To date, these devices have not incorporated all processing steps into a single microfluidic device. Here, we present a fully integrated four-layer microchip electrophoresis device for end-to-end μCE analysis of amino acids. The device consists of bonded layers of Borofloat glass wafers and a flexible PDMS membrane. We demonstrate labeling, dilution, and separation of amino acids with this device with minimal operator intervention. The solutions were placed in the appropriate reservoirs at the beginning of the experiment and all subsequent fluidic manipulations were performed via a microvalve circuit designed for autonomous investigations. The objective of this work was to develop and demonstrate a complete system that could thus be used for future *in situ* extraterrestrial exploration. All that would be required of the spacecraft probe would be to deliver an aqueous sample to a system having the capabilities described here. To the best of our knowledge, this is

the first report of a LOC automated end-to-end µCE analysis of amino acids where ***all*** of the sample preparation and chemical analysis steps are performed on a single, fully integrated device.

Experimental Section

Reagents and Solutions

All chemicals were analytical reagent grade and used as received. Sodium tetraborate ($Na_2B_4O_7 \cdot 10H_2O$) and sodium hydroxide were purchased from Fisher Scientific (Fair Lawn, NJ). Isopropanol was purchased from Sigma-Aldrich (St. Louis, MO). All aqueous solutions were prepared using 18 MΩ·cm water. The pH was adjusted using either 1 M NaOH or 1 M HCl (Sigma-Aldrich, St. Louis, MO) and measured using a glass electrode and a digital pH meter (Orion 290A, Thermo; Waltham, MA). L-valine, L-alanine, L-serine, glycine, and L-citrulline were purchased from Sigma-Aldrich (Saint Louis, MO). Pacific Blue succinimidyl ester (PB) was purchased from Invitrogen (Carlsbad, CA). Stock solutions of amino acids (10 mM in water) and Pacific Blue (20 mM in dimethylformamide (DMF)) were prepared and kept frozen (-20 °C) when not in use. The labeling reaction was performed on and off-chip by mixing amino acids and PB (200 µM) and allowing the reaction to proceed for at least 1 hour. The reaction was performed in 25 mM tetraborate buffer, pH 9.2. Other amino acid solutions were prepared by diluting the corresponding amount of stock in buffer.

Microfabrication

Multilayer microdevices were prepared as previously described with minimal modifications. [17, 27] For the µCE / pneumatic layers, 100 mm diameter 1.1 mm thick Borofloat wafers were coated with > 2000 Å aSi using LPCVD. The wafers were spin-coated with SPR 220-7 photoresist and patterned with the desired features. The aSi hard mask was patterned

using SiF_6 plasma, and the Borofloat was wet-etched using 49% HF. The electrophoretic layer was patterned first, while the pneumatic layer face was protected with blue tape. The pneumatic layer was patterned second, while the electrophoretic layer was protected with blue tape, except during backside alignment steps. Fluidic and electrophoretic access holes were drilled in the wafer with a diamond-tipped drill bit then the aSi hard mask was stripped. After dipping the wafer and a 700 mm backing wafer in AZ developer, the two wafers were manually pressed together to create a low-temperature temporary bond. This bond was solidified by bonding between two Macor blocks under weights at 668 °C for 12 hrs. A fluidic wafer was patterned and etched in a similar manner, and both the bonded two-wafer stack and the fluidic wafer were ashed with O_2 plasma prior to being bonded in a 4-layer stack utilizing a 250 mm PDMS gasket sandwiched between the glass layers.

The microfabrication process produced separation channels that were 8.5 cm long, 50 μm wide, 20 mm deep with a 1.0 cm long cross injection channel located at 0.5 cm from the anode. Pneumatic features were etched to 300 mm depth, while the fluidic features were etched to 150 mm depth. Holes were punched immediately post-assembly in the PDMS membrane to enable fluidic access between the fluidic wafer and the μCE reservoirs. The assembly of the microdevice is depicted in Figure 1. Additional fluidic reservoirs were made in 3 mm thick PDMS using a 4 mm diameter circular punch and bonded to the uppermost glass surface of the fluidic wafer. Finally, pipettor tips were placed in these PDMS fluidic reservoirs to hold larger volumes (< 1 mL) when needed.
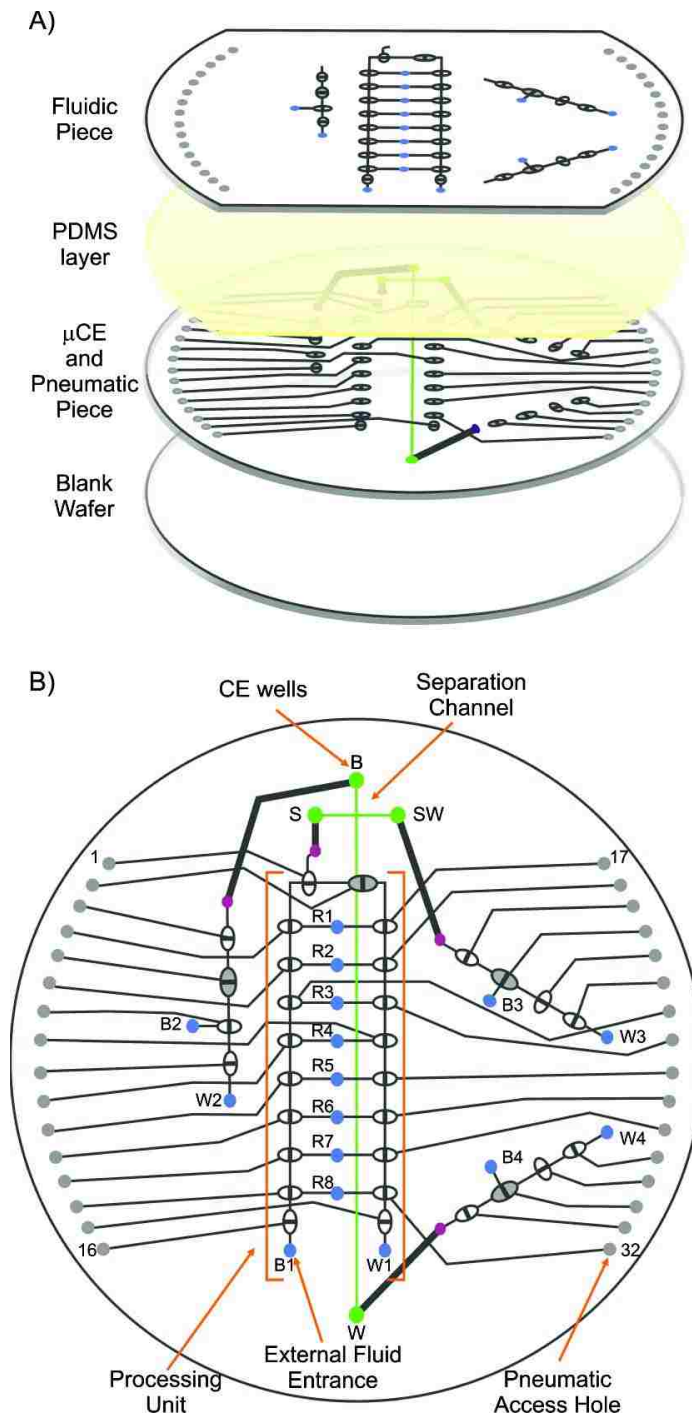
Figure 1. Microfluidic circuit for end-to-end μCE analysis. Schematic representation of A) assembly of the four-layer device and the features of each layer, and B) microfluidic circuit layout including separation channel and μCE reservoirs: sample (S), sample waste (SW), buffer (B), and waste (W), as well as fluid reservoirs. Reservoirs containing buffer for delivery to μCE wells are R1, B2, B3, and B4. Buffer reservoir B1 is used to rinse the processing unit to W1 (waste) between runs. The wells S, SW, B, W can be emptied to the respective waste reservoirs W1, W3, W2, and W4. The processing unit contains reservoirs R1 to R8 for sample, standards, and reagents handling.

Microdevice Operation

Devices were mounted inside a polycarbonate fixture designed in our laboratory (See Figure SI-1). The assembly was placed on the microscope stage for fluorescence detection. The top fixture was used to make individual pneumatic connections between each of the 32 pneumatic access holes and a manifold containing 32 solenoid valves. Depending upon the state of the solenoid valve, microvalves are either open (i.e. when solenoid is connected to vacuum) or closed (when solenoid is connected to N_2). A GAST Vacuum Pressure Pump, Xantrex XHR 300-2 DC Power Supply, National Instruments cDAQ-9172 CompactDAQ Chassis, and National Instruments 9472 8-channel Output Module were used for this purpose. Figure 1B shows a schematic drawing of the 32-valves device used for all the experiments described here. A National Instruments LabView 8.5 virtual instrument interface was employed to control opening and closing of the valves.

Microchip Capillary Electrophoresis

A LabSmith HVS448 High Voltage Sequencer (Livermore, CA) was used to control voltages applied to electrophoresis wells during injection (25 sec) and separation (200 sec). Laser-induced fluorescence detection was performed with a commercial Nikon Eclipse TE2000-U inverted microscope system. A 405 nm Melles Griot Diode Laser (CVI Melles Griot, Carlsbad, CA) was used for excitation and emission was detected by a CCD camera (Cascade 650, Photometrics). Tetraborate buffer (25 mM, pH 9.2) was used for labeling reactions and all CE separations. The separation channel was conditioned before use with 0.1 M NaOH for 10 min, followed by water and buffer for 5 min each. Initial experiments to optimize labeling conditions were performed on a commercial microchip (Micralyne Inc., Edmonton, Canada). For the four-layer device, prior to each experiment, buffer was pumped to each reservoir and a

baseline electropherogram was acquired. Then, the sample reservoir was emptied, the sample was pumped into the reservoir and the CE separation was performed. After each run, the sample was pumped in and out of the CE well for 10 cycles in order to ensure complete mixing and then the next separation was performed. During injection, 700, 1000, 0, and 900 V were applied to buffer, sample, sample waste, and waste respectively. After 25 sec the potentials were switched to 3000, 1700, 1700, and -2000 V. Data was processed using PeakFit (Systat Software Inc., San Jose CA). Electropherograms were baseline-corrected and filtered using a 0.2% Loess function. Peak migration times were corrected using Origin 8.1 (OriginLab Corporation, Northampton, MA) to account for run-to-run variations.

Off-Chip Fluorescence Measurements

A Fluorolog-3 Fluorescence Spectrometer (Horiba Jobin-Yvon) was used to determine the fluorescence of solutions of Pacific Blue. Solutions were placed in quartz cuvettes (1 cm pathlength) and the emission spectra (excitation at 405 nm, emission from 410-550 nm) were obtained in triplicate. All spectra were obtained as a ratio of corrected signal to corrected reference (Sc/Rc) to eliminate the effect of varying background radiation in the sample chamber; emission intensities are in units of counts per second per microampere (cps/μA). Spectra were processed with PeakFit (Systat Software Inc., San Jose, CA) to obtain the maximum signal.

Results and Discussion

Pacific Blue was selected as the fluorescent label for this study based on its high extinction coefficient (46,000 cm^{-1}M^{-1}) that enables low limits of detection of amino acids in extraterrestial sample extracts.[20, 32] A set of five amino acids that are well-resolved by microchip capillary electrophoresis was used as a standard mixture to demonstrate the capabilities of the device proposed here. Among the amino acids that are expected in extraterrestrial samples,[33-35]

we selected for our standard mixture two major amino acid components of meteorites[33] that have also been produced by some abiotic model syntheses[36] (alanine and glycine), two minor components of meteorites (serine and valine), and we also included a terrestrial contamination marker from the urea cycle (citrulline[37]).

In order to optimize the sensitivity of LIF to trace quantities of amino acids, we studied the response of a mixture of amino acids (Cit, Val, Ser, and Gly) labeled with Pacific Blue over a range of different experimental conditions (see SI_Figure 1 and SI_Figure 2). The highest labeling efficiency was obtained at pH ~ 9. It was also observed that a high ratio of PB to amino acid improves the labeling efficiency, we thus selected a ratio of 20 to assure the proper labeling of low concentrations of amino acids on the sample.

Device Characterization

The design of the microfluidic device used for all the experiments described here is shown in Figure 1B. There are 32 valves arranged in three sets of four valves used to pump fluid in and out of the μCE wells (B, SW, and W) and 20 valves located in the processing unit. This unit contains eight fluidic reservoirs (R1 to R8) that can be used for storage of samples, reagents, and standards as well as for performing all the sample pretreatment steps before electrophoretic separation. This unit is connected to the sample μCE well (S) so any solution placed on the fluidic reservoirs (R1 to R8) can be analyzed by the CE system.

Each microvalve consists of an etched displacement chamber on the top surface of the pneumatic manifold wafer, an elastomeric membrane layer, and a discontinuous channel structure on the bottom of the fluidic wafer. Applying vacuum to the displacement chamber pulls the membrane down, opening the valve and allowing connection of the fluidic channels across the discontinuity and movement of fluids. The valve is closed by releasing the vacuum or

applying a slight pressure. As previously described[27], by actuating three serially connected valves in a cycle, a self-priming diaphragm pump is created. These valves were fully characterized by Grover *et al.*[27] The flow rates obtained with this type of pump depend on the dimensions of the fluidic channel, the displacement chamber volume, and the valve actuation times. The actuation times also determine the total time required for each pumping step, so optimization is required in order to pump the highest volume of liquid in the least possible time. Several elastomeric polymers have been integrated with glass to form monolithic membrane microvalve devices. While fluorinated membranes have been developed in our lab and proven suitable for the extreme conditions associated with extraterrestrial analyses, we selected polydimethylsiloxane (PDMS) membranes based on their ease of fabrication for rapid prototyping.[22, 27]

In order to determine the optimal actuation time for our fluidic design, the volume of water transferred in 20 cycles from R1 to its closest and farthest neighbor reservoirs, R2 and R8 respectively, was measured for actuation times ranging from 10 to 750 msec. Figure 2 shows the pumping rate as a function of actuation time for R1 to R2 and R1 to R8 and also the total volume displaced from R1 to R2. For the minimum-distance transfer (R1-R2), the pumping rate decreases, but the volume increases with longer actuation times. At fast actuation times the valves do not fully open or close in each cycle, so less volume than the maximum is transferred in each cycle. For actuation times ³ 250 msec, the valves have enough time to fully open and close and consequently, the volume pumped per cycle no longer increases. It can also be observed in Figure 2 that the pumping rates for R1 to R8 are smaller than those for R1 to R2 for actuation times less than 500 msec. Because the fluidic resistance is higher for reservoirs and valves farther apart in the layout, longer actuation times are required to transfer the same volume

of fluid. Even though a 500 msec actuation time increases the total time required for each cycle, it was selected as the optimum value for the rest of the experiments because it permits a uniform pumping rate throughout the processing unit, simplifying the operation of the system. To evaluate chip-to-chip reproducibility, the volume pumped from R1 to each of the other reservoirs with an actuation time of 500 msec was measured for two microfluidic devices. The average volumes obtained for each device were (12 ± 1) mL and (11.2 ± 0.8) mL indicating that although the alignment may be slightly different for different devices due to deviations in human hand-to-eye coordination, the pumping rates are consistent. All valves remained functional after the device was stored for a period of eight months. Additionally, we did not observe any microdevice failure (by PDMS irreversible sealing to the glass) after approximately 100,000 actuations over a period of 10 days of continuous use.
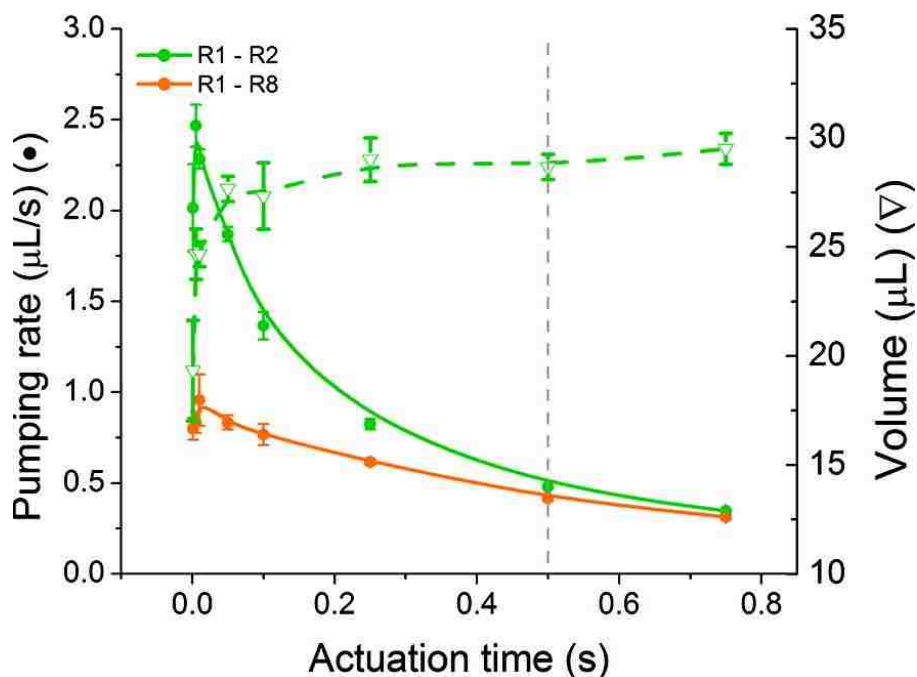
Figure 2. Pumping rate (●) and volume (Ñ) for 20 cycles pumping from R1 to R2 (─) and R1 to R8 (─). Volumes were measured in triplicates and error bars were calculated as the standard deviation of the 3 measurements.

To validate the proposed microfluidic circuit for quantitative manipulation of fluids, serial dilutions of a 20 mM PB solution were performed both manually off-chip and on-chip in duplicate. The fluorescence of the solutions was then measured and correlated to the expected concentration. Figure 3 shows the signal as a function of the concentration of PB for the three sets of sequential dilutions (20 to 0.625 mM). As can be observed in the figure, the dilutions performed using the automated pumping system correlate well with the dilutions performed manually off-chip, thus validating the system for quantitative handling of solutions prior to analysis by µCE.
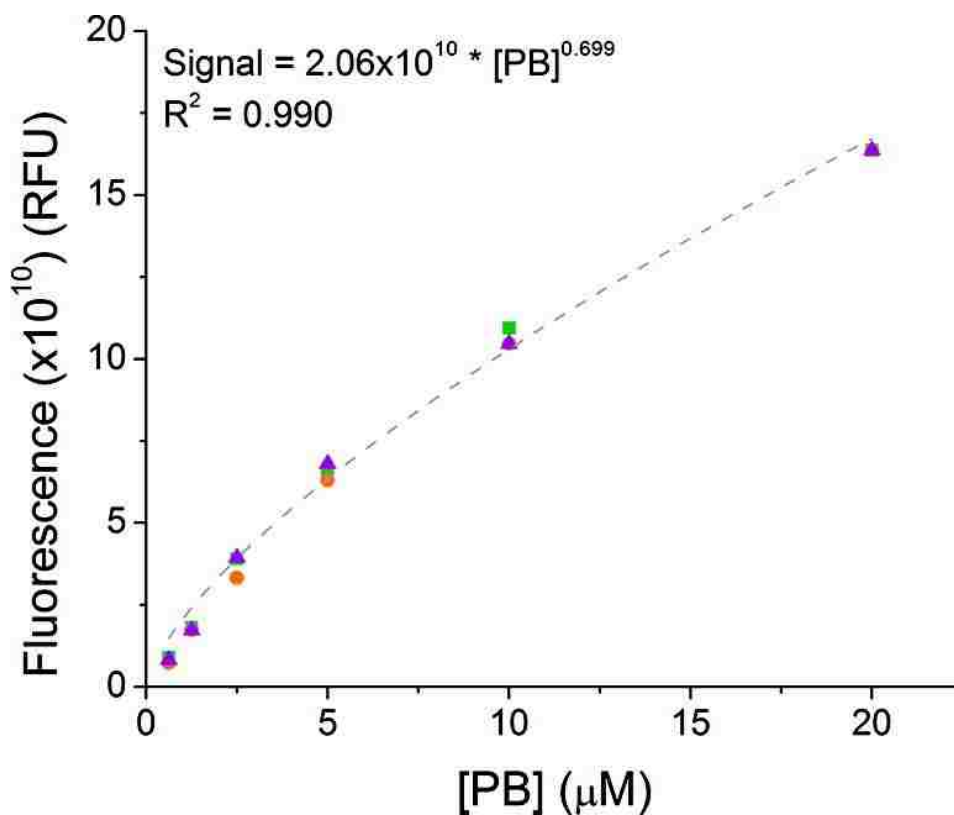
Figure 3. Fluorescence signal obtained for solutions of PB diluted sequentially from a 20 mM solution, (■) off-chip, (●) on-chip repetition 1, (▲) on-chip repetition 2. Dashed line represents the power fit for the standard dilution performed off-chip.

End-to-End Analysis

Once the operation of the processing unit was optimized and validated, an automated µCE end-to-end analysis of amino acids involving labeling, dilution, and spiking was performed. For the end-to-end analysis, R1 was filled with buffer, R2 with 50 µL of PB (500 µM), R3 with 250 µL of the three unlabeled amino acid (simulated unknown sample) mixture (10 µM each), and R8 with 250 µL of the PB-labeled amino acid standard (100 nM each). The rest of the reservoirs were used for dilution of the labeled sample (R5 and R6) and for mixing with the standard solution (R7). The sequences of mixing and dilutions performed are described briefly here; more detail is provided in the Supplementary Information. The experiments were performed in the following sequence. First, sample and dye were mixed; the solution was then left to react for at least 1 hour and then diluted to a final concentration of 160 nM. The processing unit was then rinsed to remove residual sample (labeled or unlabeled amino acids) to avoid contamination or false positives. Then, buffer was pumped to each CE well (50 µL) and a blank electropherogram was obtained (Figure 4A). The sample reservoir was emptied, filled with the amino acid standard solution, and three electrophoretic separations were acquired (Figure 4B). After analyzing the standard, the processing unit was rinsed with buffer, S was emptied and filled with buffer and a blank run was acquired again to assure that the system was clean. Next, S was emptied and then filled with the on-chip labeled-sample and electropherograms were obtained (Figure 4C). As can be observed in the figure, the sample was successfully labeled on-chip. The system was then rinsed and the blank run was acquired again. Finally, the on-chip labeled sample and the standard were mixed and pumped to S for analysis (Figure 4D). The presence of five peaks in Figure 4D indicates that the sample and the standard were well mixed on-chip. A dilution effect (smaller peaks) is observed for Ser and Gly, which were only present

in the standard, and for Ala which in only present on the simulated sample. Although each solution was measured in triplicate, Figure 4 only shows one electropherogram for clarity of data presentation.
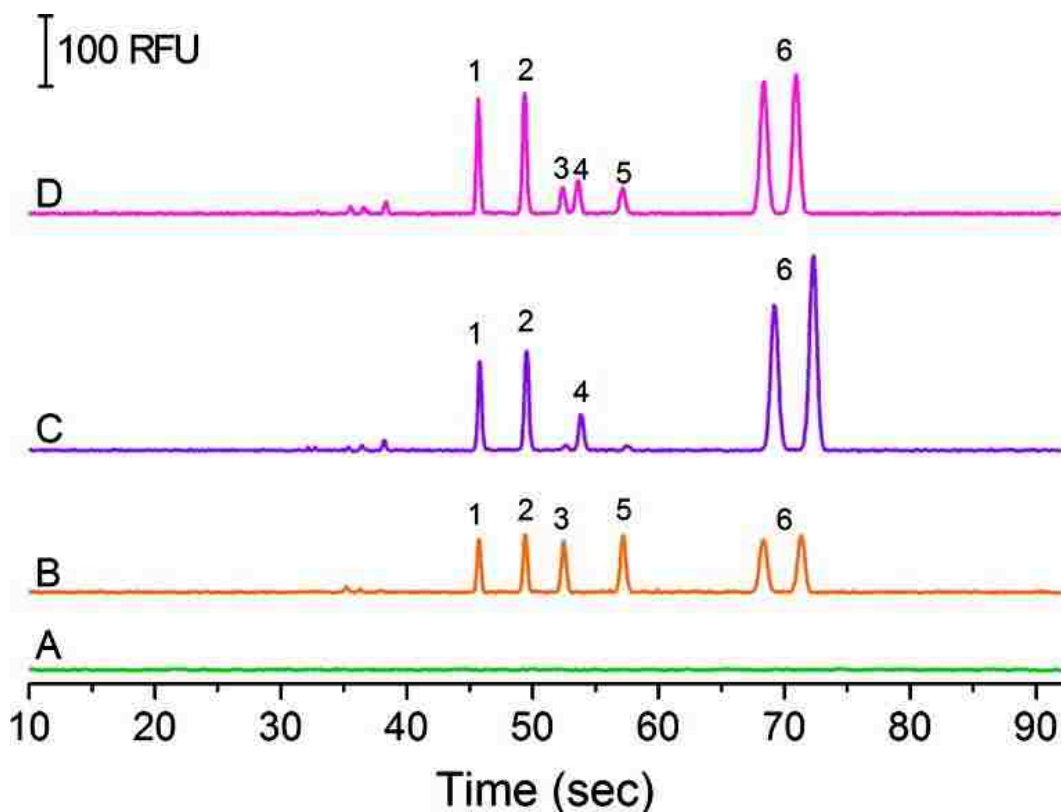
Figure 4. Results from a completely automated on-chip analysis of amino acid mixtures. Labeling and analysis of amino acid mixtures on-chip. A) blank run (buffer only), B) standard solution containing 100 nM of PB-labeled (1) Cit, (2) Val, (3) Ser, and (5) Gly. C) ~160 nM sample of (1) Cit, (2) Val, and (4) Ala diluted from 10 μM sample labeled on-chip. D) mixture of B) and C). Conditions: 25 mM tetraborate buffer pH = 9.2, V_{SEP} = 5 kV.

The sensitivity of our system was tested with the standard mixture of amino acids. Figure 5 shows the calibration curves obtained manually for solutions of Cit and Gly diluted from a stock labeled with PB. The LOD were calculated as the concentration yielding a signal-to-noise ratio (S/N) of 3. LOD for Cit, Val, Ser, Ala, and Gly were (0.94 ± 0.01), (0.70 ± 0.01), (1.17 ± 0.02), (1.05 ± 0.01), and (1.33 ± 0.02) nM respectively.

Due to the significant increase in capability represented by the novel microdevice demonstrated here and the challenge of obtaining relevant samples of astrobiological interest, the automated analysis of real samples remains outside the scope of this work. We are currently pursuing collaborations to obtain relevant samples; their autonomous analyses will be published separately.
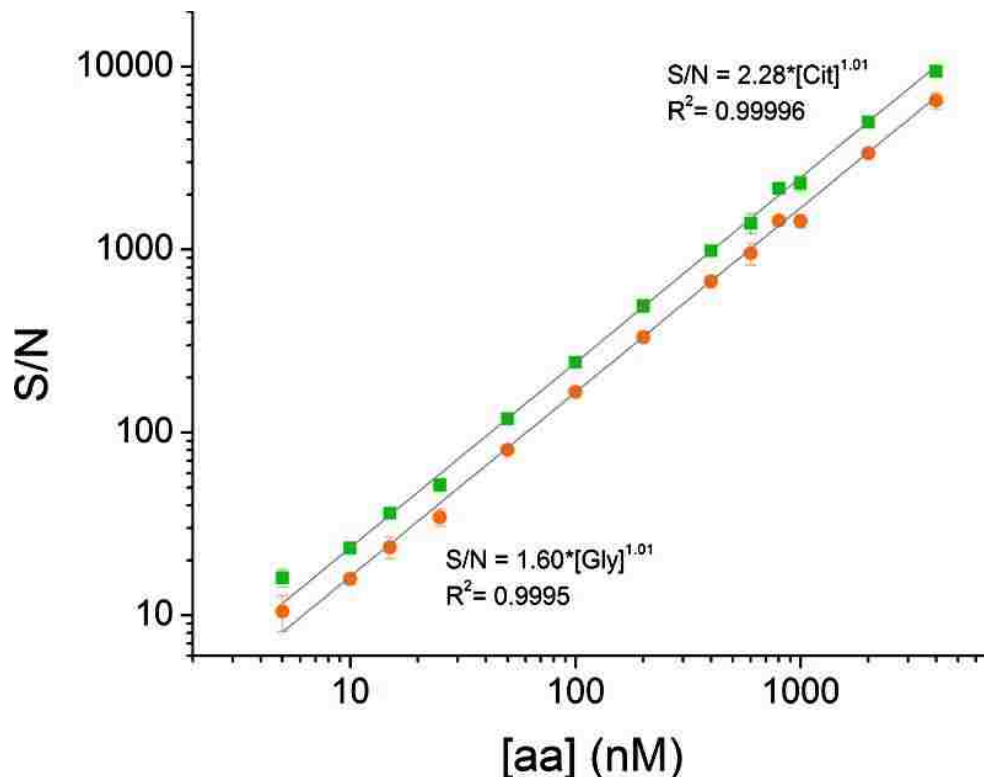
Figure 5. Calibration curves for (■) Cit, (●)Gly. Conditions: 25 mM tetraborate buffer pH = 9.2, V_{SEP} = 6 kV. Each concentration was measured in triplicates and error bars were calculated as the standard deviation of the 3 measurements.

Conclusions

This paper describes a novel four-layer fully-integrated microfluidic device that successfully executes automated end-to-end microchip capillary electrophoresis analyses. The performance of the device was demonstrated by electrophoretic analysis of a sample of amino acids labeled, diluted, and spiked on-chip. The entire process was exclusively controlled via

computer and the only intervention of the operator was to place the solutions in reservoirs prior to beginning the experiment. To our knowledge, this is the first demonstration of a completely automated end-to-end μCE analysis of amino acids on a single fully-integrated microfluidic device. This effort is critical in advancing the technology readiness level of μCE systems for future *in situ* spaceflight investigations to targets such as Mars, Europa, and Titan, *etc.* where complete automation is required. In addition, the fully autonomous fluidic processing for microchip capillary electrophoretic analyses reported here also has a number of terrestrial applications, ranging from point-of-care analyses to environmental monitoring.

Supplementary Information

Optimization of Labeling Conditions

In order to optimize the sensitivity of LIF to trace quantities of amino acids, we studied the response of a mixture of amino acids (Cit, Val, Ser, and Gly) labeled with Pacific Blue over a range of different experimental conditions. In order to assess the effect of pH on labeling efficiency, solutions containing 2 μM of each amino acid were reacted with 200 μM PB at pH values ranging from 7.0 to 10.5. Samples were then diluted to 100 nM and separated by capillary electrophoresis using a commercial microchip. SI_Figure 1 shows the peak area for serine as a function of the pH when the reaction was left to proceed for 1 and 24 hours. As can be observed in SI_Figure 1, for a 1 hour reaction, pH values between 8 and 9 give the maximum fluorescent signal. However, when the reaction was left to proceed overnight, signals decreased for pH values above 9. These results indicate that slow base catalyzed hydrolysis occurs after rapid reactions at $8 \leq pH \leq 9$. In order to obtain the highest labeling efficiency in the shortest time, labeling reactions were performed at pH ~ 9. Thus, the degradation occurring at high pH values

is avoided and the reaction occurs in only 1 hour. The same trend was observed for all the amino

acids and only serine is showed here for clarity.
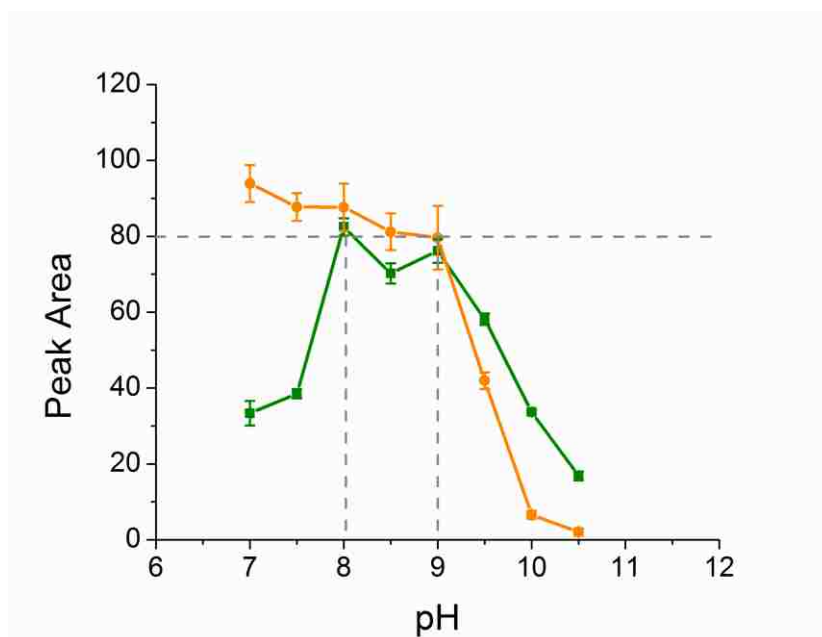
In order to determine the effect of the amino acid concentration on the efficiency of the

labeling reaction, solutions ranging from 0.50 μM to 20 μM were labeled using a ratio of 2:1 (PB

to amino acid) and pH 8.5 (as suggested by the seller) and then diluted to 100 nM and analyzed

by μCE. As shown in SI_Figure 2A, the peak intensities for the selected amino acids increase

with the concentration until reaching a maximum value for concentrations higher than 10 μM.

These results indicate that for low concentrations of amino acids, higher amounts of Pacific Blue

are required in order to enhance the labeling efficiency. The effect of the amount of Pacific Blue

on the labeling efficiency was studied by labeling 2 μM solutions of amino acids with increasing

amounts of fluorescent dye. As can be observed in SI_Figure 2B, higher ratios of PB to amino

acid improve the labeling efficiency yielding higher peak intensities. The maximum efficiency is

reached for ratios over 20. These conditions were selected in order to assure the proper labeling

of low concentrations of amino acids on the sample.

A)
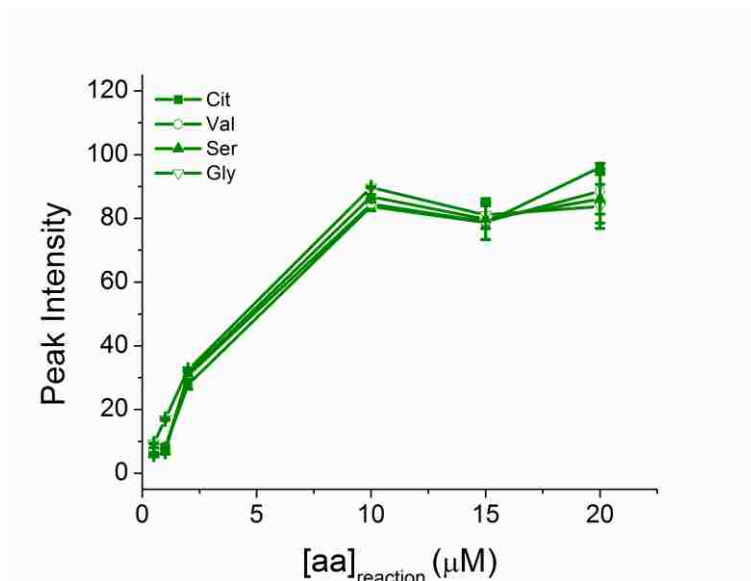
B)
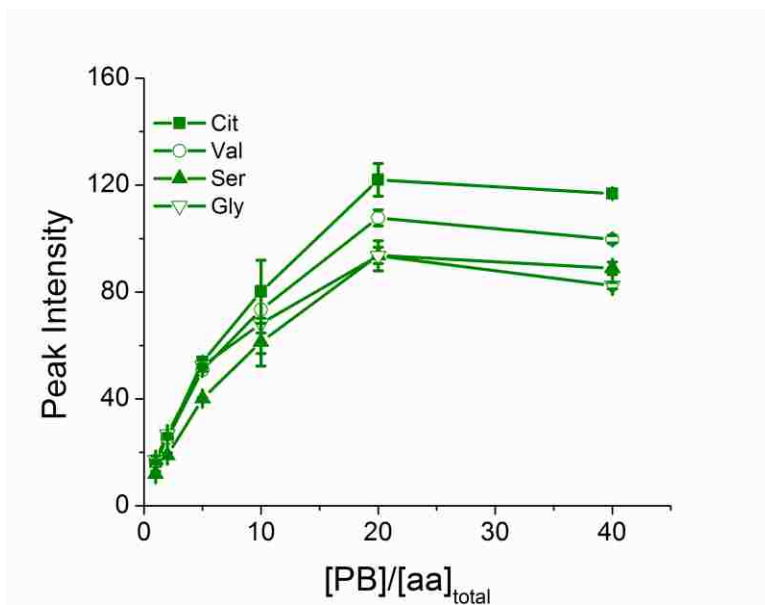
SI_Figure 2. Peak intensities for 100 nM mixtures of Cit, Val, Ser, and Gly as a function of A) the concentration on the labeling solution and B) the ratio of PB to aa.

Control of Microfluidic Device

SI_Figure 3 shows the polycarbonate mounting fixture used to hold the microchip on the microscope stage and also to apply vacuum/pressure to the valves.
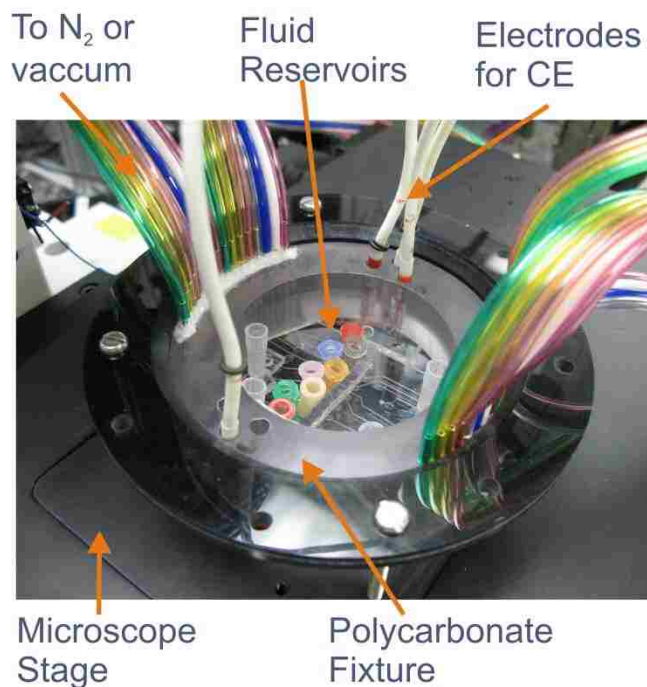
SI_Figure 3: Picture of the microfluidic device mounted on the microscope stage through a polycarbonate fixture design in our laboratory.

Pumping Sequences

The sequence of valve actuation for operating three serially connected valves as a diaphragm pump is shown in SI_Table 1. Applied vacuum places a valve in the open state, pressure places a valve in the closed state.

Sequence of valve actuation for one cycle operating three valves as a diaphragm pump.

Step	Valve		
	1	2	3
1	**Open**	Closed	Closed
2	**Open**	**Open**	Closed
3	Closed	**Open**	Closed
4	Closed	**Open**	**Open**
5	Closed	Closed	**Open**

As can be observed in the SI_Figure 4A, for the end-to-end analysis, R1 was filled with buffer, R2 with 50 µL of PB (300 µM), R3 with 250 µL of the three unlabeled amino acid mixture (10 µM each), and R8 with 250 µL of the four PB-labeled amino acid standard (100 nM each). The rest of the reservoirs were used for dilution of the labeled sample (R5 and R6) and for mixing with the standard solution. SI_Figure 4B and SI_Figure 4C depict how the fluorescent dye and the sample were mixed and how the dilution was performed, respectively.
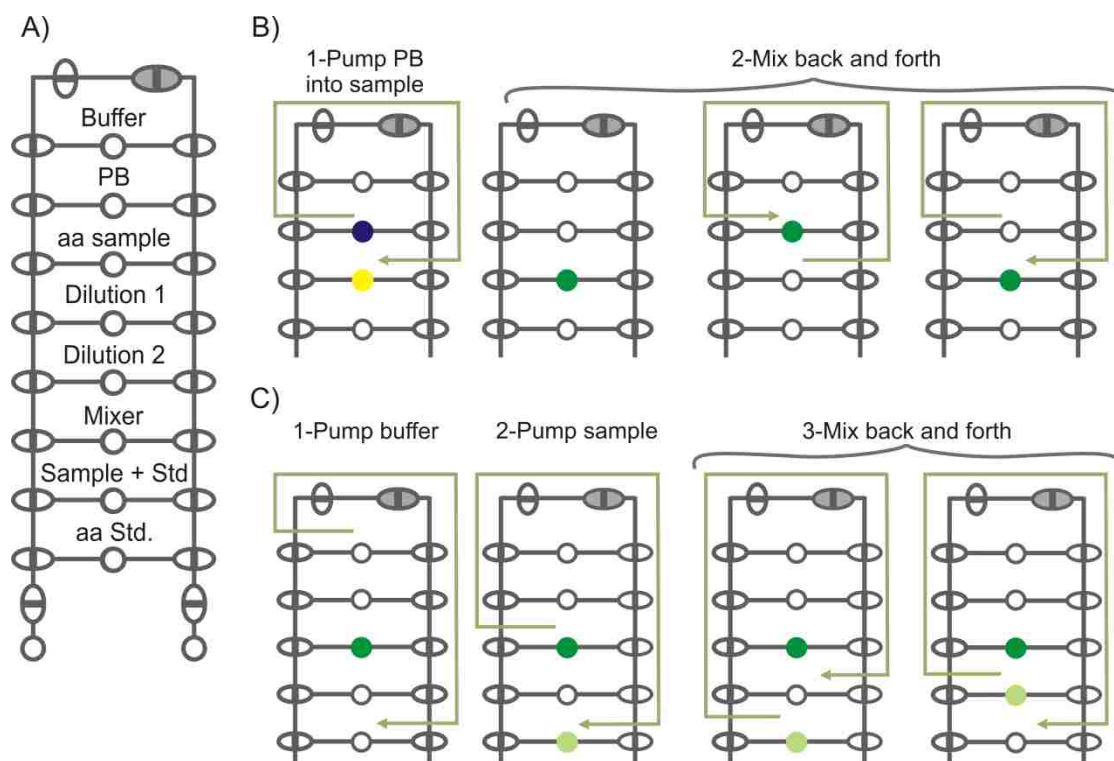
SI_Figure 4: Schematic drawing showing A) the assignment of fluid to each reservoir, B) the labeling step which involves pumping PB into the amino acid (aa) sample and then mixing several times, and C) the on-chip dilution process, consisting of three main pumping steps: buffer, sample and mixing.

SI_Table 2 shows the sequence of pumping events employed for the end-to-end analysis of amino acid indicating the fluidic reservoirs and valves involved. Solutions were placed in the processing unit as indicated in SI_Figure 4. The valves are numbered from 1 to 32 according to the diagram for the device showed in Figure 1B on the manuscript. It is worth mentioning that the pumping of buffer to S, SW, B, and W can be executed simultaneously, although they are shown as individual steps in the table for clarity.

SI_Table 1: Sequences for automated end-to-end μCE analysis of amino acids indicating the fluidic reservoirs and valves involved in each step. Electrophoretic analysis is indicated as *CE* and it was performed in triplicates.

#	Process	From	To	Valves			#	Process	From	To	Valves		
1	**Labeling Reaction**						**7**	**Buffer Run**					
	Pump PB to 3aa Mix	R2	R3	18	2	23		Pump buffer to S	R1	S	17	2	1
	Mix	R3	R2	24	2	6		Pump Buffer to B	B2	B	7	5	3
		R2	R3	6	2	24		Pump buffer to SW	B3	SW	21	20	19
	Mix	R3	R2	24	2	6		Pump Buffer to W	B4	W	29	30	31
		R2	R3	6	2	24		*CE*					
	Rinse system	B1	W1	16	2	15	**8**	**3aa-PB Dilution 2**					
2	**Dilution 1**							Empty S	S	W1	1	2	15
	Pump buffer to R4	R1	R4	17	2	10		Pump sample to W	R5	W1	11	2	15
	Pump Sample to R4	R3	R4	24	2	10		Pump 3aa sample to S	R5	S	25	2	1
	Pump buffer to R4	R1	R4	17	2	10		*CE*					
	Mix	R4	R2	8	2	6		Empty S	S	W1	1	2	15
		R2	R4	6	2	8		Rinse system	B1	W1	16	2	15
	Mix	R4	R2	8	2	6		Pump Buffer to S	R1	S	17	2	1
		R2	R4	6	2	8		Rinse system	B1	W1	16	2	15
3	**Rinse R2**							Empty S	S	W1	1	2	15
	Pump buffer to R2	B1	R2	16	2	18		Rinse system	B1	W1	16	2	15
	Empty R2	R2	W1	6	2	18	**9**	**Buffer Run**					
	Rinse system	B1	W1	16	2	15		Pump buffer to S	R1	S	17	2	1
4	**Dilution 2**							Pump Buffer to B	B2	B	7	5	3
	Pump buffer to R5	R1	R5	17	2	11		Pump buffer to SW	B3	SW	21	20	19
	Pump 3dilution 1to R5	R4	R5	8	2	10		Pump Buffer to W	B4	W	29	30	31
	Pump buffer to R5	R1	R5	17	2	11		*CE*					
	Mix	R5	R2	25	2	6	**10**	**3aa-PB + 4aa Std.**					
		R2	R5	18	2	11		Pump Dil. 2 to R7	R4	R7	8	2	13
	Mix	R5	R2	25	2	6		Pump 4aa to R7	R8	R7	32	2	13
		R2	R5	18	2	11		Mix	R7	R6	27	2	12
	Rinse system	B1	W1	16	2	15			R6	R7	26	2	13
5	**Buffer Run**							Mix	R7	R6	27	2	12
	Pump buffer to S	R1	S	17	2	1			R6	R7	26	2	13
	Pump Buffer to B	B2	B	7	5	3		Empty S	S	W1	1	2	15
	Pump buffer to SW	B3	SW	21	20	19		Pump Mix to Waste	R7	W1	13	2	15
	Pump Buffer to W	B4	W	29	30	31		Pump mix to S	R7	S	27	2	1
	CE							*CE*					
6	**4aa Standard**							Empty S	S	W1	1	2	15
	Empty S	S	W1	1	2	15		Rinse system	B1	W1	16	2	15
	Pump 4aa to Waste	R8	W1	14	2	15		Pump Buffer to S	R1	S	17	2	1
	Pump 4aa to S	R8	S	32	2	1		Rinse system	B1	W1	16	2	15
	CE							Empty S	S	W1	1	2	15
	Empty S	S	W1	1	2	15		Rinse system	B1	W1	16	2	15
	Rinse system	B1	W1	16	2	15							
	Pump buffer to S	R1	R1	17	2	1							
	Rinse system	B1	W1	16	2	15							
	Empty S	S	W1	1	2	15							
	Rinse system	B1	W1	16	2	15							

References

1. McKay, C., *Space Sci. Rev.* **2008,** *135* (1), 49-54.

2. McKay, C. P., *PLoS Biol.* **2004,** *2* (9), e302.

3. Mora, M. F.; García, C. D., *Electrophoresis* **2007,** *28* (8), 1197-1203.

4. Smith, J. T.; el Rassi, Z., *Electrophoresis* **1993,** *14* (5-6), 396-406.

5. Arvidsson, B.; Johannesson, N.; Citterio, A.; Righetti, P. G.; Bergquist, J., *J. Chromatogr. A* **2007,** *1159* (1-2), 154-158.

6. Guzman;, N. A.; Blanc;, T.; Phillips;, T. M., *Electrophoresis* **2008,** *29* (16), 3259-3278.

7. Blanes, L.; Mora, M. F.; Ayon, A.; Do Lago, C. L.; Garcia, C. D., *Electroanalysis* **2007,** *19* 2451-2456.

8. Simionato, A. V. C.; Carrilho, E.; Tavares, M. F. M., *Electrophoresis* **2010,** *31*, 1214-1226.

9. Zhou, S. Y.; Zuo, H.; Stobaugh, J. F.; Lunte, C. E.; Lunte, S. M., *Anal. Chem.* **1995,** *67* (3), 594-599.

10. Schultz, C. L.; Moini, M., *Anal. Chem.* **2003,** *75* (6), 1508-1513.

11. Garcia, C. D.; Henry, C. S., *Anal. Chem.* **2003,** *75* (18), 4778-4783.

12. Simionato, A. V. C.; Moraes, E. P.; Carrilho, E.; Tavares, M. F. M.; Kenndler, E., *Electrophoresis* **2008,** *29*, 2051-2058.

13. Dittrich, P. S.; Tachikawa, K.; Manz, A., *Anal. Chem.* **2006,** *78* (12), 3887-3908.

14. Berg, C.; Valdez, D. C.; Bergeron, P.; Mora, M. F.; Garcia, C. D.; Ayon, A., *Electrophoresis* **2008,** *29* (24), 4914-4921.

15. Jackson, D. J.; Naber, J. F.; Roussel, T. J., Jr.; Crain, M. M.; Walsh, K. M.; Keynton, R. S.; Baldwin, R. P., *Anal. Chem.* **2003,** *75*, 3311-3317.

16. Felhofer, J. L.; Blanes, L.; Garcia, C. D., *Electrophoresis* **2010,** *31* (15), 2469-2486.

17. Skelley, A. M.; Scherer, J. R.; Aubrey, A. D.; Grover, W. H.; Ivester, R. H. C.; Ehrenfreund, P.; Grunthaner, F. J.; Bada, J. L.; Mathies, R. A., *Proc. Nat. Acad. Sci.* **2005,** *102* (4), 1041-1046.

18. Hutt, L. D.; Glavin, D. P.; Bada, J. L.; Mathies, R. A., *Anal. Chem.* **1999,** *71* (18), 4000-4006.

19. Benhabib, M.; Chiesl, T. N.; Stockton, A. M.; Scherer, J. R.; Mathies, R. A., *Anal. Chem.* **2010,** *82* (6), 2372-2379.

20. Chiesl, T. N.; Chu, W. K.; Stockton, A. M.; Amashukeli, X.; Grunthaner, F.; Mathies, R. A., *Anal. Chem.* **2009,** *81* (7), 2537-2544.

21. Harrison, D. J.; Manz, A.; Fan, Z.; Luedi, H.; Widmer, H. M., *Anal. Chem.* **1992,** *64* (17), 1926-1932.

22. Hosokawa, K.; Maeda, R., *J. Micromech. Microeng.* **2000,** *10* (3), 415-420.

23. Chen, C.-F.; Liu, J.; Chang, C.-C.; DeVoe, D. L., *Lab Chip* **2009,** *9* (24), 3511-3516.

24. Weibel, D. B.; Kruithof, M.; Potenta, S.; Sia, S. K.; Lee, A.; Whitesides, G. M., *Anal. Chem.* **2005,** *77* (15), 4726-4733.

25. Unger, M. A.; Chou, H.-P.; Thorsen, T.; Scherer, A.; Quake, S. R., *Science* **2000,** *288* (5463), 113-116.

26. Grover, W. H.; Muhlen, M. G. v.; Manalis, S. R., *Lab Chip* **2008,** *8* (6), 913-918.

27. Grover, W. H.; Skelley, A. M.; Liu, C. N.; Lagally, E. T.; Mathies, R. A., *Sens. Act. A* **2003,** *89* (3), 315-323.

28. Hisamoto, H.; Funano, S.-i.; Terabe, S., *Anal. Chem.* **2005,** *77* (7), 2266-2271.

29. Willis, P. A.; Greer, F.; Lee, M. C.; Smith, J. A.; White, V. E.; Grunthaner, F. J.; Sprague, J. J.; Rolland, J. P., *Lab Chip* **2008,** *8* (7), 1024-1026.

30. Willis, P. A.; Hunt, B. D.; White, V. E.; Lee, M. C.; Ikeda, M.; Bae, S.; Pelletier, M. J.; Grunthaner, F. J., *Lab Chip* **2007,** *7* (11), 1469-1474.

31. Guillo, C.; Karlinsey, J. M.; Landers, J. P., *Lab Chip* **2007,** *7* (1), 112-118.

32. Stockton, A. M.; Chiesl, T. N.; Lowenstein, T. K.; Amashukeli, X.; Grunthaner, F.; Mathies, R., *Astrobiology* **2009,** *9* (9), 823-831.

33. Botta, O.; Bada, J. L., *Surv. Geophys.* **2002,** *23* (5), 411-467.

34. Ehrenfreund, P.; Glavin, D. P.; Botta, O.; Cooper, G.; Bada, J. L., *Proc. Nat. Acad. Sci.* **2001,** *98* (5), 2138-2141.

35. Glavin, D. P.; Dworkin, J. P.; Sandford, S. A., *Meteorit. Planet. Sci.* **2008,** *43* (1-2), 399-413.

36. Parker, E. T.; Cleaves, H. J.; Dworkin, J. P.; Glavin, D. P.; Callahan, M.; Aubrey, A.; Lazcano, A.; Bada, J. L., *Proc. Natl. Acad. Sci.* **2011,** *108* (14), 5526-5531.

37. Curis, E.; Nicolis, I.; Moinard, C.; Osowska, S.; Zerrouk, N.; Bénazeth, S.; Cynober, L., *Amino Acids* **2005,** *29* (3), 177-20

APPENDIX 2. LETTERS OF PERMISSION

Copyright Clearance Center

RightsLink

Home | Create Account | Help

ACS Publications
High quality High impact

Title: Toward Total Automation of Microfluidics for Extraterrestial In Situ Analysis

Author: Maria F. Mora, Frank Greer, Amanda M. Stockton, Sherrisse Bryant, and Peter A. Willis

Publication: Analytical Chemistry

Publisher: American Chemical Society

Date: Nov 1, 2011

Copyright © 2011, American Chemical Society

User ID

Password

☐ Enable Auto Login

LOGIN

Forgot Password/User ID?

If you're a copyright.com user, you can login to RightsLink using your copyright.com credentials. Already **a RightsLink user** or want to learn more?

PERMISSION/LICENSE IS GRANTED FOR YOUR ORDER AT NO CHARGE

This type of permission/license, instead of the standard Terms & Conditions, is sent to you because no fee is being charged for your order. Please note the following:

- Permission is granted for your request in both print and electronic formats, and translations.
- If figures and/or tables were requested, they may be adapted or used in part.
- Please print this page for your records and send a copy of it to your publisher/graduate school.
- Appropriate credit for the requested material should be given as follows: "Reprinted (adapted) with permission from (COMPLETE REFERENCE CITATION). Copyright (YEAR) American Chemical Society." Insert appropriate information in place of the capitalized words.
- One-time permission is granted only for the use specified in your request. No additional uses are granted (such as derivative works or other editions). For any other uses, please submit a new request.

BACK | CLOSE WINDOW

4/6/2013 6:58 PM

ELSEVIER LICENSE
TERMS AND CONDITIONS

Apr 16, 2013

This is a License Agreement between Sherrisse K Bryant ("You") and Elsevier ("Elsevier") provided by Copyright Clearance Center ("CCC"). The license consists of your order details, the terms and conditions provided by Elsevier, and the payment terms and conditions.

All payments must be made in full to CCC. For payment instructions, please see information listed at the bottom of this form.

Supplier	Elsevier Limited The Boulevard,Langford Lane Kidlington,Oxford,OX5 1GB,UK
Registered Company Number	1982084
Customer name	Sherrisse K Bryant
Customer address	LSU Chemistry Department
	Baton Rouge, LA 70803
License number	3130991328085
License date	Apr 16, 2013
Licensed content publisher	Elsevier
Licensed content publication	Analytical Biochemistry
Licensed content title	A capillary electrophoretic assay for acetyl coenzyme A carboxylase
Licensed content author	Sherrisse K. Bryant,Grover L. Waldrop,S. Douglass Gilman
Licensed content date	1 June 2013
Licensed content volume number	437
Licensed content issue number	1
Number of pages	7
Start Page	32
End Page	38
Type of Use	reuse in a thesis/dissertation
Portion	full article
Format	both print and electronic
Are you the author of this Elsevier article?	Yes
Will you be translating?	No
Order reference number	

118

Title of your thesis/dissertation	The Development of Capillary Electrophoresis Assays to Study Enzyme Inhibition
Expected completion date	May 2013
Estimated size (number of pages)	100
Elsevier VAT number	GB 494 6272 12
Permissions price	0.00 USD
VAT/Local Sales Tax	0.0 USD / 0.0 GBP
Total	0.00 USD
Terms and Conditions	

INTRODUCTION

1. The publisher for this copyrighted material is Elsevier. By clicking "accept" in connection with completing this licensing transaction, you agree that the following terms and conditions apply to this transaction (along with the Billing and Payment terms and conditions established by Copyright Clearance Center, Inc. ("CCC"), at the time that you opened your Rightslink account and that are available at any time at http://myaccount.copyright.com).

GENERAL TERMS

2. Elsevier hereby grants you permission to reproduce the aforementioned material subject to the terms and conditions indicated.

3. Acknowledgement: If any part of the material to be used (for example, figures) has appeared in our publication with credit or acknowledgement to another source, permission must also be sought from that source. If such permission is not obtained then that material may not be included in your publication/copies. Suitable acknowledgement to the source must be made, either as a footnote or in a reference list at the end of your publication, as follows:

"Reprinted from Publication title, Vol /edition number, Author(s), Title of article / title of chapter, Pages No., Copyright (Year), with permission from Elsevier [OR APPLICABLE SOCIETY COPYRIGHT OWNER]." Also Lancet special credit - "Reprinted from The Lancet, Vol. number, Author(s), Title of article, Pages No., Copyright (Year), with permission from Elsevier."

4. Reproduction of this material is confined to the purpose and/or media for which permission is hereby given.

5. Altering/Modifying Material: Not Permitted. However figures and illustrations may be altered/adapted minimally to serve your work. Any other abbreviations, additions, deletions and/or any other alterations shall be made only with prior written authorization of Elsevier Ltd. (Please contact Elsevier at permissions@elsevier.com)

6. If the permission fee for the requested use of our material is waived in this instance, please be advised that your future requests for Elsevier materials may attract a fee.

7. Reservation of Rights: Publisher reserves all rights not specifically granted in the combination of (i) the license details provided by you and accepted in the course of this licensing transaction, (ii) these terms and conditions and (iii) CCC's Billing and Payment terms and conditions.

8. License Contingent Upon Payment: While you may exercise the rights licensed immediately upon issuance of the license at the end of the licensing process for the transaction, provided that you have disclosed complete and accurate details of your proposed use, no license is finally effective unless and until full payment is received from you (either by publisher or by CCC) as provided in CCC's Billing and Payment terms and conditions. If full payment is not received on a timely basis, then any license preliminarily granted shall be deemed automatically revoked and shall be void as if never granted. Further, in the event that you breach any of these terms and conditions or any of CCC's Billing and Payment terms and conditions, the license is automatically revoked and shall be void as if never granted. Use of materials as described in a revoked license, as well as any use of the materials beyond the scope of an unrevoked license, may constitute copyright infringement and publisher reserves the right to take any and all action to protect its copyright in the materials.

9. Warranties: Publisher makes no representations or warranties with respect to the licensed material.

10. Indemnity: You hereby indemnify and agree to hold harmless publisher and CCC, and their respective officers, directors, employees and agents, from and against any and all claims arising out of your use of the licensed material other than as specifically authorized pursuant to this license.

11. No Transfer of License: This license is personal to you and may not be sublicensed, assigned, or transferred by you to any other person without publisher's written permission.

12. No Amendment Except in Writing: This license may not be amended except in a writing signed by both parties (or, in the case of publisher, by CCC on publisher's behalf).

13. Objection to Contrary Terms: Publisher hereby objects to any terms contained in any purchase order, acknowledgment, check endorsement or other writing prepared by you, which terms are inconsistent with these terms and conditions or CCC's Billing and Payment terms and conditions. These terms and conditions, together with CCC's Billing and Payment terms and conditions (which are incorporated herein), comprise the entire agreement between you and publisher (and CCC) concerning this licensing transaction. In the event of any conflict between your obligations established by these terms and conditions and those established by CCC's Billing and Payment terms and conditions, these terms and conditions shall control.

14. Revocation: Elsevier or Copyright Clearance Center may deny the permissions described in this License at their sole discretion, for any reason or no reason, with a full refund payable to you. Notice of such denial will be made using the contact information provided by you. Failure to receive such notice will not alter or invalidate the denial. In no event will Elsevier or Copyright Clearance Center be responsible or liable for any costs, expenses or damage incurred by you as a result of a denial of your permission request, other than a refund of the amount(s) paid by you to Elsevier and/or Copyright Clearance Center for denied permissions.

LIMITED LICENSE

The following terms and conditions apply only to specific license types:

15. **Translation**: This permission is granted for non-exclusive world **English** rights only unless your license was granted for translation rights. If you licensed translation rights you may only translate this content into the languages you requested. A professional translator must perform all translations and reproduce the content word for word preserving the integrity of the article. If this license is to re-use 1 or 2 figures then permission is granted for non-exclusive world rights in all languages.

16. **Website**: The following terms and conditions apply to electronic reserve and author websites:
Electronic reserve: If licensed material is to be posted to website, the web site is to be password-protected and made available only to bona fide students registered on a relevant course if:
This license was made in connection with a course,
This permission is granted for 1 year only. You may obtain a license for future website posting,
All content posted to the web site must maintain the copyright information line on the bottom of each image,
A hyper-text must be included to the Homepage of the journal from which you are licensing at http://www.sciencedirect.com/science/journal/xxxxx or the Elsevier homepage for books at http://www.elsevier.com , and
Central Storage: This license does not include permission for a scanned version of the material to be stored in a central repository such as that provided by Heron/XanEdu.

17. **Author website** for journals with the following additional clauses:

All content posted to the web site must maintain the copyright information line on the bottom of each image, and the permission granted is limited to the personal version of your paper. You are not allowed to download and post the published electronic version of your article (whether PDF or HTML, proof or final version), nor may you scan the printed edition to create an electronic version. A hyper-text must be included to the Homepage of the journal from which you are licensing at http://www.sciencedirect.com/science/journal/xxxxx . As part of our normal production process, you will receive an e-mail notice when your article appears on Elsevier's online service ScienceDirect (www.sciencedirect.com). That

e-mail will include the article's Digital Object Identifier (DOI). This number provides the electronic link to the published article and should be included in the posting of your personal version. We ask that you wait until you receive this e-mail and have the DOI to do any posting.

Central Storage: This license does not include permission for a scanned version of the material to be stored in a central repository such as that provided by Heron/XanEdu.

18. **Author website** for books with the following additional clauses:
Authors are permitted to place a brief summary of their work online only.
A hyper-text must be included to the Elsevier homepage at http://www.elsevier.com . All content posted to the web site must maintain the copyright information line on the bottom of each image. You are not allowed to download and post the published electronic version of your chapter, nor may you scan the printed edition to create an electronic version.

Central Storage: This license does not include permission for a scanned version of the material to be stored in a central repository such as that provided by Heron/XanEdu.

19. **Website** (regular and for author): A hyper-text must be included to the Homepage of the journal from which you are licensing at http://www.sciencedirect.com/science/journal /xxxxx. or for books to the Elsevier homepage at http://www.elsevier.com

20. **Thesis/Dissertation**: If your license is for use in a thesis/dissertation your thesis may be submitted to your institution in either print or electronic form. Should your thesis be published commercially, please reapply for permission. These requirements include permission for the Library and Archives of Canada to supply single copies, on demand, of the complete thesis and include permission for UMI to supply single copies, on demand, of the complete thesis. Should your thesis be published commercially, please reapply for permission.

21. **Other Conditions**:

v1.6

If you would like to pay for this license now, please remit this license along with your payment made payable to "COPYRIGHT CLEARANCE CENTER" otherwise you will be invoiced within 48 hours of the license date. Payment should be in the form of a check or money order referencing your account number and this invoice number RLNK501001311.
Once you receive your invoice for this order, you may pay your invoice by credit card. Please follow instructions provided at that time.

Make Payment To:
Copyright Clearance Center
Dept 001
P.O. Box 843006
Boston, MA 02284-3006

For suggestions or comments regarding this order, contact RightsLink Customer Support: customercare@copyright.com or +1-877-622-5543 (toll free in the US) or +1-978-646-2777.

Gratis licenses (referencing $0 in the Total field) are free. Please retain this printable license for your reference. No payment is required.

VITA

Sherrisse Kelly Bryant was born in Bradenton, Florida and raised in Tallahassee, Florida. Her parents are Barbara G. Kelly and the late Alexander D. Kelly, III. She received her secondary education in Monticello, Florida and Tallahassee, Florida. After graduating from Lincoln High School (Tallahassee, Florida), she began undergraduate studies at Florida Agricultural and Mechanical University where she earned a Bachelor of Science degree in Biochemistry. Immediately following her tenure as an undergraduate student, she began graduate studies at Louisiana State University (LSU) and joined Professor S. Douglass Gilman's research group. During her time at LSU, she was selected to receive the National Science Foundation Bridge to the Doctorate Fellowship (2007-2009) and the National Aeronautics and Space Agency Harriett G. Jenkins Predoctoral Fellowship (NASA JPFP, 2009-2012). She also conducted research at the NASA Jet Propulsion Laboratory (JPL) in Pasadena, California as a NASA JPFP Mini Research Award recipient (Summer 2010).She is happily married to Mark Bryant.